

# Computer methods for semi-automatic MR renogram determination

**Citation for published version (APA):**

Giele, E. L. W. (2002). *Computer methods for semi-automatic MR renogram determination*. [Phd Thesis 1 (Research TU/e / Graduation TU/e), Electrical Engineering]. Technische Universiteit Eindhoven. <https://doi.org/10.6100/IR553632>

**DOI:**

[10.6100/IR553632](https://doi.org/10.6100/IR553632)

**Document status and date:**

Published: 01/01/2002

**Document Version:**

Publisher's PDF, also known as Version of Record (includes final page, issue and volume numbers)

**Please check the document version of this publication:**

- A submitted manuscript is the version of the article upon submission and before peer-review. There can be important differences between the submitted version and the official published version of record. People interested in the research are advised to contact the author for the final version of the publication, or visit the DOI to the publisher's website.
- The final author version and the galley proof are versions of the publication after peer review.
- The final published version features the final layout of the paper including the volume, issue and page numbers.

[Link to publication](#)

**General rights**

Copyright and moral rights for the publications made accessible in the public portal are retained by the authors and/or other copyright owners and it is a condition of accessing publications that users recognise and abide by the legal requirements associated with these rights.

- Users may download and print one copy of any publication from the public portal for the purpose of private study or research.
- You may not further distribute the material or use it for any profit-making activity or commercial gain
- You may freely distribute the URL identifying the publication in the public portal.

If the publication is distributed under the terms of Article 25fa of the Dutch Copyright Act, indicated by the "Taverne" license above, please follow below link for the End User Agreement:

[www.tue.nl/taverne](http://www.tue.nl/taverne)

**Take down policy**

If you believe that this document breaches copyright please contact us at:

[openaccess@tue.nl](mailto:openaccess@tue.nl)

providing details and we will investigate your claim.

# **Computer methods for semi-automatic MR renogram determination**

**Eelco Giele**

CIP-DATA LIBRARY TECHNISCHE UNIVERSITEIT EINDHOVEN

Giele, Eelco L.W.

Computer methods for semi-automatic MR renogram determination / by Eelco L.W. Giele. -  
Eindhoven : Technische Universiteit Eindhoven, 2002.

Proefschrift. - ISBN 90-386-1890-5

NUGI 743

Trefw.: biomedische kernspinresonantie / nieren / biomedische beeldverwerking / diagnostische radiologie.

Subject headings: biomedical MRI / kidney / medical image processing / medical diagnostic computing.

© 2002, E.L.W. Giele, Geldrop

Druk: Universiteitsdrukkerij TU Eindhoven

# **Computer methods for semi-automatic MR renogram determination**

PROEFSCHRIFT

ter verkrijging van de graad van doctor aan de  
Technische Universiteit Eindhoven, op gezag van de  
Rector Magnificus, prof.dr. R.A. van Santen, voor een  
commissie aangewezen door het College voor  
Promoties in het openbaar te verdedigen op  
dinsdag 26 maart 2002 om 16.00 uur

door

**Eelco Louis Wim Giele**

geboren te Geldrop

Dit proefschrift is goedgekeurd door de promotoren:

prof.dr.ir. A. Hasman

en

prof.dr. J.M.A. van Engelshoven

Copromotor:

dr.ir. J.A. den Boer

---

## Summary

---

This thesis describes several techniques that aid in measuring MR Renograms. Renograms are curves that show the contrast agent signal enhancement in the cortex and medulla of the kidney as a function of time and are an indicator of its function. To acquire MR renograms a series of dynamic Magnetic Resonance images is generated during and after a bolus injection of contrast agent. By recording the image intensity in the two tissues the renograms are recorded.

Although the MR scanner offers cross section images of the kidney the signal in the medullary areas will in most cases contain a contribution due to cortical tissue which is included in the three dimensional image elements (voxels). By a weighted subtraction of the cortical signal from the mixed signal it becomes possible to measure pure medullary renograms. The weighting factor is determined by the cortical contribution. In this thesis several methods for determining this factor are compared and the most robust method for its calculation is presented.

To improve reproducibility and to reduce operator input, a method is described to automatically segment the kidney contour in the image series and to place the regions of interest (ROIs) that are used for the measurements. The ROI placement is based on a priori knowledge of the tissue distribution in the kidney and an analysis of the changes in contrast agent distribution during the scans.

Since the weighted subtraction results in a reduced signal to noise level, which worsens with increasing cortical contribution, the ROI is reduced by removal of areas with a high cortical contribution. This is done by a method which uses matched image filtering to find pixels with a high contribution, leading to a net increase in signal to noise ratio.

The development of the algorithms was done using image series of transplanted kidneys. The images obtained from this type of kidney are suitable for that purpose, since they show no breathing induced movement. To be able to use the same techniques on native kidneys which do move with breathing, a movement

---

correction method is needed. In this thesis several movement correction methods are described and compared for performance.

At the end of this thesis the MR scanner settings used to generate the image series for our research are reviewed. Based on the developed methods and advances in technology a new set of scanner parameters is suggested that should result in renograms that have the same shape but a better signal to noise ratio.

---

# Contents

---

<b>Summary</b>	<b>5</b>
<b>Contents</b>	<b>7</b>
Chapter 1	
<b>Introduction</b>	<b>11</b>
1.1 The kidney .....	11
1.2 MR renograms .....	14
1.3 Outline of the thesis .....	15
Chapter 2	
<b>Determination of ROI location, size and shape.</b>	<b>19</b>
2.1 Introduction .....	19
2.2 Partial volume effect.....	20
2.3 Materials .....	21
2.4 Partial volume correction algorithm .....	22
2.5 Onion ring ROIs .....	23
2.6 Results .....	24
2.7 Conclusions and Discussion .....	27
2.8 References .....	28
Chapter 3	
<b>Evaluation of two cortical fraction estimation algorithms for the calculation of dynamic magnetic resonance renograms.</b>	<b>29</b>
3.1 Abstract.....	29
3.2 Introduction .....	29
3.3 Materials, subjects and scan method.....	31
3.3.1 Analysis .....	32
3.3.2 Estimation of the cortical fraction .....	33
3.3.3 Determination of the accuracy of the cortical fraction calculations .....	34
3.3.4 Choice of estimation interval.....	35
3.4 Results .....	36
3.5 Discussion and Conclusions. ....	39
3.6 References .....	39



## Contents

---

### Chapter 4

<b>Reduction of noise in medullary renograms from dynamic MR Images</b>	<b>43</b>
4.1 Abstract.....	43
4.2 Introduction .....	43
4.3 Materials .....	44
4.4 Methods .....	45
4.4.1 Determination of ROIs .....	45
4.4.2 Determining the cortical fraction.....	46
4.4.3 Method to decrease $f_c$ .....	48
4.4.4 Noise estimation .....	50
4.5 Results .....	50
4.6 Discussion.....	54
4.7 Conclusion .....	57
4.8 References .....	57

### Chapter 5

<b>Movement correction of the kidney in dynamic MRI scans using FFT phase difference movement detection.</b>	<b>59</b>
5.1 Abstract.....	59
5.2 Introduction .....	59
5.3 Materials .....	61
5.4 Methods .....	62
5.5 The PDMD marker image.....	68
5.6 Results .....	70
5.7 Discussion.....	73
5.8 Conclusion .....	76
5.9 References .....	76

### Chapter 6

<b>Optimal scanner settings for semi automatic renogram determination.</b>	<b>81</b>
6.1 Abstract.....	81
6.2 Introduction .....	81
6.3 Slice thickness. ....	82
6.3.1 Signal to noise ratio versus slice thickness.....	84
6.3.2 Cortical fraction versus slice thickness.....	85
6.3.3 Signal to noise ratio versus cortical fraction.....	87
6.3.4 Relative medullary signal to noise ratio versus slice thickness. ....	87
6.3.5 Discussion.....	88
6.4 Slice orientation.....	89
6.5 Single or multi slice.....	90
6.5.1 Experiments .....	90
6.5.2 Discussion.....	92

---

6.6 Conclusions .....	93
6.7 Acknowledgement .....	93
6.8 References .....	93
Chapter 7	
<b>Discussion and Conclusions</b> .....	<b>97</b>
7.1 General discussion .....	97
7.2 Conversion of images to numerical data.....	97
7.2.1 Segmentation .....	98
7.2.2 ROI placement.....	99
7.2.3 ROI size .....	100
7.2.4 Exclusion of pixels from the medullary ROI.....	101
7.2.5 Movement correction.....	101
7.2.6 Suggested changes of scanner settings .....	103
7.3 Usability of techniques for other clinical research .....	103
7.4 Contribution of this research to the clinical use of MR renography.....	104
7.5 Image processing .....	104
7.5.1 Registration: no sub-pixel accuracy.....	104
7.5.2 Interpolation.....	105
7.5.3 Registration methods .....	105
7.5.4 Processing speed.....	107
7.6 Recommendations for further research.....	107
7.7 Conclusions .....	108
7.8 References .....	109
Appendix A	
<b>Use of a Dynamic 3D Computer Model of the Kidney for Validation of Analysis Methods and Scan Parameters in Dynamic MRI of the Kidney.</b> .....	<b>111</b>
Introduction .....	111
Materials/Method.....	112
Use of the model.....	112
Conclusion .....	113
Acknowledgement .....	114
References .....	114
Appendix B	
<b>Automated quantitative evaluation of diseased and non-diseased renal transplants with MR – renography.</b> .....	<b>115</b>
Introduction .....	115
Material and methods. ....	117
Results. ....	120
Discussion.....	123

---

Contents

---

References .....	126
<b>Samenvatting</b>	<b>129</b>
<b>Dankwoord</b>	<b>131</b>
<b>Curriculum Vitae</b>	<b>133</b>

# Chapter 1

---

## Introduction

---

### 1.1 The kidney

The kidneys in a normal adult measure 11 to 14 cm in length from pole to pole and are located retroperitoneally in the lumbar region and form as highly vascular organs an integral part of the systemic circulation. They are concerned with the regulation of the volume and composition of the extracellular fluid and with the elimination of waste products. Each kidney is composed of about 2 – 3 million very tiny tubular structures called "nephrons". The most proximal part of such a nephron is the glomerulus in which the vascular system is closely related to the tubuli and where the blood is filtered. The tubule part of the nephron follows a typical path. Its most proximal part is very tortuous, then the tubule straightens and takes a direct course toward the centre of the kidney, there it makes a hairpin turn and returns in a straight line back to the outer part of the kidney. At that level many nephrons join in straight collecting tubules transporting the urine to the renal hilum and pelvis. The glomeruli are predominantly located in the outer 8 mm of the kidney called the cortex of the kidney and the tubuli are concentrated within the pyramids also called the medulla of the kidney (figure 1.1). Cortex and medulla together are called the renal parenchyma. Filtration in the glomerulus and complex interactions between the vascular bed and the tubular epithelium account for the definitive function of the kidneys.

A large variety of diseases can affect the different anatomic elements of the kidney. This can occur unilaterally or bilaterally and all these diseases can also be present in a transplanted kidney. Renal transplantation is the treatment of choice in patients with chronic end-stage renal disease, therefore many renal transplant patients are living now and they also are subject to diagnostic techniques. These transplants are nearly always placed heterotopically in an extraperitoneal location in the iliac fossa in the pelvis.

## Introduction

---

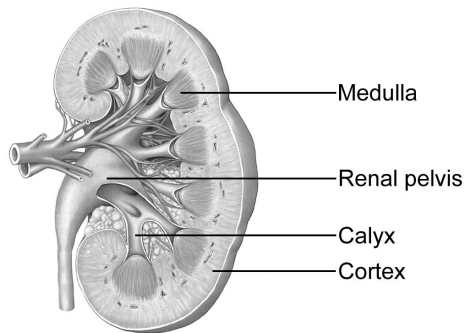


Figure 1.1: Cross section of the kidney.

Many diagnostic techniques are available to detect abnormalities in renal morphology or renal function. Each technique has its own limitations and possibilities. Urine and blood sample tests give only an impression about the function of both kidneys together. Imaging tests, on the other hand, give morphologic information about each kidney separately and allow for the detection of renal stones, mass lesions or obstructions of the urinary tract. For these roentgenograms, computed tomography or ultrasound examinations are the diagnostic tests of first choice. However the so called medical nephropathies which are diseases of the glomeruli, tubules and interstitial tissue of the renal parenchyma, thus diseases on a microscopic level only without affecting the gross anatomy of the kidney, can not be detected with imaging techniques and often need a radionuclide scan or even a renal biopsy to make a definite diagnosis.

Radionuclide studies provide predominantly functional data and their ability to visualise functional renal tissue, which can not be imaged radiographically, is an advantage of this method. Its inability to show precise anatomical detail is, however, an important drawback. With this technique the flow of a radionuclide tracer through the renal parenchyma can be followed over time with a high temporal but a limited spatial resolution. This method is particularly useful in the post renal transplant management because it can deliver information about renal perfusion, renal filtration and renal excretion. Radionuclide techniques cannot locate functional abnormalities inside the renal parenchyma and cortical and medullary function cannot be differentiated accurately.

MRI has the attractive potential for functional kidney imaging by a technique that parallels the radionuclide study principle but may compare favourably in performance because it offers high temporal and spatial resolution as well as good soft tissue contrast. The presence of an intravenously injected MR contrast medium can be followed over time in the renal cortex and medulla separately. This can be

done simultaneously and the changes in signal intensities of cortex and medulla can be displayed graphically (figure 1.3). These are called MR renograms.

In this study we have used the low molecular Gd-DTPA dimeglumine as MR contrast medium. This Gd chelate diffuses fast into the extracellular space after an intravenous injection and it is immediately subject to renal excretion. This excretion is exclusively determined by the glomerular filtration without any tubular reabsorption. Because most of the water is reabsorbed in the tubulus a high concentration of Gd-DTPA may be reached in the medulla. Therefore, the cortical renogram can be considered as a reflection of the renal perfusion and a medullary renogram as a visualisation of the function of the nephron concerning its filter and reabsorption capacity.

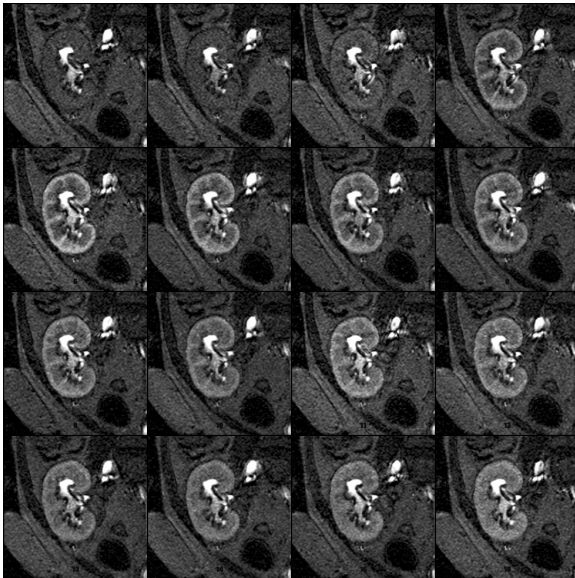


Figure 1.2: A dynamic series of images of an implanted kidney. In the dynamic scan an image is generated every 2 seconds. Displayed is every second image, covering the first 64 seconds. Ten seconds after the scan started contrast agent was injected. In these images the arrival of the contrast agent can be seen as well as its distribution pattern over the kidney.

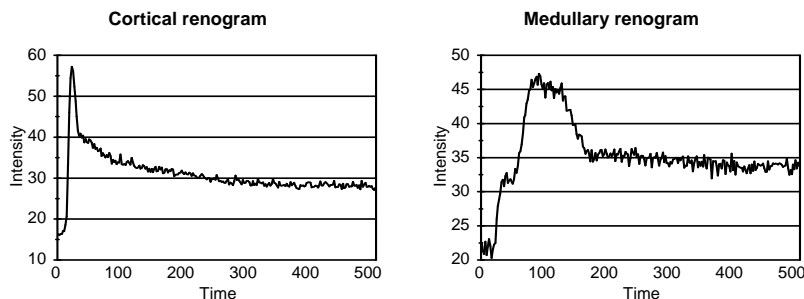


Figure 1.3: Cortical and medullary renogram, showing the average intensity of the pixels in the cortex and medulla, and thus give a measure for the contrast agent concentration.

## 1.2 MR renograms

At the onset of the study it was unclear if the intended diagnostic contribution, new functional information of the kidney obtained from MR renograms, could be realised. It was clear however that it would be a difficult task. So next to the optimal choice of data acquisition method, a considerable effort was devoted to optimise the data analysis. This thesis deals with steps in both domains.

The proof of the value of this undertaking is of course if MR renograms are actually useable in clinical practice and offer advantages over already existing methods. Our study was performed simultaneously with a clinical research project that investigated this question. In appendix B we reproduce some of the clinical results to indicate the progress made in that respect.

### *The MR technique*

The flow of the contrast agent through the kidney is tracked by collecting a series of images during the passage of a bolus of the contrast agent. This agent is rapidly injected intravenously in the arm as a bolus. During its transport through the lungs, the heart and the aorta the bolus is only slightly diluted so that its concentration in the blood that enters the kidney is elevated for a short time only (about 10 s). The observation of the evolution of the subsequent changes in the contrast agent concentration during the cortical arterial phase requires a high temporal resolution. This in turn causes a low signal to noise ratio in the images. High concentrations of the contrast agent, in particular in the nephrons requires a very heavily T1 weighted scan sequence, again at the cost of signal to noise ratio, especially at low contrast agent concentrations. Finally the long duration of the nephronal passage requires scan series of at least five minutes. To fulfil all these conditions

simultaneously, we used a single slice spoiled FFE method with a time resolution of two seconds and a total duration of 256 images (512 s). Figure 1.2 shows 16 images from such a series. The images have an in-plane spatial resolution of about 1.5 mm in both directions, sufficient to separate cortex and medulla. By selection of a small slice thickness, 6 mm, we aimed to maintain this separation in the third dimension so that the medullary renogram would be retrievable. This retrieval turned out to be a major hurdle and an important part of this thesis is devoted to its solution.

### 1.3 Outline of the thesis

#### *Finding the regions of interest (ROIs)*

By drawing regions of interest (ROIs) over the cortex and medulla in the obtained images the signal intensity of the cortex and medulla can be calculated for each image.

Since the measurements are based on 256 images and placing ROIs in each image would be far too time consuming automatic ROI definition is mandatory to make the method useable for daily practice. This is relatively simple in renal transplants because they do not move during respiration inside the human body and is thus more difficult in native kidneys because they move over considerable distance due to breathing. Therefore, MR renography of the native kidneys poses an additional problem because of the need for motion correction. In chapter 2 the problems of locating the kidney and positioning the required ROIs in a reproducible and meaningful way are discussed.

As mentioned, medullary renograms could be a valuable addition for diagnosing certain diseases. While measuring the cortical renogram is mainly a matter of careful selection of the ROI placement (regions with only cortical tissue are found near the periphery of the cross-section of the kidney) measuring the pure medullary renogram is more complicated since medullary and cortical tissue usually overlap. Since cortical and medullary renograms have different shapes the hypothesis is that the location of medullary regions can be obtained by searching for areas with signals that are minimally correlated with the cortical signal.

The signal to noise ratio of the renograms is among other things determined by the slice thickness. The thicker the slice, the higher this ratio. However, with thicker slices the chance that voxels will contain both cortical and medullary tissue increases. The resulting renogram of medullary regions will therefore probably contain a cortical contribution. From the study reported in chapter 2 it became clear that ROIs covering only medullary tissue were very difficult to find, even with a



slice thickness of 6 mm. We therefore call the ROI used to retrieve the medullary signal a mixed ROI. To obtain the medullary renogram a method has to be developed that removes the cortical contribution to the signal of the mixed ROI. We assumed that the temporal shapes of cortical and medullary signals are invariant of the location in the kidney. In that case the partial volume occupied by the cortical tissue (called the cortical fraction) can be determined and the cortical contribution to the signal can be removed by weighted subtraction.

### *Optimal determination of the cortical fraction*

The noise present in the signals not only reduces the quality of the signals, but also decreases the accuracy and increases the difficulty with which the cortical fraction can be determined. Since there are several different methods for determining this cortical fraction we compare them in chapter 3 and select the one that has the most stable performance with noisy signals.

### *Noise reduction of medullary renograms*

Weighted subtraction indeed results in a medullary renogram as was shown in the clinical research project but also results in an increased noise level of the medullary signal. The higher the cortical fraction, the higher the noise level and the lower the signal to noise ratio of the medullary renogram, so it is of interest to reduce the cortical fraction in the mixed ROI. The approach is described in chapter 4 where we use matched image filtering to remove pixels with a high cortical fraction from the mixed ROI. Since as a result the signal to noise ratio of the mixed signal decreases, we described the balance of both effects on the signal to noise ratio of the medullary signal.

### *Motion correction*

In the first chapters we focused on transplanted kidneys. The main reason was that they show no movement during scanning. To measure renograms of native kidneys a motion correction is needed. A new method that is suitable for motion estimation is described and compared to existing methods in chapter 5. This new method was necessary because the short imaging time used to generate renograms results in low signal-to-noise ratio images and the arrival and subsequent passage of contrast agent changes the contrast distribution in the images. Therefore the brightness distribution of the object (the kidney) to be detected in the image changes from image to image.

### *A critique on scanner parameter settings.*

Since the study was carried out using parameter settings decided on early in the study we investigated what parameters would be optimal given the methods

---

described in the earlier chapters. In chapter 6 the sensitivity of the methods to some important parameters (slice thickness, single or multi-slice and slice orientation) is presented.

*Discussion and conclusions*

All methods and results presented in the main part of this thesis and the total of the technical progress made are discussed in chapter 7. Table 1.1 summarizes the status of the various items which have been researched for this thesis. Everything which is implemented can be used for clinical research and has been used for validation purposes. Everything which is noted as being in use is now part of the standard procedure to generate MR renograms.

Table 1.1: Status of the various items of this research.

Item	Evaluated	Implemented	In use for clinical series
ROI shape and placement	Chapter 2	+	+
Estimate of cortical fraction ( $f_c$ )	Chapter 3	+	+
Rejection of high $f_c$ pixels	Chapter 4	+	-
Movement correction	Chapter 5	+	+
Thick multi slice scan	Chapter 6	-	-

## Introduction

---

## Chapter 2

---

# Determination of ROI location, size and shape.

---

### 2.1 Introduction

In dynamic MR a single slice through the body is selected and this slice is repeatedly imaged with the MRI scanner. Administration of a contrast agent during the recording of the series enables the visualisation and measurement of perfusion related dynamic processes that take place per tissue region visualized in this slice.

To extract functional information use is made of regions of interest (ROIs). A ROI is a closed contour that is placed over the image and defines an area which can be used for calculating statistics. These measurements include, but are not limited to, surface area, average pixel intensity of all the pixels enclosed by the ROI and the standard deviation of these pixel intensities. In dynamic MR of a non-moving tissue a ROI is placed over the tissue of interest in one image and copied to all the other images. This makes it possible to measure the average pixel intensity of the tissue during a scan. In combination with a contrast agent this allows for a record of the history of the contrast agent concentration in that tissue.

In the kidney cortical and medullary tissue are present in a pattern which suggests that dynamic MR of the kidney may be used to investigate these tissues separately. In our approach to dynamic MR of the kidney a slice is chosen that cuts through the kidney and the contrast agent Gd-DTPA is injected intravenously. We use a short scan time of one image every two seconds combined with recording over a longer period, and expect that the fast arrival at and distribution of the contrast agent over the cortex as well as the slower uptake in and excretion by the medulla can be visualised and quantified. The graphical displays of the concentration of contrast agent in cortex and medulla as a function of time are called renograms.

Potential advantages of MR renograms over scintigraphy are the higher spatial resolution of MR and the availability of cross section images instead of the

Determination of ROI location, size and shape.

---

projection images obtained via scintigraphy. In particular the combination of these allows for the separate observation of the cortex and medulla.

In this chapter the problem of selection of cortical and medullary ROIs in dynamic kidney scans will be discussed. The two main problems that have to be dealt with concern the partial volume effect, which often makes the selection of pure medullary tissue impossible, and the segmentation of the kidney despite the high noise levels in dynamic MRI.

Performance aspects of the proposed technique will be tested on dynamic MR scans obtained from a series of kidney transplant patients. Transplanted kidneys do not move appreciably with breathing and for the analysis of dynamic scans, ROI copying is feasible without a movement correction. Native kidneys do move with breathing, and necessitate a method for movement correction.

## **2.2 Partial volume effect**

MRI makes images of a three dimensional volume, with as smallest unit the volume element (voxel). The pixels that can be viewed in images generated by an MRI scanner are two dimensional representations of these three dimensional voxels. The size of the voxels is determined by the operator of the MRI scanner. Its horizontal and vertical dimensions are equal to the size of the pixels. The pixel size is determined by the area of the field of view (for kidney images typically somewhere around 40x40 cm) and the image matrix size (typically 256x256). Voxel thickness is determined by the slice thickness setting (in our experiments typically 6 mm). The signal to noise ratio of the voxel signal approximately increases linearly with the volume when all other parameters remain the same.

A problem with large voxels is that the volume they enclose can contain more than one tissue type, and the larger they become the larger the chance that this happens. This problem is called the partial volume effect. The different tissue types have curved borders and occupy limited volumes. For a given tissue type, its sensitivity for partial volume effects depends on these geometrical effects so the extent of partial volume effect depends on the dimensions of the voxel relative to those of the volume of the tissue of interest. In our dynamic scans, with a time resolution of 2 seconds, a slice thickness of 6 mm was considered to be minimally needed to obtain a decent image quality. Combined with the other two dimensions (1.6x1.6 mm) this results in a fairly tall voxel (figure 1.2).

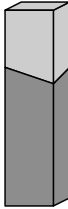


Figure 2.1: Schematic representation of a voxel with partial volume effect. The top of the voxel equals the pixel size. The height represents the slice thickness. The pixel intensity is a weighted average of the intensities of both tissues.

### 2.3 Materials

Nine patients with renal transplants were scanned twice (for other research purposes as well). The second examination was performed between 1 and 2 weeks after the first. For this study we consider these 18 series as independent examinations. The patients had no clinical signs of dysfunction of the transplanted kidney (for instance their creatinine clearances ranged between 25 and 91 ml/min, avg 61 ml/min). Approval was obtained from the medical ethical commission of the hospital and informed consent was obtained from all patients.

MR examinations were made with a Philips ACS-NT MR scanner (1.5T) (Philips Medical Systems, Best, The Netherlands) and included a dynamic scan. The selection of the slice location was based on a T1 weighted multislice scan angled through the longitudinal axis of the kidney. Of this oblique scan, the slice that showed the largest surface of renal tissue was chosen. For the dynamic scan we used T1-FFE for a strongly T1 weighted spoiled GE sequence (TR/TE/flip = 11 ms/3.4 ms/60°) with 400 mm field of view and a slice thickness of 6 mm. The resolution is 256 x 256 pixels, resulting in pixels of 1.56 x 1.56 mm<sup>2</sup>. We obtained 256 images of a single coronal slice through the implanted kidney, with a frequency of 1 image per 2 seconds.

The contrast agent, Gd-DTPA dimeglumine (Schering), was injected (dose 0.05 mmol/kg) in the ante-cubital vein as a rapid bolus (5 ml/sec) using a MR compatible injector pump (Medrad Spectris, Medrad, Maastricht, the Netherlands) during imaging, at the start of scan 6. We verified that 256 images sufficed to record the major signal changes related to the passage of the agent through cortex and medulla.

All examinations were stored on magneto-optical disks and transported to a Sun Sparc 20 which was used to analyse the data using an EasyScil software platform (Philips Medical Systems, The Netherlands).

Determination of ROI location, size and shape.

---

## 2.4 Partial volume correction algorithm

Examination of the kidney shows that the outer layer of the kidney contains only cortical tissue. It also shows that increasing the slice thickness does not lead to the inclusion of other tissues in the voxels at the boundary of the cross-section if this cut is located at the broadest part of the kidney. Only when the slice thickness increases so much that the voxels leave the kidney, partial volume effect will occur. However, the tissues that will then be included do not show up in the MR scans.

For the medulla it is not possible to guarantee that selected voxels contain only medulla. Since in MR scans small levels of partial volume effect (<30%) are not visible, it is safe to assume that the medullary ROI will always contain cortical tissue and the medullary renogram obtained in this way therefore always will contain a cortical component. It will be shown in the next paragraph that it is possible to make a correction for the cortical component of the medullary renogram. The positioning of the ROI is therefore less problematic.

Since the partial volume effect is always present a method is needed to determine its magnitude and is able to remove it. It appears that the problem can be solved by taking advantage of the way the contrast agent passes through the kidney.

The cortex, which is responsible for distributing the blood over the kidney receives a bolus of the contrast agent and within 2 to 3 images (4-6 seconds) after arrival of the contrast agent at the kidney the concentration in the cortex reaches its maximum. The contrast agent reaches the medulla via a filtration process, which is slow. Thus, when the contrast agent concentration in the cortex reaches its peak value, no contrast agent has yet entered the medulla. Any early enhancement of the pixels in a medullary region therefore will be due to the enhancement of cortical tissue that is present in the corresponding voxels.

We assume that the cortical tissue in the medullary ROI will produce the same enhancement as the cortical tissue in the cortical ROI. Since the cortical tissue only occupies a fraction of the total volume determined by the medullary ROI, the early enhancement per pixel of the medullary ROI therefore will be equal to this cortical fraction multiplied by the enhancement per pixel observed over the cortical ROI. By subtracting from the medullary renogram the cortical renogram weighted by the cortical fraction a 'pure' medullary renogram can be determined. We have developed an algorithm that determines the cortical fraction and we have shown that the subtraction procedure produces 'pure' medullary renograms [1].

The method depends on the availability of a region of interest that contains only cortical tissue. Since as discussed earlier the periphery of the kidney contains no medullary tissue the ROI should be drawn there.

As we have argued, a correction for partial volume effect is always needed. This makes it easier to define a medullary ROI; no careful selection of medullary regions is needed any more, since the contribution of included cortical tissue to the enhancement can now be corrected. The problem of automatically placing a ROI is now reduced to locating an area in the kidney that contains as much medullary tissue as possible (it can be shown that an increase in cortical fraction increases the noise in the pure medullary signal). The shape of the ROI appears to be not that important anymore. In the next sections we will show how the circumference of the kidney can be determined. This outline will then be used to construct different ROIs within the kidney.

## 2.5 Onion ring ROIs

Although segmentation of the kidney in a single image is not possible due to the low signal to noise ratio of the images, segmentation can be achieved using several images from a dynamic series. To do this the kidneys should not move. Because we are studying transplanted kidneys this is indeed the case.

Since the contrast agent is injected at the start of scan 11 the first 10 images are guaranteed not to contain any contrast agent. By averaging these first 10 images a background image is created. The signal to noise ratio of this image is improved over that of a single image because of the averaging. The next 30 images are also averaged. Since in most of these 30 images the contrast agent is present in the kidney the resulting image will show an enhanced kidney. Subtraction of both average images results in an image that shows the kidney and no other tissues. Thresholding now suffices to segment the kidney resulting in a binary image (1's where there is kidney, 0's for the rest of the image). To close possible gaps in the kidney contour a hull function is used.

Now we have to determine the shape and location of the ROIs within the kidney cross-section so that one region contains cortical and the other medullary tissue. In the binary image it is easy to create rings with boundaries that are parallel to the circumference of the kidney using an erosion filter. Erosion with one-pixel results in a binary image of the kidney with a one-pixel wide layer on the outside removed. It is of course also possible to obtain images that have had more pixels eroded. Subtraction of the original and an eroded image leaves a ring that follows the contour of the kidney and that has a thickness equal to the number of pixels



Determination of ROI location, size and shape.

---

eroded. Since the resulting ROIs are layered and follow the outside contour, we call them onion rings.

This ring shape is easily and reproducibly obtainable so we decided to use it for the ROIs. The question has still to be answered where the ROIs should be located within the kidney and what the 'thickness' of the ROIs should be.

Thicker rings have a better signal to noise ratio. The cortical ROI should be thin enough to contain only cortex. The inner ring should preferably contain as much medulla as possible.

To determine an optimal ring thickness 15 onion rings of one pixel thickness were created. The rings are numbered from 1 to 15, with 1 the outermost ring and 15 the innermost ring. Before the rings are determined a line was drawn manually to exclude areas which were clearly visibly polluted with veins or other tissue. This line also served to exclude the hilum from the measurements. In order to determine locations where medullary tissue is present, the intensity curves generated from the various rings were determined and correlated. Since the outer rings only contain cortical tissue it is expected that rings in the medullary area will produce intensity curves with a different shape that therefore have a low correlation with the cortical curves. In the next section the correlation results are presented.

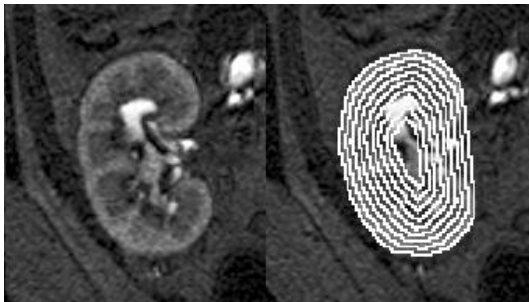


Figure 2.2: MR image of a kidney and the same image with the odd numbered onion rings displayed in it.

## 2.6 Results

The signal for each ring is calculated. Figure 2.2 shows some example curves of different rings in the same kidney. It can clearly be seen that some curves resemble each other and some are different.

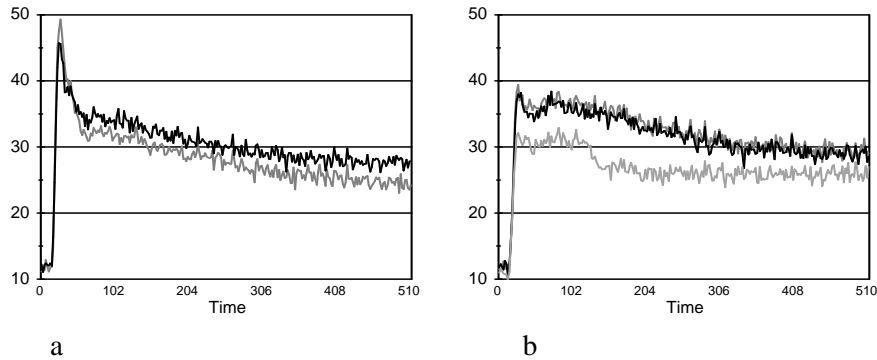


Figure 2.3: Curves of ring 2 and 3 (a) and ring 6, 7 and 10 (b) from the same kidney.

For each signal the correlation with the other signals of the same kidney is calculated. Highly correlated rings can be grouped together to form a larger ROI. Since these groupings depend on the specific kidney shape we want a general indication of which rings can be combined. For each combination of rings the averages over all kidneys are displayed in table 2.1.

Table 2.1: Averages of the correlations between the rings. Correlations over 0.9 are shaded grey.

	2	3	4	5	6	7	8	9	10	11	12	13	14	15
1	0.92	0.91	0.88	0.83	0.79	0.76	0.74	0.73	0.70	0.66	0.60	0.57	0.57	0.57
2		0.97	0.92	0.85	0.80	0.76	0.74	0.72	0.69	0.65	0.58	0.56	0.56	0.56
3			0.96	0.91	0.86	0.82	0.80	0.78	0.75	0.71	0.64	0.61	0.60	0.59
4				0.96	0.93	0.90	0.87	0.85	0.82	0.77	0.69	0.65	0.63	0.60
5					0.97	0.95	0.93	0.90	0.87	0.80	0.72	0.67	0.63	0.60
6						0.97	0.95	0.93	0.89	0.82	0.74	0.67	0.62	0.59
7							0.97	0.94	0.89	0.82	0.74	0.66	0.60	0.58
8								0.95	0.90	0.81	0.74	0.67	0.61	0.59
9									0.90	0.80	0.74	0.67	0.61	0.60
10										0.91	0.84	0.77	0.71	0.63
11											0.89	0.82	0.75	0.64
12												0.89	0.80	0.67
13													0.85	0.70
14														0.80

These averages give an indication of which rings can be combined. Important is that the rings which will be grouped together should have a high correlation in all kidneys. By determining the minimum correlation values over all patients for each ring, it is possible to find the worst cases and to combine only those rings that have a consistent high correlation in every kidney.

Determination of ROI location, size and shape.

Table 2.2: Minimum correlations between the rings. Correlations over 0.8 are coloured grey.

	2	3	4	5	6	7	8	9	10	11	12	13	14	15
1	0.80	0.78	0.78	0.68	0.60	0.55	0.49	0.46	0.38	0.05	-0.05	-0.03	-0.09	-0.08
2		0.92	0.81	0.69	0.59	0.51	0.45	0.41	0.38	0.06	-0.05	-0.04	-0.27	-0.21
3			0.91	0.79	0.70	0.62	0.56	0.52	0.46	0.13	0.02	0.04	-0.15	-0.10
4				0.93	0.86	0.82	0.78	0.72	0.53	0.21	0.09	0.10	-0.08	-0.04
5					0.94	0.90	0.88	0.82	0.56	0.22	0.11	0.10	-0.04	-0.01
6						0.95	0.92	0.86	0.60	0.27	0.14	0.15	-0.04	-0.00
7							0.94	0.90	0.53	0.20	0.08	0.09	-0.03	0.01
8								0.88	0.46	0.16	0.04	0.08	0.14	0.17
9									0.42	0.06	-0.02	-0.05	-0.01	0.11
10										0.70	0.61	0.18	-0.03	0.01
11											0.61	0.12	-0.13	-0.06
12												0.71	0.50	0.06
13													0.64	0.14
14														0.21

A graphical representation of these numbers is given in figure 2.4 and figure 2.5 which show the correlations of the signals of each ring compared to the signals of their more distal neighbours. The results of each correlation with the 1st inward ring, the 2nd inward ring, etc are shown.

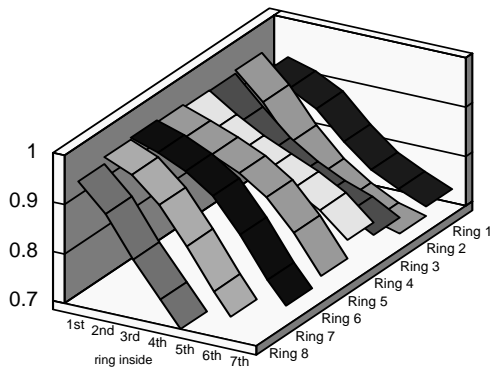


Figure 2.4: Average correlation between the signal of a ring and the signals of all rings located more distally.

As can be concluded from table 2.1 and figure 2.4, ring 1 does not correlate highly with any of the other rings. Ring 2 and 3 only have a high correlation with the rings directly adjacent to them. Ring 6 has a high correlation with ring 7, 8 and 9 (1st, 2nd and 3rd). This suggests that ring 2 and 3 have a similar dynamic behavior as have rings 6, 7, 8 and 9. It can be inferred from the figure 2.5 that the signals of rings 2 and 3 hardly correlate with the signals of rings 6,7,8 and 9.

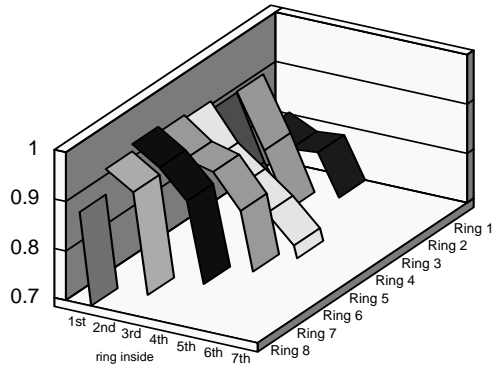


Figure 2.5: Minimum correlation between the rings and all those located more inward.

Table 2.2 and figure 2.5 show the minimum observed values for the correlations. Although the values are lower and the drop is sharper, the same pattern can be observed as in table 2.2 and figure 2.5.

Based on these correlations two ROIs can be defined. A cortical ROI, consisting of ring numbers 2 and 3 and a medullary ROI containing a mix of cortical and medullary tissue consisting of ring numbers 6,7,8 and 9. These are shown in figure 2.6.



Figure 2.6: The inner and outer ROI, based on the onion ring 2&3 for the outer and 6-9 for the inner ROI.

## 2.7 Conclusions and Discussion

The kidney is difficult to segment on a frame to frame basis. Placing ROIs on the cortex and medulla is therefore difficult, especially when ROIs are needed that cover only cortical tissue or only medullary tissue. In fact we observed that ROIs containing only medullary tissue are almost impossible to obtain. Such regions are

Determination of ROI location, size and shape.

---

however needed to obtain time-enhancement curves representing only cortical or medullary tissue. We could show that a ROI covering pure cortical tissue and a ROI covering both cortical and medullary tissue are sufficient for determining both a pure cortical and medullary renogram. Because of the physiology a time-enhancement curve of a medullary ROI always starts with a pure cortical component when cortical tissue is included. The cortical fraction can be determined from the intensity of this component.

We have shown that onion ring like regions can be used for determining locations for placing ROIs. The advantage of onion ring style segmentation is that the segmentation is relatively simple and fairly robust in a dynamic scan series. The disadvantage that this procedure does not result in a ROI that contains only medullary tissue is not a problem since the partial volume effect has to be corrected anyway.

Since a pure medullary renogram is obtained by subtracting the cortical renogram weighted by the cortical fraction from the time-enhancement curve obtained from the mixed ROI, the signal to noise ratio decreases with increasing cortical fraction. Therefore the medullary ROI probably has to be adapted in such a way that the cortical fraction is as small as possible. We hypothesize that regions in the medullary area with a relatively high cortical fraction can be identified on a pixel by pixel basis by correlating the time-activity curve of each pixel with the cortical renogram. Again a high correlation implies a relatively high cortical fraction. We will investigate this hypothesis in chapter 4.

## 2.8 References

- 1 J. A. de Priester, J. A. den Boer, E. L.W. Giele, M. H.L. Christiaans, A. Kessels, A. Hasman, J. M.A. van Engelshoven. MR Renography: An Algorithm for Calculation and Correction of Cortical Volume Averaging in Medullary Renographs. JMRI 2000;12:453–459.

## Chapter 3

---

# Evaluation of two cortical fraction estimation algorithms for the calculation of dynamic magnetic resonance renograms.

---

*E.L.W. Giele MSc, J.A. de Priester MD, J.A. Blom PhD, J.A. den Boer PhD, J.M.A. van Engelshoven PhD, A. Hasman PhD*

COMPUTER METHODS AND PROGRAMS IN BIOMEDICINE; 67/3:169-176(2002)

### 3.1 Abstract

With the high resolution of dynamic MRI scans it is possible to measure cortical renograms directly, but due to partial volume effects this is impossible for medullary renograms. With weighted subtraction of the cortical renogram from a mixed renogram it becomes possible to extract the medullary renogram.

For this subtraction the fraction of cortical tissue, present in the region of interest in which the mixed renogram is determined, has to be calculated. We have evaluated two algorithms for calculation of the cortical fraction. Both algorithms use the fact that during an interval after the start of the cortical enhancement no medullary enhancement occurs. One algorithm calculates the ratio between the slopes of both enhancement curves. The other is based on minimising the medullary signal values using a least squares error method. Using a computer model of the renograms and measurements on real patients we analysed the accuracy of both methods and determined the best parameters for each.

### 3.2 Introduction

Dynamic Magnetic Resonance Imaging (MRI) has been in use for some time to retrieve functional information of organs in the human body. In the case of the

kidney, dynamic MR imaging is attractive because of its high temporal and spatial resolution, providing the possibility to separate the functional behaviour of cortex and medulla. This is a feature that is not available with scintigraphic techniques.

Thus far, most of the literature has focussed on cortical MR Renography (MRR). The (patho)physiologic information contained in medullary MRR's, however, could be valuable in providing information about diseases primarily affecting the medulla (ie. toxic nephropathy) or affecting the medulla in the early stage (ie, urinary tract obstruction, tubulointerstitial diseases)[1-3].

In dynamic MRI of the kidney [4-16], use is made of the contrast agent Gd-DTPA. The uptake in and passage through the kidney of this agent is monitored. Separate monitoring of cortex and medulla is done by placing regions of interest (ROI) over both tissues, and measuring the average signal intensity under these ROIs for each sequential image.

In various studies using this technique, the ROIs were defined manually and aimed at the direct selection of cortex and medulla [4-9,11-14,16]. The complex shaped medullary pyramids border the cortical radial structures. In cases where the border between the cortical and medullary structure is parallel to and in the scan plane, the presence of cortical tissue may not be detected and cortical tissue will be erroneously included in the ROI selected for the measurement of the medullary signal which then becomes a mixed signal. Another disadvantage of manual selection of the medulla is that the quality of the selection depends on the cortico-medullary contrast during the early phase of enhancement, which in diseased kidneys is often weak. The cortical signal, however, can be measured unambiguously when a ROI is chosen along the periphery of the kidney.

Since the initial period of the mixed signal contains only cortical signal, this period can be used to estimate the cortical fraction in the mixed signal. The medullary signal can be obtained from the mixed signal by weighted subtraction of the cortical signal from the mixed signal [17,18].

We developed an automatic algorithm to determine the correct weighting factor and used it in a series of subjects to prove the feasibility of the method. This was primarily done for monitoring the function of transplanted kidneys. Transplanted kidneys do not move thus no movement corrections are needed.

In this contribution we evaluate, via simulation, the accuracy with which the cortical fraction can be determined. We compare two alternatives for determining the cortical fraction. The accuracy of the cortical fraction determination depends on the number of data points that are taken into account in the calculation. The

number of data points is limited because only the initial period of the mixed signal, where the signal is only due to the cortical contribution, is considered. Since the start of the medullary signal cannot be directly determined from the signals, this could result in a bias in the calculated fraction. In this contribution we study what bias results when data points are taken into account that contain a medullary component. The situation is simulated and the results are compared with patient studies.

In the next section the material and methods are described. Then the results are presented and discussed.

### **3.3 Materials, subjects and scan method**

Data was obtained from MRI scans on volunteers and nine patients with renal transplants. The latter were scanned twice; the second examination was performed between 1 and 2 weeks after the first. For this study we consider these 18 series as independent examinations. The patients had no clinical signs of dysfunction of the transplanted kidney (for instance their creatinine clearances ranged between 25 and 91 ml/min, avg 61 ml/min). Approval was obtained from the medical ethical commission of the hospital and informed consent was obtained from all patients.

Data was also generated by a computer simulation. The data of two patients with different cortical curves was used as input for a computer model of the dynamic behaviour of the kidney[19]. This model generated the average signal intensities of the cortex and medulla. By weighted addition of these signals and the addition of noise ROI signals were generated.

MR examinations were made with a Philips ACS-NT MR scanner (1.5T, gradient strength 10mT/m, slew rate 15T/m/sec) (Philips Medical Systems, Best, The Netherlands) and included a dynamic scan. The selection of the slice location was based on a T1 weighted multislice scan angled through the longitudinal axis of the kidney. Of this oblique scan, the slice that showed the largest surface of renal tissue was chosen. For the dynamic scan we used T1-FFE for a strongly T1 weighted spoiled GE sequence (TR/TE/flip = 11 ms/3.4 ms/60°) with 400 mm field of view and a slice thickness of 5 mm. The resolution is 256 x 256 pixels, resulting in pixels of 1.56 x 1.56 mm<sup>2</sup>. We obtained 256 images of a single coronal slice through the implanted kidney, with a frequency of 1 image per 2 seconds. A contrast agent, Gd-DTPA dimeglumine (Schering), was injected (dose 0.05 mmol/kg) in the ante-cubital vein as a rapid bolus (5 ml/sec) using a MR compatible injector pump (Medrad Spectris, Medrad, Maastricht, the Netherlands) during imaging, at the start of scan 11. We verified that 256 images suffice to



record the major signal changes related to the passage of the agent through cortex and medulla.

All examinations were stored on magneto-optical disks and transported to a Sun Sparc 20 which was used to analyse the data using an EasyScil software platform (Philips Medical Systems, The Netherlands).

### 3.3.1 Analysis

Based on the assumption that the outer layer of the kidney only contains cortical tissue, a cortical ROI is drawn in the strongly enhanced images and copied to all remaining images of the series. This is possible because transplanted kidneys do not show movement [17]. A second ROI is drawn concentric to the cortical ROI. It is of smaller size and located more centrally in the kidney. This inner ROI contains both medullary and cortical tissue. Both ROIs are semi-automatically derived from the outer contour of the kidney (figure 3.1)(for details see [17]). To maximize signal to noise, both ROI areas should be large. In addition the second ROI should contain as little cortical tissue as possible [17].

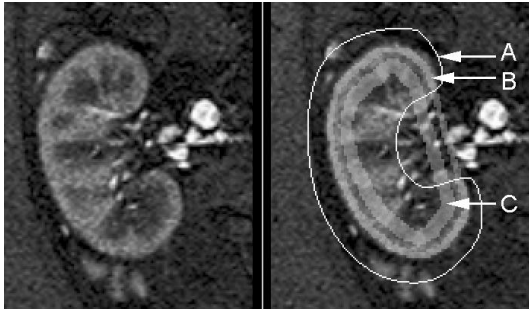


Figure 3.1: Kidney image and image with outer ROI(B) and inner ROI(C). The program measures the signal of the inner and outer ROI within the closed line(A) thus excluding the calix

The arrival and uptake of the contrast agent in the kidney is visible in the signals from both ROIs; a cortical signal  $s_c(t)$  measured in the outer ROI and a mixed signal  $s_i(t)$ , measured in the inner ROI. These signals are measured by calculating the average pixel intensities as a function of time. The pixel intensities are scaled by the software and range from 0 to 255. This scaling remains constant for all the images in a dynamic scan but can differ between different scans. The medullary signal  $s_m(t)$  can be determined from the mixed signal and the cortical signal via

$$s_m(t) = \frac{s_i(t) - f_c \cdot s_c(t)}{1 - f_c} \quad (3.1)$$

where  $f_c$  is the cortical fraction. The concentration of the contrast agent was so low that the magnitude of the signal is proportional to the concentration of the contrast agent.

In figure 3.2-a both the cortical and the mixed signal are displayed. These signals are generated with a computer model with a known  $f_c$ , using the cortical and medullary signals as explained above and by adding artificial gaussian noise. Figure 3.2-b shows the mixed signal again, together with the original medullary signal (as used in the simulation) and the medullary signal as calculated from the mixed and cortical signal.

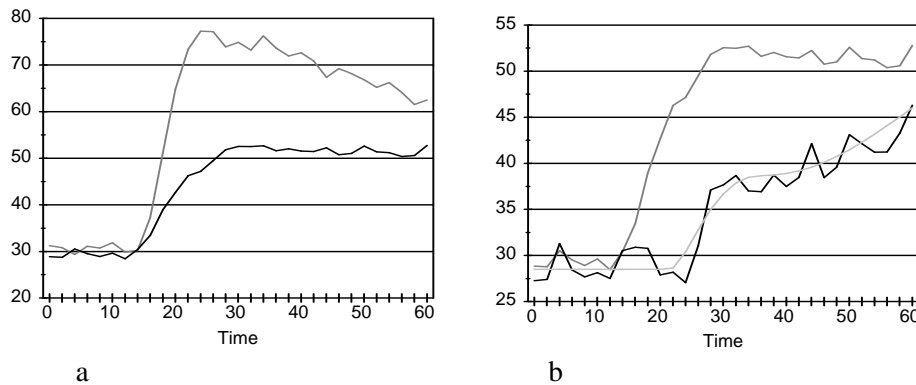


Figure 3.2: a: Simulated cortical signal (grey) and mixed signal (black). b: The mixed signal (dark grey), the medullary signal used as input for the calculation of the mixed signal (light grey) and the medullary signal (black) as calculated by our algorithm.

### 3.3.2 Estimation of the cortical fraction

Because the microvascular system of the medulla is connected in series with that of the cortex, the contrast agent arrives later in the medulla than in the cortex. As a consequence, the initial rise of the signal of the mixed (inner) ROI, before medullary enhancement, must be due to the cortical tissue in the inner ROI [18]. At the image rate of our dynamic series (one image per 2 seconds) this initial period is long enough to cover several images.

We considered two approaches that use this period to calculate the cortical fraction. In both approaches the signal level before contrast arrival is assumed to be constant. Arrival of the contrast agent in the cortical tissue is assumed to occur at the time just before enhancement. Both approaches require the selection of an estimation interval starting after arrival at the cortex and ending before arrival of the contrast agent at the medulla and both use the intensities of the cortical and

mixed signals. The noise in the dynamic MRI signal will give rise to a random error in the calculated cortical fraction; a systematic error will occur when the estimation interval includes data points that in fact contain medullary enhancement.

#### *Linear approach*

The easiest method to compute the cortical fraction is by using a linear fit on the signal during the initial period of contrast arrival. Straight lines are fitted through both the upslopes of the cortical and the mixed signal and the ratio of the slopes of both lines is assumed equal to the relative amount of cortical tissue in the mixed ROI, the cortical fraction. The non-linearity of the signal slope limits the accuracy of the linear fit. In many cases the cortical signal intensity started to decrease during the latest part of the initial period. Using data points during the decrease lowers the slope of the linear fit and invalidates the calculation.

#### *Least squares error approach*

Instead of direct calculation, this is an iterative method based on the least squares error. An arbitrary value for  $f_c$  is chosen and based on this value the medullary signal is calculated from the mixed signal. If  $f_c$  is chosen correctly, the calculated medullary signal will remain at its background level (average signal intensity before contrast injection, this is also calculated from the mixed and cortical signal) in the estimation interval since there is no medullary enhancement. The squared differences between background level and the calculated signal are summed and the optimal value for  $f_c$  is determined by iteratively varying  $f_c$  until the least squares error (LSE) is minimized. Due to signal noise the LSE will never reach zero. The advantage of this method is that all data points until the start of medullary enhancement can be used.

#### *3.3.3 Determination of the accuracy of the cortical fraction calculations*

The accuracy of the cortical fraction is determined with help of artificially generated data. As discussed earlier the data is obtained with a model. The noise used to simulate MR scanner noise is Gaussian white noise. Figure 3.3 shows examples of real data and artificial data. The examples illustrate their similarity and thus suggest the validity of this way of data simulation. The artificial datasets simulate real ROI signals from dynamic MR scans, and offer the added information of the true cortical fraction  $f_c$ . This knowledge allows an assessment of the accuracy of the determination of  $f_c$  from the distribution of the observed values of  $f_c$  using a sufficiently large number of artificial datasets.

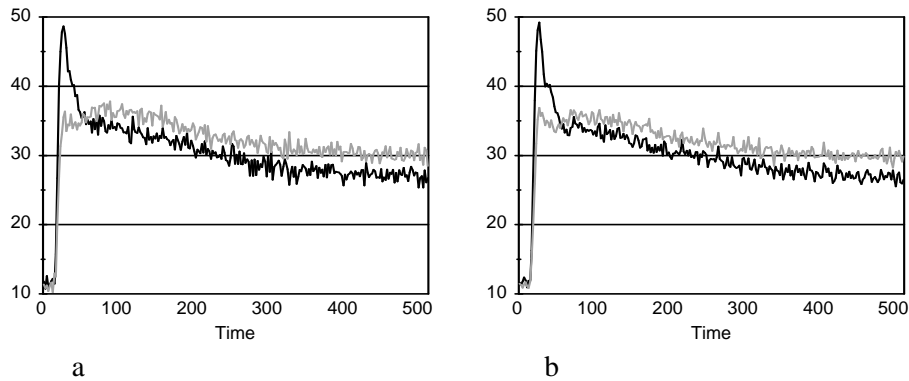


Figure 3.3: Cortical (black) and mixed cortico-medullary (grey) signal versus time obtained in a real dynamic scan (a) and by simulation (b). The vertical axis is in instrumental units, i.e. the scale in which the MR system presents the data.

#### 3.3.4 Choice of estimation interval

Determining  $f_c$  with the linear approach limits the estimation interval to the upward slope of the cortical signal. The LSE approach can use all data points that occur before the start of the enhancement of the medullary tissue. Since this start cannot be observed directly we determined how sensitive  $f_c$  is for the presence of a medullary contribution in the estimation interval. In the simulation we know of course when the medullary signal starts. Since the starting point of medullary enhancement is patient dependent, we studied the dependence of  $f_c$  on the estimation interval in the earlier mentioned MRI examinations.

By increasing the length of the estimation interval the LSE algorithm uses more samples, thereby reducing the influence of the signal noise and thus reducing the random error. If the estimation interval encloses the start of the medullary enhancement, this enhancement will be considered cortical enhancement and the resulting  $f_c$  will become higher, introducing a systematic error. This error will cause overcompensation of the mixed signal in the period before the start of the medullary enhancement, resulting in undershoot of the calculated medullary signal in that period, as shown in figure 3.4. Because of the noise in the signal the presence of a small undershoot cannot always be reliably detected.

We examined the influence of the number of samples in the estimation interval on the value of  $f_c$  in both simulated and measured patient data. By relating the total errors to the noise induced errors we tried to find the optimal number of samples.

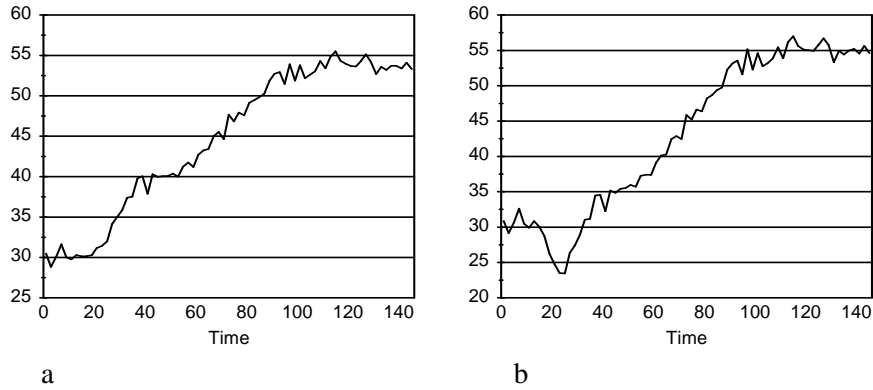


Figure 3.4: The calculated medullary signal with a correct value for  $f_c$  (a) and with an overestimated  $f_c$  (b).

### 3.4 Results

#### *Accuracy*

We constructed cortical and medullary signals by using the MRIs of two different patients. Artificial cortical and mixed signals were generated at five different data noise levels and three different cortical fractions. Each of those 30 combinations was simulated 500 times. The noise levels were chosen to resemble those present in the real data. This level varied between patients, possibly due to patient size and movement, and is influenced by slice thickness, pixel size and MR parameters.

In table 3.1 the standard deviation (SD) of  $f_c$  estimated from these data sets is presented as a function of the true value of  $f_c$  and the noise level. The used noise levels are expressed as the SD of the pixel value, given in instrumental units. The values of the cortical fractions that we used correspond roughly to the range of values that we encountered in our patient series. Both the linear and the LSE method for calculating the cortical fraction were applied to each signal. An estimation interval of four data points was used for both the linear approach and the LSE method. The observed mean values of  $f_c$  are not given; the first three decimals were equal to the true value of  $f_c$ .

Table 3.1a,b: The SD of  $f_c$  calculated from 500 artificial data sets for different values of  $f_c$  and data noise for two modelled patients (sampling period of four data points).

$f_c$	0.20			0.40			0.60		
Data noise	LSE	Linear	Lin/LSE	LSE	Linear	Lin/LSE	LSE	Linear	Lin/LSE
0.2	0.0055	0.0081	1.49	0.0063	0.0083	1.31	0.0070	0.0091	1.31
0.6	0.0176	0.0235	1.34	0.0193	0.0234	1.21	0.0217	0.0265	1.22
1.0	0.0283	0.0380	1.34	0.0268	0.0408	1.52	0.0302	0.0393	1.30
1.4	0.0297	0.0506	1.70	0.0345	0.0559	1.62	0.0425	0.0608	1.43
1.8	0.0400	0.0683	1.71	0.0426	0.0709	1.66	0.0437	0.0734	1.68

$f_c$	0.20			0.40			0.60		
Data noise	LSE	Linear	Lin/LSE	LSE	Linear	Lin/LSE	LSE	Linear	Lin/LSE
0.2	0.0064	0.0084	1.30	0.0079	0.0100	1.27	0.0069	0.0090	1.31
0.6	0.0186	0.0258	1.39	0.0202	0.0272	1.35	0.0237	0.0299	1.27
1.0	0.0301	0.0414	1.38	0.0331	0.0479	1.45	0.0335	0.0560	1.67
1.4	0.0363	0.0587	1.62	0.0348	0.0642	1.84	0.0405	0.0683	1.69
1.8	0.0451	0.0750	1.66	0.0522	0.0826	1.58	0.0654	0.0902	1.38

The results indicate that the SD of  $f_c$  increases roughly proportional to the data noise. They also indicate that the accuracy of determining  $f_c$  hardly depends on the actual value of  $f_c$ . Compared to the linear method, the estimation of  $f_c$  with the LSE method has a 1.46 (on average) times lower SD, and thus a higher accuracy for each individual determination of  $f_c$ . The SD is so small that medullary curves calculated with the real  $f_c$  minus the SD and  $f_c$  plus the SD do not differ enough to show a visible difference.

#### *Choice of estimation interval*

To determine the influence of the number of samples in the estimation interval on  $f_c$  we again simulated signals with an  $f_c$  of 0.2 and 0.4 and a noise level comparable to that in the patient data (in the tables represented as noise level 1).

Using the model of one patient, signals were calculated 20 times and the cortical fraction was determined for different estimation intervals, ranging in length from 3 to 10 data points. The medullary signal starts 4 samples after the start of the cortical signal. The estimated  $f_c$  values are plotted in the scatter graph in figure 3.5. Also shown is the average value of  $f_c$ .

Evaluation of two cortical fraction estimation algorithms for the calculation of dynamic magnetic resonance renograms.

---

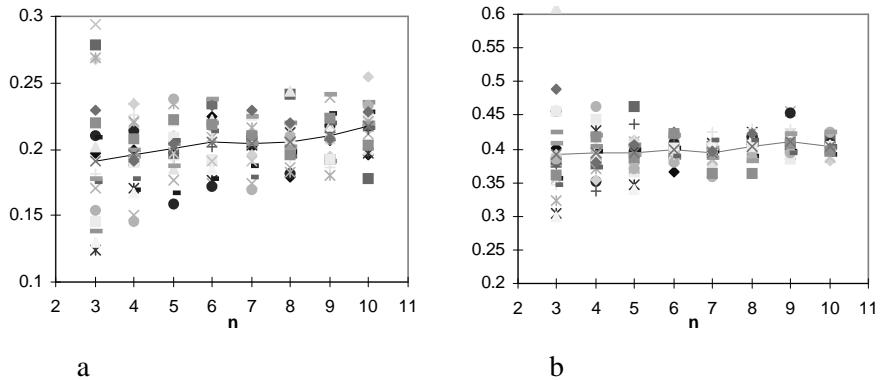


Figure 3.5: The cortical fractions calculated from the simulations. a) Signals generated with  $f_c=0.2$ ; b) signals generated with  $f_c=0.4$ . The averages are indicated with a line.

As can be seen in the simulated data set, there is a slight rising trend representing the systematic error caused by using too many samples. The random error caused by the noise is larger than the systematic error, especially for  $n < 6$ .

Also for each of the 18 dynamic MRI scans the cortical fractions for the various estimation intervals were calculated. Since the cortical fraction in this case is different for each patient the average  $f_c$  value determined from an estimation interval of 4 points was subtracted from each  $f_c$  value.

In figure 3.6 the scatter in the  $f_c$  values for a given length of the estimation interval is due to differences between patients.

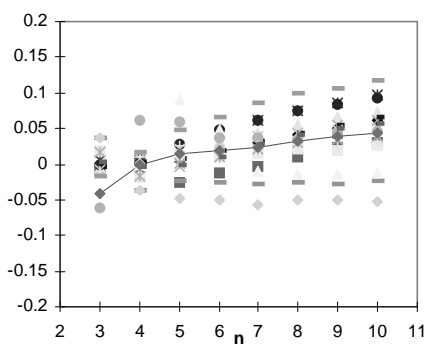


Figure 3.6: Normalized cortical fractions calculated from the patient data. The average is shown with a line.

### 3.5 Discussion and Conclusions.

Earlier [18] we introduced a method for determining the cortical and medullary signals from patients with transplanted kidneys using dynamic MRI studies. We demonstrated the feasibility of the method but we could not determine the accuracy of the method. To do that, simulation is needed so that the results of applying the method can be compared with the actual situation.

The value of the method that we introduced depends on the accuracy with which the cortical fraction can be determined. The cortical fraction in a ROI with cortical and medullary tissue can be determined by comparing the initial rise of the corresponding mixed signal with that of the signal determined from a cortical ROI. The estimation can be performed either by fitting the curves with a straight line or by the use of a LSE approach. The simulations show that the latter approach has a higher accuracy. Also the SD of  $f_c$  is relatively small. When the medullary curve as estimated by the method is compared with the actual medullary curve, it is apparent that the error in  $f_c$  does not lead to systematic errors in the estimated medullary curve.

In both simulated and real patient data the estimated cortical fraction slightly increases with the length of the estimation interval because the algorithm considers medullary signal to be cortical signal. To prevent this bias in the determination of  $f_c$  the choice of the number of samples to be included in the estimation interval has to be kept low. Using 6 or less of the first samples after cortical enhancement shows a smaller bias in  $f_c$  is than the random error in  $f_c$ . Using more than 6 samples does not reduce the random error any more, but it increases the bias. Thus, using the first 6 samples after cortical enhancement gives the most accurate estimate of the cortical fraction.

### 3.6 References

- 1 R Cronin, W Henrich. Toxic nephropathy. In: Brenner BM, editor. Brenner and Rector's the kidney. New York: WB Saunders; 1996. p 1597-1654.
- 2 R Rubin, R Cotran, N Tolkoff-Rubin. Urinary tract infection, pyelonephritis and reflux nephropathy. In: Brenner BM, editor. Brenner and Rector's the kidney. New York: WB Saunders; 1996. p 1597-1654.
- 3 R Semelka, K Corrigan, S Ascher, J Brown, R Colindres. Renal corticomedullary differentiation: observation in patients with differing serum creatinine levels. Radiology 1994; 190: 149-152.



Evaluation of two cortical fraction estimation algorithms for the calculation of dynamic magnetic resonance renograms.

---

- 4 R Kikinis, G von Schulthess, P Jäger, et al. Normal and Hydronephrotic Kidney: Evaluation of Renal Function with Contrast-enhanced MR Imaging. *Radiology* 1987; 165:837-842.
- 5 P Heintz, Ch Ehrenheim, H Hundeshagen. Gd-DTPA in MRI and 99m Tc-DTPA in the examination of the perfusion of transplanted kidneys. *Diagnostic Imaging International* 1988: November, Supplement.
- 6 P Choyke, J Frank, M Girton, et al. Dynamic Gd-DTPA-enhanced MR Imaging of the Kidney: Experimental Results. *Radiology* 1989; 170:713-720.
- 7 M Carvlin, P Arger, H Kundel, et al. Use of Gd-DTPA and Fast Gradient-Echo and Spin-Echo MR Imaging to Demonstrate Renal Function in the Rabbit. *Radiology* 1989; 170:705-711
- 8 R Semelka, H Hricak, E Tomei, A Floth, M Stoller. Obstructive Nephropathy: Evaluation with Dynamic Gd-DTPA-enhanced MR Imaging. *Radiology* 1990; 175:797-803.
- 9 H Munechika, D Sullivan, Hedlund, et al. Evaluation of Acute Renal Failure with Magnetic Resonance Imaging Using Gradient-Echo and Gd-DTPA. *Invest Radiol* 1991; 26:22-27
- 10 O Hélénon, E Attlam, C Legendre, et al. Gd-DOTA-enhanced MR Imaging and Color Doppler US of Renal Allograft Necrosis. *RadioGraphics* 1992; 12:21-33.
- 11 Th Vestring, K Dietl, A Fahrenkamp, et al. Die Rindennekrose der Transplantatniere. *Fortschr. Röntgenstr* 1992; 156,6: 507-512
- 12 P Ros, J Gauger, C Stoupis, et al. Diagnosis of Renal Artery Stenosis: Feasibility of Combining MR Angiography, MR Renography, and Gadopentetate-Based Measurements of Glomerular Filtration Rate. *AJR* 1995; 165:1447-1451.
- 13 R Sharma, R Gupta, H Poptani, et al. The Magnetic Resonance Renogram in Renal Transplant Evaluation using Dynamic Contrast Enhanced MR Imaging. *Transplantation* 1995; 59: 1405-1409
- 14 N Grenier, H Trillaud, C Combe, et al. Diagnosis of Renovascular Hypertension: Feasibility of Captopril-Sensitized Dynamic MR Imaging and Comparison with Captopril Scintigraphy. *AJR* 1996;166:835-843.

- 15 T Roberts, Physiology Measurements by Contrast-Enhanced MR Imaging: Expectations and Limitations. JMRI 1997; 7:82-90
- 16 D Szolar, K Preidler, Ebner, et al. Functional Magnetic Resonance Imaging of Human Renal Allografts during the Post-Transplant Period: Preliminary Observations. Magnetic Resonance Imaging 1997; 15:727-735
- 17 E Giele, J de Priester, J Blom, J den Boer, J van Engelshoven, A Hasman. Reduction of noise in medullary renograms from dynamic MR Images. Journal of Magnetic Resonance Imaging. JMRI 2000;11:149-155
- 18 J. A. de Priester, J. A. den Boer, E. L.W. Giele, M. H.L. Christiaans, A. Kessels, A. Hasman, J. M.A. van Engelshoven. MR Renography: An Algorithm for Calculation and Correction of Cortical Volume Averaging in Medullary Renographs. JMRI 2000;12:453-459.
- 19 DenBoer JA, DePriester JA, Geerlings MJHM, et al. Quantitative model description of dynamic MRI enhancement data of the kidney. JMRI, submitted.

Evaluation of two cortical fraction estimation algorithms for the calculation of dynamic magnetic resonance renograms.

---

## Chapter 4

---

# Reduction of noise in medullary renograms from dynamic MR Images

---

*E.L.W. Giele MSc, J.A. de Priester MD, J.A. Blom PhD, J.A. den Boer PhD, J.M.A. van Engelshoven PhD, A. Hasman PhD*

JOURNAL OF MAGNETIC RESONANCE IMAGING 11:149–155 (2000)

### 4.1 Abstract

Dynamic magnetic resonance images of the kidney can be used to acquire separate renograms of cortex and medulla. A high quality cortical renogram can be determined directly from a region of interest (ROI) placed in the cortex. Due to partial volume effects, part of the signal from a ROI placed in the medulla is caused by cortical tissue. By subtracting a fraction of the cortical signal from the cortico-medullary signal a more pure medullary renogram can be determined.

A side-effect of this subtraction is an increase in noise level. The noise level increases with larger partial volume fractions. Using a matched image filter it is possible to exclude those areas from the ROI that have a high partial volume content, thus reducing the amount of cortical signal that has to be separated from the medullary signal. Noise reductions of up to 50% have been achieved in the medullary renogram with an average reduction of 23%.

### 4.2 Introduction

A new diagnostic test to measure renal perfusion and renal function is Dynamic Magnetic Resonance Imaging (Dynamic MRI) of the kidney after bolus injection of a contrast agent [1-13]. Based on the high temporal and spatial resolution of MRI, this technique provides the opportunity to quantitatively follow intravenously injected MR contrast medium (Gd-DTPA) in both cortical and medullary renal

tissues and to separate these tissues functionally [1-6,8-13]. This method has the potential to establish diagnosis and prognosis of acute and chronic renal failure, particularly in renal transplants. Analysis of the cortical contrast uptake enables to differentiate acute cortical necrosis from rejection which is not reliable possible with nuclear or ultrasound scans [8] and analysis of medullary contrast uptake might facilitate the diagnosis of urinary tract obstruction and diseases primarily affecting the medulla.

However, in the individual images of the dynamic MRI scans cortical and medullary renal tissue are often hard to differentiate and computer based segmentation of these tissues has thus far not been possible. Manual definition of ROIs [1-6,8-11,13] is very time consuming and introduces user bias. In order to make semi-automatic segmentation possible, we developed an algorithm that is based on general assumptions about the location in the images of renal cortex and medulla. The outer 5 millimeter of a kidney includes cortical tissue only whereas the remaining more central located renal parenchyma includes both cortical and medullary tissue. Therefore signal intensities of a region of interest in the central located renal parenchyma after injection of an MR contrast medium provide a mixture of cortical and medullary signals. Our algorithm separates the cortical and medullary functional information. The feasibility of such a separation is based on the assumptions that there is a time delay in contrast agent appearance between cortex and medulla, and that the cortical and medullary signals are location independent. On the basis of these assumptions the cortical volume fraction in the cortico medullary ROI can be determined and its value can be used as the weight factor for weighted subtraction of the cortical signal from the cortico medullary signal.

A typical property of dynamic MRI scans is due to the short time per image: each pixel contains non-negligible noise. This results in noisy images and thus noisy signals from the ROIs. Due to the subtraction process, the medullary renogram which is retrieved from the cortico-medullary signal contains even more noise. This paper introduces a technique to maximize the signal-to-noise ratio in the computed medullary signal.

### **4.3 Materials**

The MR examinations were made with a Philips ACS-NT MR scanner (1.5T, gradient strength 10mT/m, slew rate 15T/m/sec)(Philips Medical Systems, Best, The Netherlands) and included a dynamic scan. For this dynamic scan we used T1-FFE, a strongly T1 weighted spoiled GE sequence (TR/TE/flip = 11ms/3.4ms/60) with a 400 mm field of view and a slice thickness of 5 mm. The resolution is 256 x

---

256 pixels, resulting in pixels of  $1.56 \times 1.56 \text{ mm}^2$ . We obtained 256 images of a coronal slice through the implanted kidney, with a frequency of 1 image per 2 seconds. The selection of the slice location was based on planscans (SE: TR/TE=182/10) and a multislice oblique scan (T1-weighted, SE: TR/TE=550/14) angled through the longitudinal axis of the kidney. Of this oblique scan, the slice that showed the largest surface of renal tissue was chosen. The contrast agent Gd-DTPA was injected (dose 0.05 mmol/kg) in the ante cubital vein as a rapid bolus (5 ml/sec) using an MR-injector pump (Medrad Spectris, Medrad, Maastricht, the Netherlands) during imaging, at the moment when scan 11 starts. We verified that 256 images suffice to record the major signal changes related to the passage of the agent through cortex and medulla.

Nine patients with renal transplants were scanned twice (for other research as well) using this protocol, the second examination between 1 and 2 weeks after the first. For this study we consider these as 18 separate examinations. The patients had no clinical signs of dysfunction of the transplanted kidney (creatinine clearances ranged between 25 and 91 ml/min, avg 61 ml/min). Approval was obtained from the medical ethical commission of the hospital and informed consent was obtained from all patients.

All examinations were stored on magneto-optical disks and transported to a Sun Sparc 20 which was used to analyse the data using EasyScil software (Philips Medical Systems, The Netherlands).

## 4.4 Methods

### 4.4.1 Determination of ROIs

The ROIs that were used to define cortical and cortico-medullary areas were the same over the entire dynamic series for each patient. Transplanted kidneys are located in the lower abdomen and per consequence no breathing related movement occurs. This was verified by visual inspection of each of the scans. The kidney is segmented from the surrounding tissue by subtracting the average of 10 images preceding contrast injection from the average of 30 images after injection.

Using an erosion filter, a 2 pixel ( $\approx 3 \text{ mm}$ ) wide onion-ring-like section is generated along the entire outer margin of the kidney; such a ROI is shown in figure 4.1. It has a clearance of one pixel from the kidney border. This section is called the outer ROI and is assumed to contain cortical tissue only. The second or inner ROI is also an onion-ring-like section. It is located more inwardly to include medullary tissue. It is 4 pixels ( $\approx 6 \text{ mm}$ ) removed from the inner edge of the outer ROI and is 4 pixels

thick. A manual procedure is used to exclude the calix and, if desired, the major veins.

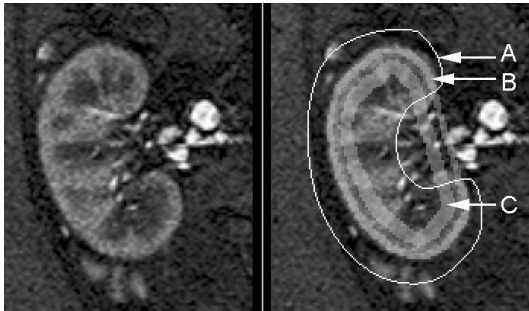


Figure 4.1: Kidney image and image with outer ROI(B) and inner ROI(C). The program measures the signal of the inner and outer ROI within the closed line(A) thus excluding the calix

#### 4.4.2 Determining the cortical fraction

By determining the average pixel intensity in the ROIs (the sum of the intensities of all pixels in the ROI divided by the number of pixels in that ROI) and repeating this for all 256 images, two time-dependent signals are generated. The signal of the outer ROI  $s_c(t)$  is called the cortical renogram; the signal of the inner ROI  $s_i(t)$  is a combination of the cortical and the as yet unknown medullary renogram.

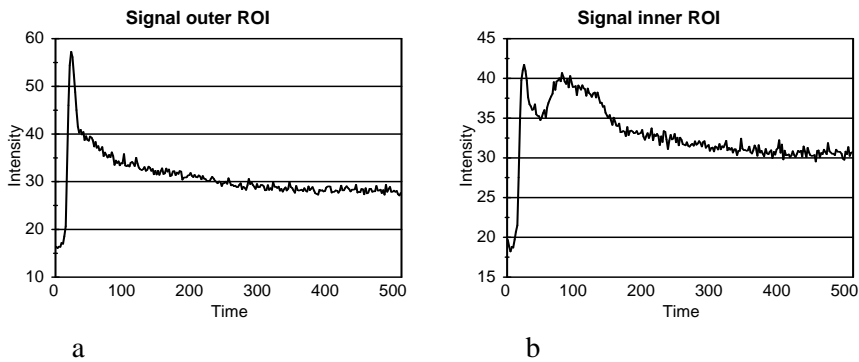


Figure 4.2: Cortical renogram (a) and inner ROI signal (b)

The volume fraction of cortical tissue in the inner ROI is called  $f_c$ . This is the mean of the cortical fractions  $f_{ci}$  of each voxel. There are hardly any voxels with  $f_{ci}=0$  because of in-slice as well as through-slice partial volume effects. The contribution of the voxels to the cortical fraction is inhomogeneously distributed over the entire inner ROI and, because of the low signal to noise ratio in each individual image, this contribution cannot be easily estimated.

---

The signal measured in the inner ROI  $s_i(t)$  is a mix of medullary signal  $s_m(t)$  and cortical signal  $s_c(t)$ , where both signals contribute to the measured signal according to their respective fractions, so

$$s_i(t) = f_c \cdot s_c(t) + (1 - f_c) \cdot s_m(t) \quad (4.1)$$

Here we have assumed that the signal of the cortical tissue in the inner ROI is identical to the cortical signal from the outer ROI. If the cortical fraction  $f_c$  were known, the medullary signal could be computed by subtracting the cortical signal multiplied by its cortical fraction  $f_c$  from the mixed signal and scaling. From formula 1 it follows that:

$$s_m(t) = \frac{s_i(t) - f_c \cdot s_c(t)}{1 - f_c} \quad (4.2)$$

We determine  $f_c$  by using the inherent delay of about 10 seconds between the arrival times of the contrast agent in cortex and medulla. Due to the fact that there is such a delay, the composite signal contains no medullary signal during the first few images after contrast injection: the rise in  $s_i(t)$  during this period must be due to cortical contribution only. During the early rise, therefore, equation (4.1) can be rewritten as

$$s_i(t) = f_c \cdot s_c(t) \quad (4.1a)$$

and, given the measured signals  $s_i$  and  $s_c$ , we can solve the value of  $f_c$ .

Since the signals  $s_i$  and  $s_c$  are noisy, a least squares approach is indicated to obtain a reliable value for  $f_c$ . Also, we correct for a possible non-zero offset. Thus, the best estimate of  $f_c$  is taken to be that value that minimizes the difference between the signal  $s_m(t)$  from the first five images after contrast arrival (the time of contrast arrival is marked by the first point in the upslope) and the signal before contrast arrival (background level).



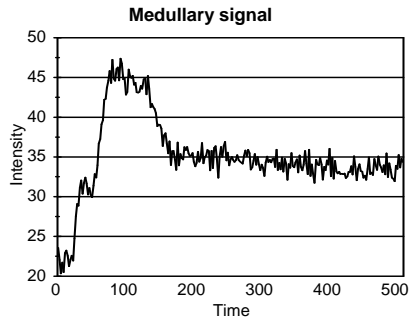


Figure 4.3: Calculated medullary renogram

#### 4.4.3 Method to decrease $f_c$

All methods to determine a reliable medullary renogram are hindered by the partial volume effect, which is quantified by  $f_c$ . Removing pixels from the inner ROI with high  $f_{ci}$  decreases  $f_c$ . This is attractive because it reduces the factor  $1/(1-f_c)$  by which the noise in the calculated medullary renogram is amplified. However, removing pixels from the ROI decreases the ROI size, and this in turn increases the noise level of the inner ROI signal: it is then averaged over fewer pixels, so the net result usually is an increase of noise in the calculated medullary renogram. It was our hypothesis that by selectively excluding the pixels with the highest cortical contribution from the inner ROI,  $f_c$  can be decreased while still keeping the inner ROI area large enough, resulting in a net gain in signal to noise.

To exclude pixels in the ROI that have the highest cortical contribution, a matched image filter is used to locate those pixels in the inner ROI of which the signal shows the strongest similarity to the cortical signal.

First, each image is convoluted with a gaussian filter, reducing image noise and slightly blurring every image before it is used in the matched filter operation (gauss filter parameters  $\sigma=1$ , filter width=3x3 pixels).

The pixel values at scantime  $t$  are denoted as a function  $p_{x,y}(t)$ , where  $x$  and  $y$  are the co-ordinates of the pixel. The matched image filter calculates the inproduct,  $P_{x,y}$ , for each pixel of its signal  $p_{x,y}(t)$  and the cortical signal  $s_c(t)$ . The inproduct is calculated over the first  $T$  samples, where we used  $T=100$ .

$$P_{x,y} = \frac{\sum_{t=1}^{t=T} s_c(t) p_{x,y}(t)}{\sqrt{\sum_{t=1}^{t=T} (s_c(t))^2 \sum_{t=1}^{t=T} (p_{x,y}(t))^2}} \quad (4.3)$$

The inproduct  $P_{x,y}$  by definition varies between -1 and +1. Since all pixels in our images have a positive value, the inproduct cannot be lower than 0. In the inner ROIs of all our data sets, the values  $P_{x,y}$  were always over 0.9. This was due to the high signal offset of both  $p_{x,y}(t)$  and  $s_c(t)$ .

The resulting "cortex similarity image"  $P$ , of which  $P_{x,y}$  are the pixels, is an image with high pixel values in all those points with a signal highly similar to the cortical signal.

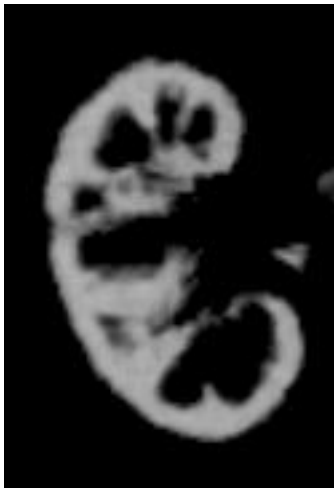


Figure 4.4: Cortex similarity image, the result of the matched image filter

By thresholding this image, a binary mask is created of all cortex-similar tissues, where the mask contains all pixels that have a value higher than the threshold. All the pixels in the mask are removed from the inner ROI, resulting in a masked inner ROI containing fewer pixels. The pixels that are eliminated are those which are most cortex-like, and thus the cortical fraction of the (masked) inner ROI decreases.

The threshold value determines how close the pixels in the mask resemble the cortical signal. A higher threshold value means a closer resemblance to the cortical

signal, causing a smaller mask, and thus a larger masked inner ROI with a higher cortical fraction.

#### 4.4.4 Noise estimation

To estimate the noise in the masked inner ROI signal, we used the tail of this signal (the last 150 samples, i.e. the last 300 seconds), where the signal shows a smooth decay of contrast agent concentration in the renal tissues. We defined the noise level  $\sigma_i$  of the signal as the standard deviation of the noise present in the tail. By fitting the tail signal with a suitable smooth function, the standard deviation of the residue provides a measure of the noise level. Since reliably fitting with an exponential was unsuccessful, we approximated the tail of the signal by five straight line segments, each 30 samples long. The noise level of the masked inner ROI signal is expressed as a fraction of the noise level in the unmasked inner ROI signal. The latter level is obtained using a threshold of 1.0, i.e. no masking. The noise level in the medullary signal was estimated for thresholds between 0.98 and 1.0, increasing the threshold in steps of 0.001. This range appeared to be large enough to include the noise level minima.

## 4.5 Results

In our 18 data sets the average area of the outer ROI was 402 pixels ( $\approx 980 \text{ mm}^2$ ) with a standard deviation of 34 pixels ( $\approx 85 \text{ mm}^2$ ). The inner ROI had an average area of 612 pixels ( $\approx 1500 \text{ mm}^2$ ) and a standard deviation of 62 pixels ( $\approx 150 \text{ mm}^2$ ).

Table 4.1 shows for one data set the area of the masked inner ROI and the relative noise level of the signal as a function of the thresholds. A relative noise level of 1 means that the noise level in the corresponding signal is equal to that of the signal of the original ROI. All other data sets show comparable results.

Also shown by table 4.1 is that the ROI size decreases with decreasing threshold while the noise in the inner ROI signal increases. In figure 4.5 the noise level is presented as function of ROI size. The noise level should, in theory, be inversely proportional to the square root of the area. This theoretical curve is shown as well. The difference between the two curves stems from spatial correlation between pixels.

Table 4.1: Threshold, resulting area of the inner masked ROI, relative noise level in the mixed signal, cortical fraction and relative noise in the medullary signal.

Threshold	Inner ROI area (pixels)	relative noise level of $s_i(t)$ ( $\sigma_{i,Th}/\sigma_{i,Th=1}$ )	Cortical fraction $f_c$	relative noise level of $s_m(t)$ ( $\sigma_{m,Th}/\sigma_{m,Th=1}$ )
1.000	614	1.000	0.585	1.000
0.999	614	1.000	0.585	1.000
0.998	614	1.000	0.585	1.000
0.997	605	1.003	0.579	0.985
0.996	561	1.026	0.545	0.930
0.995	519	1.058	0.509	0.890
0.994	472	1.090	0.471	0.852
0.993	434	1.148	0.441	0.852
0.992	413	1.168	0.424	0.845
0.991	383	1.203	0.402	0.845
0.990	365	1.235	0.392	0.858
0.989	346	1.259	0.379	0.860
0.988	328	1.289	0.373	0.883
0.987	310	1.304	0.363	0.881
0.986	292	1.356	0.353	0.908
0.985	274	1.418	0.338	0.929
0.984	255	1.472	0.322	0.945
0.983	244	1.509	0.309	0.953
0.982	231	1.543	0.304	0.969
0.981	220	1.582	0.294	0.984
0.980	200	1.649	0.284	1.019

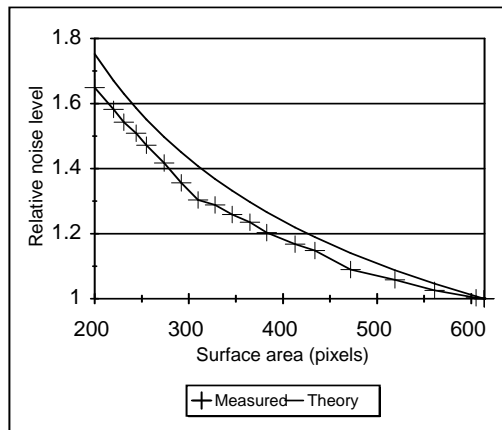


Figure 4.5: Noise level vs. ROI size of the masked inner ROI and the theoretical expectation for this curve according to equation (4.4)

The cortical fraction in the masked inner ROI is also shown in table 4.1, together with the relative noise in the calculated medullary signal (relative to the noise in the medullary signal without masking), both as function of the threshold.

Decrease of the threshold results in a reduction of  $f_c$ , and as a result the noise level in the calculated medullary signal initially decreases. After a further decrease of the threshold this trend is reversed, so that an optimal threshold is found for which the noise level of the reconstructed medullary signal is minimal. Figure 4.6 gives a graphical impression of this noise level as function of ROI size.

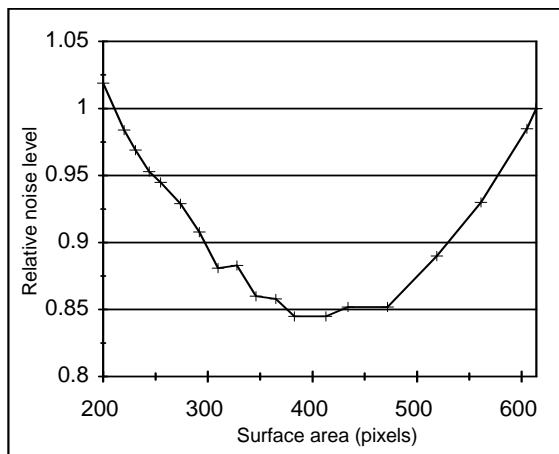


Figure 4.6: Noise level in the medullary renogram as a function of ROI size

The optimal threshold in this example is 0.992 and the resulting noise level of the medullary renogram is 85 % of what is obtained using the unmasked inner ROI as source of the medullary signal. Figure 4.7 shows the mask at the optimal threshold as an overlay on the similarity image for the data set used in table 4.1. One can see that the mask appears to remove preferentially those pixels that correspond to renal columns, i.e. extensions of the cortex located between the medullary areas.

All remaining data sets were treated in the same way to find the minimum noise level in  $s_m(t)$ ; the results are summarised in table 4.2.

Table 4.2 shows that a reduction of the noise level in the medullary signal could be reached in all dynamic scans. The average relative noise level at optimum threshold is 77% (SD 16%). The value of the optimal threshold and the achieved reduction in noise level at that threshold differs for each dynamic scan. No prediction could be made concerning the optimal threshold or the noise reduction that can be achieved for individual dynamic scans. The mean of the cortical fraction at optimal threshold is 0.3; this is a reduction by almost a factor 2 compared to the unmasked inner ROI.



Figure 4.7: The cortical similarity image with the entire inner ROI (a) and the cortical similarity image with the reduced inner ROI, thresholded at optimal value (b)

Table 4.2: Relative noise level at optimum threshold, optimal threshold value and the cortical fraction before and after masking at optimal threshold for each dynamic scan. (Note that, since slice location is slightly different between the first and second scan, the cortical fraction also changes between scans)

Dynamic scan (patient.session)	Relative noise level of $s_m(t)$ at optimal threshold	Optimal threshold	Cortical fraction without masking	Cortical fraction at optimal threshold
1.1	0.937	0.997	0.331	0.257
1.2	0.906	0.995	0.431	0.306
2.1	0.746	0.983	0.500	0.222
2.2	0.901	0.995	0.510	0.385
3.1	0.845	0.992	0.585	0.424
3.2	0.829	0.991	0.488	0.310
4.1	0.656	0.985	0.540	0.258
4.2	0.942	0.991	0.430	0.323
5.1	0.633	0.985	0.588	0.198
5.2	0.507	0.980	0.582	0.122
6.1	0.867	0.992	0.718	0.577
6.2	0.745	0.990	0.720	0.542
7.1	0.780	0.992	0.632	0.406
7.2	0.822	0.988	0.615	0.200
8.1	0.449	0.983	0.711	0.292
8.2	0.448	0.985	0.613	0.236
9.1	0.948	0.985	0.324	0.136
9.2	0.944	0.992	0.307	0.200
Average	0.772 (SD 0.16)		0.535	0.300

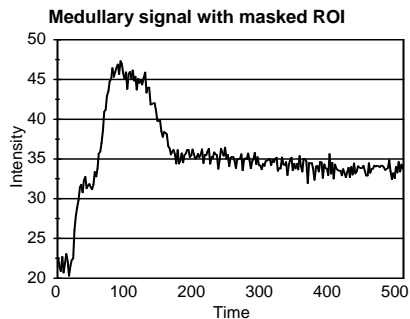


Figure 4.8: Medullary signal obtained after optimal masking. (Compare with figure 4.3)

In figure 4.8, the medullary renograms of the case shown in figure 4.4 with optimal masking is shown. Figure 4.3 shows the same renogram without masking. Apart from the difference in noise level, one can see no systematic changes: the two curves carry the same information.

## 4.6 Discussion

The noise per pixel in dynamic MR images of the kidney is relatively high. The usual means for improving signal to noise ratio (long repetition time and signal averaging) cannot be applied because of the required temporal resolution. Three seconds per image is already considered long (13), so we reduced this to 2 seconds per image, which was the best we could achieve without major loss of image quality.

The signal level is low because of the strong T1 weighting required to avoid signal saturation during bolus passage and the unfavorable anatomic location of the kidney (we used the main body coil as receive coil). Our method would not function if signal saturation at high concentrations of Gd-DTPA (1,3,8,12), would be present. To prevent saturation, we also used a low dose of contrast agent of 0.05 mmol/kg.

In the inner ROI, the fraction of cortical tissue is usually considerable: the ROI includes pixels that represent mostly or only cortical tissue. These pixels cannot be isolated based on visual clues only: the irregular three dimensional shape of the renal columns in combination with the large slice thickness creates, with high probability, areas of through-plane partial volume effect in medullary ROIs. Nor can these pixels be isolated on the basis of the contrast between cortex and medulla: the relatively high noise in the dynamic MR kidney image prevents this. To cope with the noise, a way out is to make use of the consistencies in the signal

---

during the dynamic scan. One way to do this is with a matched filter technique: elimination of pixels which are very cortex-like from the inner ROI reduces the noise in the obtained medullary renograms.

For the matched filter, use is made of “negative selection”: to increase the medullary contribution in the mixed signal, the filter identifies pixels with a high cortical contribution which are then removed from the inner ROI. Unlike the medulla, the location of at least part of the cortex is known: the periphery of the kidney. Assuming that the dynamic behaviour in this part of the cortex is also representative for the remaining cortex, the cortical signal can be obtained from a ROI at the periphery. Comparison of the global shape of filtered and unfiltered medullary renograms confirms that the peripheral cortical signal is a good representative of the cortical signal elsewhere in the kidney.

The gaussian spatial filter used to reduce image noise reduces the sharpness. The reduction in sharpness only slightly influences the shape of the mask that is used to remove pixels from the inner ROI and therefore can be tolerated. When no gauss filter is used, some pixels that are very noisy will be excluded from the mask even though they are cortical, and remain therefore in the inner ROI. Since our aim is to reduce noise, a method that retains very noisy pixels is counterproductive.

The similarity image generated by the matched image filtering looks like one of the images with cortical enhancement and no medullary enhancement, so one may wonder whether these images can be used directly instead of first calculating the similarity image. However the high amount of noise in the latter images prevents the use of a reliable thresholding technique: the number of frames that can be used is much smaller than the number of frames used in the calculation of the similarity image. Experiments have shown that even after smoothing, 25% of the pixels remaining in the ROI are different from the pixels in the ROI obtained with the similarity image. These are pixels which therefore do not behave as cortex.

We estimated the noise in the signal of the inner ROI and in the calculated medullary renograms. The use of a piecewise linear approach to calculate the noise in a smoothly decaying tail of the signal is the source of a small error. However, this error stays the same for all different thresholds, since the mean temporal behaviour of the medullary signal does not change.

The noise in the ROI signal and the calculated renogram includes a noise source that may be the result of motion of the kidney perpendicular to the image plane. Even at small amplitude, this type of motion will give an increased MR signal because new, unsaturated spins will be excited. Although non-negligible, this noise



source can be regarded as independent of the normal pixel noise and will not depend on the size of the filtered inner ROI.

Two mechanisms determine the noise in the medullary renogram. First, the noise level in the inner ROI is a function of the ROI area. When the noise per pixel is uncorrelated, the relative noise is inversely proportional to the square root of the area of the ROIs:

$$\sigma_{roi} = \frac{\sigma_{pixel}}{\sqrt{Area_{roi}}} \quad (4.4)$$

with  $\sigma_{ROI}$  the standard deviation of the noise in the inner ROI signal and  $\sigma_{pixel}$  that of the noise in individual pixels.  $Area_{ROI}$  is the area of the ROI in pixels, i.e. the ROIs number of pixels, and increasing it will reduce the noise level in the signal.

Second, due to the way the medullary renogram is calculated (formula 4.2), an increased cortical fraction in the inner ROI will result in an increased noise level in the renogram. If  $\sigma_c$  is the standard deviation of the noise in the cortical signal,  $\sigma_i$  that of the inner ROI signal and  $\sigma_m$  that of the calculated medullary signal,  $\sigma_m$  follows from

$$\sigma_m = \sqrt{\frac{\sigma_i^2 + f_c^2 \sigma_c^2}{(1 - f_c)^2}} \quad (4.5)$$

which is valid if the noise in both signals is uncorrelated.

Together, equation (4.4) and (4.5) illustrate that the best way to reduce noise is to reduce the cortical fraction in the ROI while keeping the ROIs area as large as possible.

Since neither the optimal noise reduction nor the optimal threshold to achieve the best noise reduction were predictable, optimal thresholds to arrive at optimal medullary renograms had to be determined for each case. For our data sets, a large number of sequential thresholds were used. The curve in figure 4.6 shows the noise level as a function of the ROI size. The curve's smoothness suggests that a smarter algorithm should be able to find the optimum more efficiently. Since such an added feature would make our method faster but not better, we have not investigated this approach yet.

The overall conclusion is that our correction method decreases the noise in medullary renograms. In our set of 18 cases, the obtained decrease in noise level varied from 5 to 55%. Moreover, the proposed algorithm is incapable of producing worse results than without filtering. Although in some signals noise reduction is marginal, the noise reduction that can be achieved in other cases is a factor of 2 or even better. In addition the contribution of the cortical signal has been eliminated in all cases. In our opinion this is sufficient justification for the use of this method. This is especially so since the extra computational effort occurs during off line data processing and burdens neither the patient nor the scanner.

#### **4.7 Conclusion**

Matched image filtering makes it possible to eliminate cortex-like pixels from the medullary ROI. This improves the signal-to-noise ratio of medullary renograms acquired from dynamic MR kidney scans, while eliminating the cortical contribution. The noise reduction can be as large as a factor of 2 or more. With less noise, a more reliable clinical interpretation of the resulting corrected medullary renogram is possible.

#### **4.8 References**

- 1 Kikinis R, Schulthess von G, Jäger P, et al. Normal and Hydronephrotic Kidney: Evaluation of Renal Function with Contrast-enhanced MR Imaging. *Radiology* 1987; 165:837-842.
- 2 Heintz P, Ehrenheim Ch, Hundeshagen H. Gd-DTPA in MRI and 99m Tc-DTPA in the examination of the perfusion of transplanted kidneys. *Diagnostic Imaging International* 1988: November, Supplement.
- 3 Choyke P, Frank J, Girton M, et al. Dynamic Gd-DTPA-enhanced MR Imaging of the Kidney: Experimental Results. *Radiology* 1989; 170:713-720.
- 4 Carvlin M, Arger P, Kundel H, et al. Use of Gd-DTPA and Fast Gradient-Echo and Spin-Echo MR Imaging to Demonstrate Renal Function in the Rabbit. *Radiology* 1989; 170:705-711
- 5 Semelka R, Hricak H, Tomei E, Floth A, Stoller M. Obstructive Nephropathy: Evaluation with Dynamic Gd-DTPA-enhanced MR Imaging. *Radiology* 1990; 175:797-803.

- 6 Munechika H, Sullivan D, Hedlund, et al. Evaluation of Acute Renal Failure with Magnetic Resonance Imaging Using Gradient-Echo and Gd-DTPA. *Invest Radiol* 1991; 26:22-27
- 7 Hélénon O, Attlam E, Legendre C, et al. Gd-DOTA-enhanced MR Imaging and Color Doppler US of Renal Allograft Necrosis. *RadioGraphics* 1992; 12:21-33.
- 8 Vestring Th, Dietl K, Fahrenkamp A, et al. Die Rindennekrose der Transplantatniere. *Fortschr. Röntgenstr* 1992; 156,6: 507-512
- 9 Ros P, Gauger J, Stoupis C, et al. Diagnosis of Renal Artery Stenosis: Feasibility of Combining MR Angiography, MR Renography, and Gadopentetate-Based Measurements of Glomerular Filtration Rate. *AJR* 1995; 165:1447-1451.
- 10 Sharma R, Gupta R, Poptani H, et al. The Magnetic Resonance Renogram in Renal Transplant Evaluation using Dynamic Contrast Enhanced MR Imaging. *Transplantation* 1995; 59: 1405-1409
- 11 Grenier N, Trillaud H, Combe C, et al. Diagnosis of Renovascular Hypertension: Feasibility of Captopril-Sensitized Dynamic MR Imaging and Comparison with Captopril Scintigraphy. *AJR* 1996;166:835-843.
- 12 Roberts, T. Physiology Measurements by Contrast-Enhanced MR Imaging: Expectations and Limitations. *JMRI* 1997; 7:82-90
- 13 Szolar D, Preidler K, Ebner, et al. Functional Magnetic Resonance Imaging of Human Renal Allografts during the Post-Transplant Perio: Preliminary Observations. *Magnetic Resonance Imaging* 1997; 15:727-735

## Chapter 5

---

# Movement correction of the kidney in dynamic MRI scans using FFT phase difference movement detection.

---

*E.L.W. Giele MSc, J.A. de Priester MD, J.A. Blom PhD, J.A. den Boer PhD, J.M.A. van Engelshoven PhD, A. Hasman PhD, M. Geerlings*

JOURNAL OF MAGNETIC RESONANCE IMAGING 14:741–749 (2001)

### 5.1 Abstract

To measure cortical and medullary MR renograms, regions of interest are placed on the kidney in images acquired using dynamic MRI. Since native kidneys move with breathing and breathholding techniques are not feasible, movement correction is necessary. In this contribution we compare three correction methods; based on image matching, on phase difference movement detection and on cross-correlation respectively. The phase difference movement detection based method shows the best performance and is able to determine the movement of a kidney in our test series in 68% of the scans with no visible deviation and in 88% of the scans if a one-pixel deviation is considered acceptable.

### 5.2 Introduction

Dynamic Magnetic Resonance Imaging after administration of a contrast agent has been in use for some time to retrieve functional information on organs in the human body [1-14]. In the case of the kidney, dynamic MRI is attractive because it offers high temporal and spatial resolution and allows separation of the functional behaviour of cortex and medulla.

During dynamic MRI contrast agents, like Gd-DTPA, enter the arterial space and the interstitium as well as the nephrons and increase the image intensity in both cortex and medulla. If separate regions of interest (ROIs) are placed over cortical and medullary tissue in each frame, two time intensity signals are obtained. If care is taken to avoid saturation effects [1, 2, 18], the image intensity is an indication of the contrast agent concentration and the uptake in and passage through the kidney of the agent can be monitored.

In various publications describing this technique, MR renograms were determined from ROIs that were defined manually and aimed at direct selection of cortex and medulla [1-7,9-12,14]. Since the complex-shaped medullary pyramids border the cortical tissue throughout the kidney many voxels contain a mix of cortical and medullary tissue. Cortical regions at the periphery of the kidney are free of medulla, but in medullary regions there is always a mix of cortical and medullary tissue.

As was shown by de Priester et al. [15] the pure medullary signal can be obtained from the mixed signal by weighted subtraction of the cortical signal. In addition we described an algorithm [16] to automatically determine the correct weighting factor and tested its use in a series of subjects. The signals were recorded from ROIs that were automatically copied after manual segmentation of one of the images early in the dynamic series. The images later in the series lack the contrast for reliable segmentation. Use of these ROIs is only justified when the kidney has a constant shape and position in each image. This is the case for transplanted kidneys and we could show that in that situation the medullary signal could reliably be retrieved. [16,17].

In native kidneys breathing results in kidney movement. For our dynamic scan, breath holding is not feasible (the entire scan takes more than 8 minutes at a temporal resolution of 2 seconds per image) and at least in the early part of the scan we cannot allow large time gaps. Also, it has been shown [23] that even during breath holding the diaphragm is not motionless.

In the dynamic image series of the native kidney a movement correction should be made before the above mentioned signal retrieval method can be applied. Fortunately, the breathing movement does not cause appreciable rotation or distortion of the kidney so that in a suitably angulated coronal plane the kidney cross-section in the images has a constant shape. Subjective survey of our scans shows that the movement of the kidney due to breathing results in a Head to Feet (HF) shift that is normally well within 10 pixels, although slightly larger values sometimes occur. The Left to Right (LR) shift is in most cases zero or one pixel.

We hypothesize that an adequate movement correction can be performed by only shifting the image.

It is possible to perform this shifting manually, but given the large number of scans used for the renogram that is a time consuming job. To automatically measure signal intensities in dynamic MRI studies when motion is present, a method is therefore needed to automatically retrieve the kidney position in each scan.

We designed and tested three approaches and compared their performance. The first approach, called image matching, shifts a part of the image that contains the kidney systematically step by step over another image and for each step determines the similarity between the partial image and the area that it overlays in the other image[24]. The second approach uses Fourier transformation and is called phase difference movement detection (PDMD). The idea behind this approach is that the movement of an object between two images can be estimated by determining the difference of the phase spectra of both images [25]. This phase difference is proportional to both the spatial frequency and the movement distance. The third approach determines the cross-correlation [26] of two images to locate the kidney in the second image. In this contribution we describe all three approaches and evaluate them on a set of images obtained from five patients.

### **5.3 Materials**

Movement correction was tested on dynamic kidney scans obtained from five patients. Approval was obtained from the medical ethics commission of the hospital and informed consent was obtained from all patients.

MR examinations were made with a Philips ACS-NT MR scanner (1.5T, gradient strength 10mT/m, slew rate 15T/m/sec) (Philips Medical Systems, Best, The Netherlands) and each included a dynamic scan of a single slice. The selection of the slice location was based on a multislice scan (T1-weighted, SE: TR/TE=550/14) angled through the longitudinal axis of both kidneys. The slice that showed the largest surface of renal tissue was chosen. For the dynamic scan we used T1-FFE for a strongly T1 weighted spoiled GE sequence (TR/TE/flip = 11 ms/3.4 ms/60°) with 400 mm field of view and a slice thickness of 5 mm. The resolution is 256 x 256 pixels, resulting in pixels of 1.56 x 1.56 mm<sup>2</sup>. We obtained 256 images of a single coronal slice through both kidneys, with a frequency of 1 image per 2 seconds. A contrast agent, Gd-DTPA dimeglumine (Schering), was injected (dose 0.05 mmol/kg) in an antecubital vein as a rapid bolus (5 ml/sec) using a MR compatible injector pump (Medrad Spectris, Medrad, Maastricht, the Netherlands) during imaging, at the start of scan 11. We verified that 256 images

suffice to record the major signal changes related to the passage of the agent through cortex and medulla.

All examinations were stored on magneto-optical disks and transported to a Sun Sparc station which was used to analyse the data using EasyScil software (Philips Medical Systems, The Netherlands).

## 5.4 Methods

We assessed the three methods (image matching, phase difference movement detection and cross-correlation) for their ability to estimate the movement distance of both kidneys between each of the images from the dynamic scan.

Each of the algorithms operates in a number of steps. Per step a “reference image” is compared to a “search image” and the estimated kidney movement vector (the shift) between these images is determined. There are two ways of expressing the shift between images during the dynamic series; absolute or incremental. When measuring absolute movements, one single image is always used as reference image and the movement of the kidney in the search images is determined with respect to the kidney location in the reference image (1-2, 1-3, 1-4, etc). When measuring in the incremental way, the movement of the kidney between subsequent images (1-2, 2-3, 3-4, etc) is determined, the first image of each pair being the reference image.

During the scan the contrast within the kidney as well as between the kidney and the surrounding tissue changes significantly because of the contrast agent redistribution. This makes the estimates of absolute movement difficult because a reference image taken at maximum enhancement is not at all similar to images later in the series. For that reason we chose the incremental way for calculation and comparison of the methods.

All methods start from a single high contrast image in which a kidney contour is drawn manually. The contour is then used to convert the image into a binary kidney image of which the pixels inside the contour have a value 1 and outside the contour a value 0.

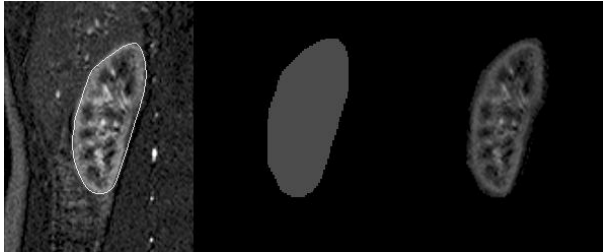


Figure 5.1: On the left the kidney contour as drawn by the operator, in the middle the mask and on the right the masked image.

This binary kidney image is used to construct a mask. Only pixels within the mask have values different from 0, the remaining part of the mask image contains zeroes. The mask is multiplied with each of the images in the dynamic series and the result is called a “masked image”. Mask size and mask pixel values differ per method.

In case of the image matching method the mask is binary. In case of the PDMD and cross-correlation method the mask contains pixel values between 0 and 1. A further use of the contour of the kidney is to support the operator when checking whether the calculated shift is correct. To this end each search image is displayed translated over the calculated shift and the contour is shown overlaying the image. If the movement is correctly determined the kidney border should coincide with the contour. When the operator judges that this is not the case, he adjusts the image position manually and in this way a more correct shift is obtained. Both calculated shift and manual adjustment are recorded as a vector containing the values of the shift in both directions, expressed as integer numbers of pixels.

#### *Image matching method.*

The first reference image is the masked image obtained from the image that was used by the operator to draw the contour. The similarity of the next (non masked) image (the search image) with the reference image is then determined for each of a number of trial shifts. The trial shift (x,y) of the search image relative to the reference image ranges over all positions that could be reached by the moving kidney. The similarity is expressed as the inproduct of the vectors that represent both images. The shift leading to the highest inproduct value is the one that provides the estimated movement of the kidney from reference to search image. This shift of the kidney is then recorded.

After the shift of the kidney has been determined, the search image becomes the reference image for calculating the next movement. The obtained shift is applied to the mask so that it should again cover the kidney. Because of rounding off or other errors this may not be the case. Therefore an operator has to check the location of



the mask directly after the kidney movement between two images has been estimated. This procedure is repeated until the end of the series. Since the initial image (the manually contoured image) is usually not the first image in the series, the procedure is also performed backward to the beginning of the series.

We tested this algorithm with three different masks. The first mask was obtained from the binary kidney image by dilation (growing) with two pixels. This mask therefore covers the kidney and a small area around it. The second mask is derived by dilating the first mask with another 4 pixels. The third mask is derived from the first mask by subtracting an image that is obtained by eroding this first mask with 4 pixels. The result is a 4 pixel wide ring around the contour of the kidney, covering the rim of the cortex and peripheral fat.

#### *Image matching algorithm*

The similarity between the masked image (the mask  $m$  multiplied by the reference image ( $a$ ) and the shifted search image ( $b$ ) is determined by

$$R_{ab}(x, y) = \frac{\sum_{i=1}^N \sum_{j=1}^M m_{i,j} a_{i,j} b_{i+x,j+y}}{\sqrt{\sum_{i=1}^N \sum_{j=1}^M m_{i,j} a_{i,j}^2} \cdot \sqrt{\sum_{i=1}^N \sum_{j=1}^M m_{i,j} b_{i+x,j+y}^2}} \quad (5.1)$$

where  $(x,y)$  represents the shift between image  $a$  and  $b$ . All images are of the size  $N \times M$  where  $N$  and  $M$  are sufficiently large to contain the mask. The similarity can be regarded as the inproduct of two vectors (representing the masked image and the search image), both having as many dimensions as the image has pixels.

The  $(x,y)$  coordinates resulting in the the highest value of the inproduct  $R_{ab}$  represent the estimated movement vector . An example of the distribution of values of  $R_{ab}$  is plotted in figure 5.2. The inproduct usually has a single maximum that can be found with an accuracy of one pixel.

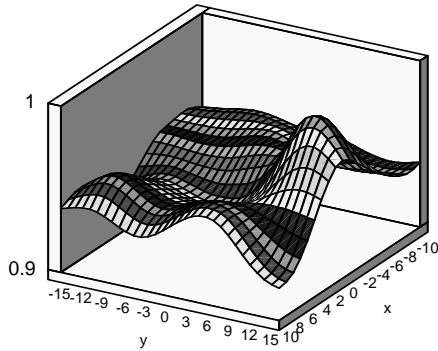


Figure 5.2: Example of a plot of  $R_{ab}$  obtained from a pair of images from a dynamic MR kidney series.

#### *Phase Difference Movement Detection (PDMD) method*

In the PDMD method the mask is derived from the binary kidney image in three steps. In the first step the binary image is filtered with a wide non-isometric gaussian filter (with a standard deviation in the LR-direction of 5 and in the HF-direction of 20 pixels). A new binary image is obtained by giving pixels that exceed a threshold of 0.1 the value 1 and the remaining pixels a value 0. The area covered by the non-zero pixels is large enough to always contain the kidney. Finally this new image is again filtered, now with an isometric gaussian filter (standard deviation 10 pixels in both directions) to remove sharp edges. The resulting mask contains pixels with values between 0 and 1. A cross section of the mask is presented in figure 5.3. The mask remains at a stationary position; it is considered large enough to cover the actual kidney position in alle images.

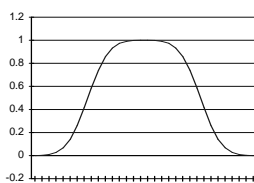


Figure 5.3: Cross section of the floating value mask used in the PDMD and cross correlation method.

Movement correction is again determined between subsequent images. The method starts with the first image in the series. In this case both the reference and the search image are multiplied with the mask. Using the PDMD algorithm (see next section) the shift is calculated and recorded. This process is repeated to determine the movement between the second and the third image, etc.

## Movement correction of the kidney in dynamic MRI scans using FFT phase difference movement detection.

---

After the calculation of the shifts between three subsequent images, the shift between the first and third image is also directly calculated using the same method. If this shift differs by one pixel from the sum of the two previous shifts this difference is considered to be due to rounding off and the shift between the second and third image is corrected. If the difference is more than one pixel one of the three calculations must have contained an error, but since it is unknown which of the calculations this is, no corrections are made.

An operator checks the resulting shifts and corrects possible errors. Since the mask does not have to be repositioned the operator can perform this check after the whole series of images has been processed.

### *PDMD algorithm*

Fourier transformation resolves an image or a signal into its frequency components, resulting in an amplitude and a phase spectrum. Two images containing identical objects, one of them moved with respect to the other, will have the same amplitude spectrum. The phase spectrum will always be in the range  $[-\pi, \pi]$ . The phase spectrum of the image after movement contains at each spatial frequency an additional phase shift (in relation to the image before movement) proportional to both the movement of the object and the spatial frequency, as shown for a one-dimensional object in figure 5.4. By subtracting the phase spectra of both images the phase difference spectrum is obtained. From this the movement distance of the object can be estimated.

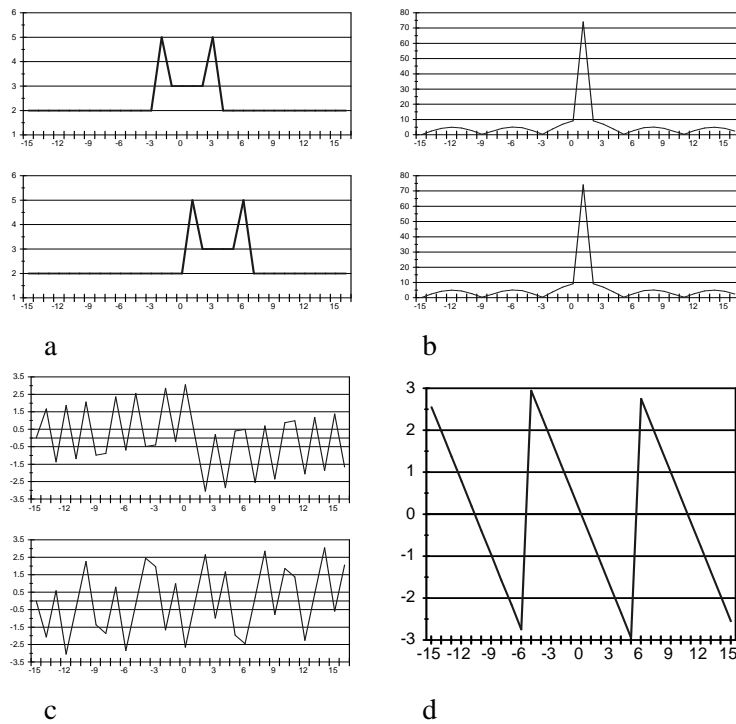


Figure 5.4: A signal and the same signal shifted (a), with the corresponding amplitude (b) and phase spectra (c). The difference of both phase spectra is shown in (d)

Noise in the signals will manifest itself in the amplitude and the phase spectra. Especially the high frequency parts of the spectra get distorted, as shown in figure 5.5.

## Movement correction of the kidney in dynamic MRI scans using FFT phase difference movement detection.

---

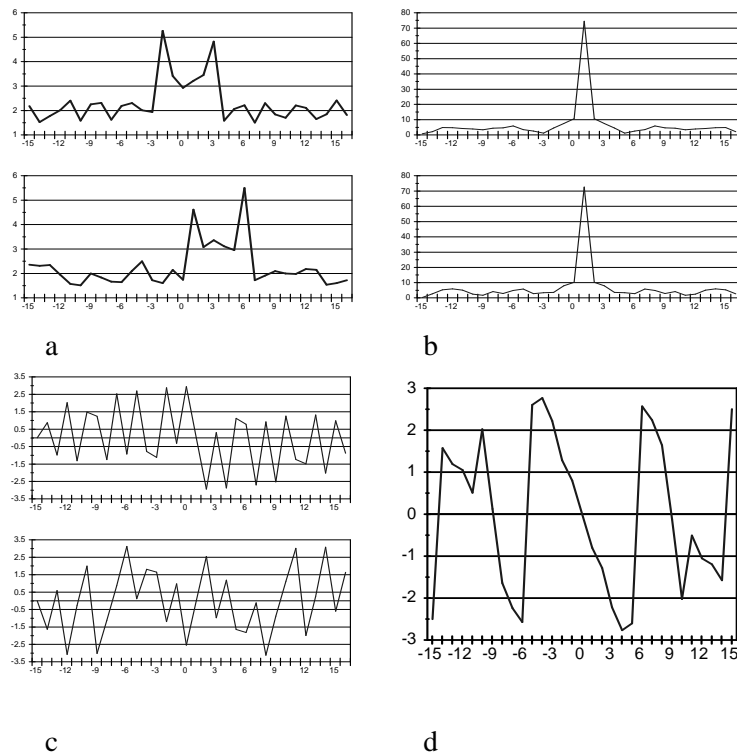


Figure 5.5: The same signals as in figure 5.4 now after the addition of noise

### 5.5 The PDMD marker image

To explain how the movement is estimated, suppose we have an image only containing a delta peak in its center. Fourier transformation of this image results in a flat amplitude spectrum and a phase spectrum that is zero everywhere. When the delta peak is shifted the same amplitude spectrum is obtained but the phase spectrum shows a phase that increases linearly with the frequency. The slope is determined by the shift. We apply this idea in the reverse order: we replace the phase spectrum of the delta peak by the phase difference spectrum obtained in the way described above. We then will, after inverse FFT, obtain an image containing a delta peak shifted from the origin over the same distance as the object moved from one image to the other. In general the presence of noise will cause a widening of the shifted delta peak.

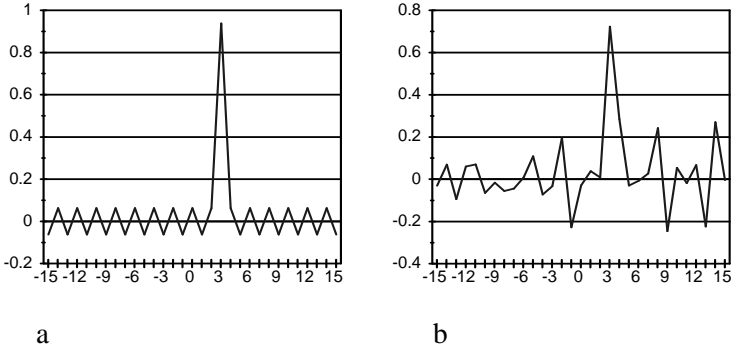


Figure 5.6: One dimensional synthetic PDMD image, (a) based on the clean signals in figure 5.4 and (b) based on the noisy signals of figure 5.5.

The PDMD procedure is as follows. After masking and Fourier transformation of the images acquired with the MRI scanner, the phase difference spectrum is determined. This phase difference spectrum is combined with a flat amplitude spectrum. After inverse FFT an image is obtained containing a sharp peak, approaching a delta shape, but usually widened because of noise. To reduce high frequency noise in this image, we convolute with a gaussian filter. The position of the maximum of the peak is the estimated movement distance of the kidney.

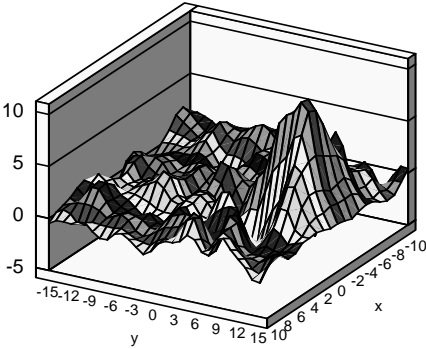


Figure 5.7: Example of a contour plot of a PDMD image obtained from the same pair of images as used for figure 5.2.

*Cross-correlation method*

Cross-correlation is a well known method that is used both for signals and images. The implementation was adapted to our situation. Using the same mask as with the PDMD method, all consecutive image pairs are cross-correlated. Cross-correlation values for different shifts can relatively easy be determined via the Fourier domain

## Movement correction of the kidney in dynamic MRI scans using FFT phase difference movement detection.

---

by multiplying the Fourier transform of the masked reference image with the complex-conjugated Fourier transform of the masked search image and then transforming back. This results in an image as displayed figure 5.8. The maximum intensity in the image indicates the estimated movement.

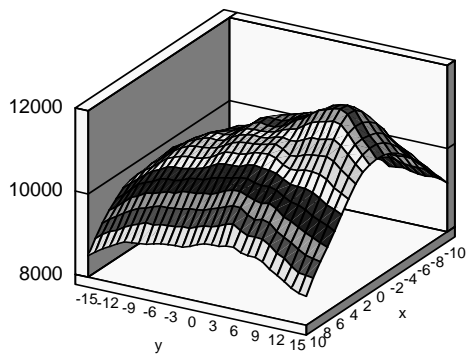


Figure 5.8: Example of a contour plot of the cross-correlation values determined from the same pair of images as used in figure 5.2 and figure 5.7.

## 5.6 Results

To measure the performance of the movement correction methods we used the data of five patients. Since each patient has two kidneys, this resulted in 10 series of 255 movements each. After the movement correction, the results were reviewed by an operator and his manual adjustments were recorded.

All the results presented here concern the adjustments needed to reach the operator position along the vertical (HF) axis. Since the horizontal movements were minor the observed shifts in that direction are not reported.

### *Image matching method*

The images of two patients were used to determine the influence of the mask size on the accuracy of the image matching method. The locations determined by one operator were taken as the gold standard. In table 5.1 a breakdown per error size of the resulting errors in the matching method are presented. The results of the small and the large mask closely resembled each other, with the small mask giving slightly better results for small errors. The small mask did suffer more from large errors. The mask which selected only the cortex-periphery junction had the worst results, with far less correct results and a very high number of totally wrong results.

Table 5.1: Breakdown of errors observed in the image matching method for three different masks.

Error size (pixels)	0	1	2	3	4	>4
Small mask	301	368	181	79	34	57
Large mask	284	379	199	93	36	29
Cortex-periphery junction	168	274	187	116	97	178

### Method comparison

The data in table 5.2 shows the differences in performance of the three methods. In this table the average results of all 10 series are shown for the three methods. From these results it is clear that the PDMD method is the better performer. Since the performance depends on contrast distribution in the images the results vary per patient. We used the Kruskal Wallis test which shows that the results between these methods are significant ( $P < 0.001$ ). We also calculated the difference in performance for each patient in comparison with the PDMD method. The minimum and maximum differences over all ten series are also shown in the table.

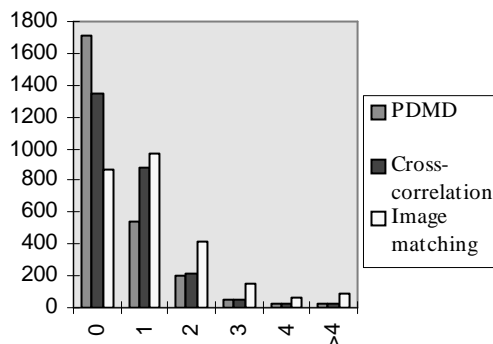


Figure 5.9: Graphical comparison of errors in the three different methods as presented in table 5.2.



Movement correction of the kidney in dynamic MRI scans using FFT phase difference movement detection.

Table 5.2: Breakdown of the error rates observed in three methods (image matching, cross- correlation and PDMD). Also shown are minimum and maximum score differences per series. These are the differences compared between the respective method and the PDMD method for each series.

Error size	0		1		2		3		4		>4	
Image matching	865 (34%)		968 (38%)		414 (16%)		157 (6%)		62 (2%)		84 (3%)	
Cross-correlation	1350 (53%)		881 (35%)		217 (9%)		52 (2%)		29 (1%)		21 (1%)	
PDMD	1714 (67%)		546 (21%)		198 (8%)		51 (2%)		20 (1%)		21 (1%)	
min/max (PDMD-IM)	38	121	-81	13	-45	-2	-20	0	-8	0	-26	0
min/max (PDMD-CC)	6	56	-49	10	-12	6	-5	10	-2	1	-10	4

*Contrast phase dependence*

As mentioned before, the contrast in the kidney changes drastically during the scan. To determine how this influences the accuracy of the PDMD method we divided the dynamic series into four scan phases: the first phase (I) consists of the first 10 images. These images are taken before the contrast agent was injected.. The second phase (II) consists of the next 30 images with high contrast and the largest signal in the cortex. In the next phase (III) of 60 images the part of the bolus that is excreted to the nephronal channels is assumed to still reside in the kidney [17], causing moderate enhancement in cortex as well as medulla. The last phase (IV) is characterized by a much lower contrast between kidney and surroundings. Table 5.3 shows the results. Since the number of images is different in each phase, the errors are given in percentages. Figure 5.10 presents the same information graphically.

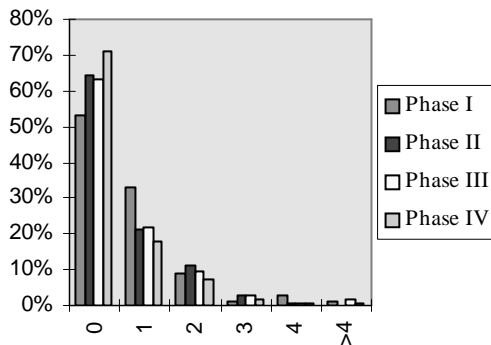


Figure 5.10: Breakdown of differences in each of the phases as presented in table 5.3.

Table 5.3: Percentage breakdown of errors in the PDMD method for four phases in the dynamic scan

Error size	0	1	2	3	4	>4
scan phase I	53%	33%	9%	1%	3%	1%
scan phase II	64%	21%	11%	3%	1%	0%
scan phase III	63%	22%	10%	3%	1%	2%
scan phase IV	71%	18%	7%	2%	1%	1%

The percentual breakdown of the errors shows that the distribution does not change much between the different phases. It can be noted that the first phase, where no contrast agent is present, has the worst results and the last phase, during which the slow wash out of contrast agent occurs, has the best results.

## 5.7 Discussion

In this contribution we have investigated three different methods for automatically locating the image position of a moving native kidney. Several other movement correction methods are known in literature but for reasons we will describe these were not useable for our purposes.

One of these possible movement correction methods is based on feature extraction as suggested by Gerig [22]. In each image the contour of the kidney is determined by an edge detection filter. The kidney contour of the first image is used to locate the position of the contour in the subsequent images. The use of an edge detection filter in these images requires a relatively low noise level which we did not achieve in our scans because of the short scan time (time resolution of 2 seconds per image). Especially the late images in our series have a low contrast with respect to the surroundings and do not allow contour detection.

A method developed specifically to determine abdominal movement is the use of navigator images interleaved in the dynamic image acquisition. Since the navigator echo has to be implemented by the manufacturer of the MRI scanner, not every scanner is equipped with it. This was also the case with our scanner which did not offer the navigator echo. Therefore our method is entirely based on post-processing methods and is thus independent of the scanner.

From brain imaging with MRI two other types of image registration are known which are suited for motion compensation. One method is based on image transformation [Friston,19], the second one on segmentation [Woods, 20].

Image transformation as described by Friston modifies an image via a combined spatial and intensity transformation to resemble a reference image. By minimizing the sum of squares of the differences in the pixel values between the two images an optimal correction is achieved. This method is independent of the actual image content and does not need segmentation or information, like shape or location, about the object. We tested the Friston algorithm and showed that although the method was able to accurately correct the kidney position, the image intensity became distorted. We assume that the large movement of the kidney is cause of this artefact. Since our aim is to record the changes in image intensity, the Friston method can not be used.

The movement correction by Woods segments each image and then calculates the shift between the segmented images. Since in segmented images the location of the tissue of interest is known, this technique is suitable for both small and large movements. A prerequisite for a segmentation method is a signal to noise ratio high enough to reliably perform segmentation. As discussed earlier, in the case of our dynamic renal MRI scans there are a large number of images where the contrast between the kidney and the surrounding tissue is too low for contour detection, let alone reliable segmentation.

Because of the problems mentioned we did not test these methods but only the three described in this article. Although at least two of the investigated methods perform relatively well, further studies are necessary to improve the technique in order to reduce operator intervention time. With the best method the operator must still make corrections in about 20% of the 255 images.

#### *Round off drift*

The disadvantage of using an incremental method is that the resulting movement estimate is susceptible to drift. Every time the movement is estimated, the obtained shift is rounded up or down to the nearest entire pixel. This results in a maximum error of a half pixel after each calculation. Already after two steps this may result in an error of more than half a pixel that will then be rounded off to one pixel. With a uniform error distribution the chance that this happens is  $1/4$ . Since our primary concern was to determine and compare the accuracy of alternative methods, we decided to use a very simple drift correction algorithm. After two calculations the movement between the first and third image is calculated and compared with the sum of the two individual movement corrections. In case the difference between the sum and the direct calculation is zero, no drift is assumed to be present. If the difference is one pixel, this is considered to be caused by drift, and the last movement is modified accordingly. A difference more than one pixel can not be caused by drift alone. In such a case no action is undertaken. On the other hand a difference of one pixel does not have to be caused by drift and the method may

---

introduce another error. We envisage to upgrade the PDMD method to sub-pixel accuracy to further reduce the problem of possible drift.

#### *Influence of mask size in the image matching method*

In the image matching method, the masks with the best performance are those that contain the entire kidney. The mask that only contains the cortical-peripheral junction has the worst performance. The small size of this mask makes it very vulnerable to noise. The difference in performance between the two larger masks is relatively small. Since image matching depends on the contrast of transitions in the image, enlarging the mask does not add useful information.

The main disadvantage of the image matching method is that an operator has to check the results of each step before the method can continue. As was explained earlier after each matching step the current search frame becomes the new reference frame. Since the kidney has moved, the mask has to be shifted to its required position. If an error in the determination of the kidney location is made the mask will not exactly overlay the kidney. The masked reference image will then not present the kidney area correctly. To prevent this an operator has to check the location of the mask with respect to the kidney and make corrections when needed.

#### *PDMD method*

Of the three methods the PDMD method has the highest percentage of error free shifts. It scores approximately equal to the cross correlation method as far as large errors are concerned but achieves a higher accuracy, resulting in less errors with a size of one pixel.

Since the PDMD method is not very sensitive to the background, a large mask can be used. Smoothing of the edges is important to keep the energy in the amplitude spectrum of the mask low. A sharp mask would contribute too much energy to the spectrum, the method would detect the location of the mask instead of the location of the kidney. Even then the mask can be made large enough to remain stationary, always containing the kidney, irrespective of its movement. The stationary mask is one of the main advantages of PDMD method because the calculations can all be performed by the computer without operator intervention. The operator can now check the calculations afterwards and if necessary correct them.

#### *Cross-correlation method*

As can be concluded from the experiment the cross-correlation method is better than the image matching method. Like the PMPD method, the correlation method does not need operator intervention during the calculations. The method works quickly and provides stable results. The fact that it performs not as well as the

PDMD method may be due to the fact that the distribution of cross-correlation values is characterized by a smooth peak. This may explain the relatively large occurrence rate for error size 1, when compared with the PDMD method.

#### *Change in accuracy during the scan*

As shown in table 5.3, the error rate of the PDMD method does not deteriorate strongly during the late (low contrast) scans. The added rates of error sizes 0 and 1 during the four different dynamic scan phases are almost constant. We assume that this is due to the fact that the method does not depend on pixel intensities (the amplitude spectrum is ignored), but on the coherence between the pixel intensities.

## **5.8 Conclusion**

We tested three post processing scanner independent methods for movement correction of the kidney. The preferred method appears to be the phase difference movement detection method. Both the size and the number of corrections are significantly lower when compared with the other methods.

Full agreement between the movements measured by the PDMD method and the operator occurs in 68% of the measurements and in 88% an error size of at most one pixel is obtained. The PDMD is fairly independent of the contrast situation in the images. In our series the method performed equally in all four contrast phases (pre-contrast, cortical enhancement, medullary enhancement and wash-out). With this performance the operator workload is significantly reduced and the algorithm therefore is of important clinical value for dynamic kidney MR of noisy images.

Noisy images result when the scan parameters are driven in the direction of high temporal and spatial resolution with a close to linear contrast agent concentration response. Earlier, in implant patients we have shown that such scans can be used to obtain dynamic scans of outstanding quality, especially when evaluated with methods for automatic determination of cortical and medullary signals. This work shows that extension of the use of these dynamic scans to native kidneys is possible.

## **5.9 References**

- 1 R Kikinis, G von Schulthess, P Jäger, et al. Normal and Hydronephrotic Kidney: Evaluation of Renal Function with Contrast-enhanced MR Imaging. *Radiology* 1987; 165:837-842.

- 
- 2 Takeda M, Katayama Y, Tsutui T, Komeyama T, Mizusawa T. Does Gd-DTPA enhanced MRI of the kidney represent tissue concentration of contrast media in the kidney: In vivo and in vitro study. *Mag. Res. Im.* 1994; 12:421-427.
  - 3 P Heintz, Ch Ehrenheim, H Hundeshagen. Gd-DTPA in MRI and 99m Tc-DTPA in the examination of the perfusion of transplanted kidneys. *Diagnostic Imaging International* 1988: November, Supplement.
  - 4 P Choyke, J Frank, M Girton, et al. Dynamic Gd-DTPA-enhanced MR Imaging of the Kidney: Experimental Results. *Radiology* 1989; 170:713-720.
  - 5 M Carvlin, P Arger, H Kundel, et al. Use of Gd-DTPA and Fast Gradient-Echo and Spin-Echo MR Imaging to Demonstrate Renal Function in the Rabbit. *Radiology* 1989; 170:705-711
  - 6 R Semelka, H Hricak, E Tomei, A Floth, M Stoller. Obstructive Nephropathy: Evaluation with Dynamic Gd-DTPA-enhanced MR Imaging. *Radiology* 1990; 175:797-803.
  - 7 H Munechika, D Sullivan, Hedlund, et al. Evaluation of Acute Renal Failure with Magnetic Resonance Imaging Using Gradient-Echo and Gd-DTPA. *Invest Radiol* 1991; 26:22-27
  - 8 O Hélénon, E Attlam, C Legendre, et al. Gd-DOTA-enhanced MR Imaging and Color Doppler US of Renal Allograft Necrosis. *RadioGraphics* 1992; 12:21-33.
  - 9 Th Vestring, K Dietl, A Fahrenkamp, et al. Die Rindennekrose der Transplantatniere. *Fortschr. Röntgenstr* 1992; 156,6: 507-512
  - 10 P Ros, J Gauger, C Stoupis, et al. Diagnosis of Renal Artery Stenosis: Feasibility of Combining MR Angiography, MR Renography, and Gadopentetate-Based Measurements of Glomerular Filtration Rate. *AJR* 1995; 165:1447-1451.
  - 11 R Sharma, R Gupta, H Poptani, et al. The Magnetic Resonance Renogram in Renal Transplant Evaluation using Dynamic Contrast Enhanced MR Imaging. *Transplantation* 1995; 59: 1405-1409

- 12 N Grenier, H Trillaud, C Combe, et al. Diagnosis of Renovascular Hypertension: Feasibility of Captopril-Sensitized Dynamic MR Imaging and Comparison with Captopril Scintigraphy. *AJR* 1996;166:835-843.
- 13 T Roberts, Physiology Measurements by Contrast-Enhanced MR Imaging: Expectations and Limitations. *JMRI* 1997; 7:82-90.
- 14 D Szolar, K Preidler, Ebner, et al. Functional Magnetic Resonance Imaging of Human Renal Allografts during the Post-Transplant Period: Preliminary Observations. *Magnetic Resonance Imaging* 1997; 15:727-735
- 15 J. A. de Priester, J. A. den Boer, E. L.W. Giele, M. H.L. Christiaans, A. Kessels, A. Hasman, J. M.A. van Engelshoven. MR Renography: An Algorithm for Calculation and Correction of Cortical Volume Averaging in Medullary Renographs. *JMRI* 2000;12:453-459.
- 16 E Giele, J de Priester, J Blom, J den Boer, J van Engelshoven, A Hasman. Reduction of noise in medullary renograms from dynamic MR Images. *Journal of Magnetic Resonance Imaging*. *JMRI* 2000;11:149-155
- 17 E Giele, J de Priester, J Blom, J den Boer, J van Engelshoven, A Hasman. Evaluation of two cortical fraction estimation algorithms for the calculation of dynamic magnetic resonance renograms. Accepted for publication in *Computer Methods and Programs in Biomedicine*.
- 18 DenBoer JA, DePriester JA, Geerlings MJHM, et al. Quantitative model description of dynamic MRI enhancement data of the kidney. *JMRI*, submitted.
- 19 K Friston, J Ashburner, C Frith, J Poline, J Heather, R Frackowiack. Spatial Registration and Normalization of Images. *Human Brain Mapping* 1995; 2:165-189
- 20 Woods RP, Cherry SR, Mazziotta JC. Rapid automated algorithm for aligning and reslicing PET images. *Journal of Computer Assisted Tomography* 1992;16:620-633.
- 21 Swenne CA, van Bommel JH, Hengeveld SJ, Hermans M. Pattern recognition for ECG monitoring; An interactive method for the classification of ventricular complexes. *Comput Biomed Res* 1973; 5:150-160

- 22 Gerig G, Kikinis R, Kuoni W, von Schulthess GK, Kübler O. Semiautomated ROI Analysis in Dynamic MR Studies. Part I: Image Analysis Tools for Automatic Correction of Organ Displacements. *JCAT* 1991; 15(5):725-732
- 23 Holland A, Goldfarb J, Edelman R. Diaphragmatic and Cardiac Motion during Suspended Breathing: Preliminary Experience and Implications for Breath-hold MR Imaging. *Radiology* 1998; 209:483-489
- 24 Pratt W.: *Digital Image Processing*. John Wiley, New York 1978
- 25 G Yang, P Burger, J Panting, P. Gatehouse, D Rueckert, D Penell, D Firmin. Motion and deformation tracking for short-axis echo-planar myocardial perfusion imaging. *Medical Image Analysis* 1998; 2:285-302
- 26 D.C. Champeney. *Fourier transforms and their physical applications*. Academic Press, 1973.



Movement correction of the kidney in dynamic MRI scans using FFT phase difference movement detection.

---

## Chapter 6

---

# Optimal scanner settings for semi automatic renogram determination.

---

*E. Giele, J.A. den Boer, J.A. de Priester, H. v Mameren, J.M.A. van Engelshoven, A. Hasman*

JOURNAL OF MAGNETIC RESONANCE IMAGING: SUBMITTED

### 6.1 Abstract

In our previous research we developed algorithms to determine cortical and medullary renograms of native and transplanted kidneys. We used scanner settings that were limited by technological constraints at the start of our research. In this contribution we re-evaluate these settings and based on the progress in scanner technology and the properties of our algorithms we suggest better ones. By switching from 6 to 12 mm slice thickness not only the SNR of the images will be improved but the SNR of the renograms as well. The presence of noise caused by through slice movement can be reduced by using a multi slice technique and measuring in the middle slice.

### 6.2 Introduction

Dynamic Magnetic Resonance Imaging of the kidney after administration of a contrast agent has been studied for some time with the aim to obtain clinically useful functional information of this organ [1-14]. When we started our study in this domain, we designed a data acquisition method which, given the requirements for data analysis, was judged to constitute the best scan method available. Some of the MR technique factors chosen at that time are reconsidered in this contribution. To understand the reasons behind our choice of data acquisition method, the global description of the entire procedure is given first. Table 6.1 shows the presently used scan parameters.

During the scan, following intravenous bolus injection, the extracellular contrast agent Gd-DTPA enters the arterial space, the interstitium as well as the nephrons and increases the image intensity in both cortex and medulla. By placing separate regions of interest (ROIs) over cortical and medullary tissue in each frame, two time-intensity signals (TI-signals) are obtained which are called MR Renograms. The temporal resolution (frame-to-frame time) of the scan is sufficient to resolve the events even during the fast arterial phase. Care is taken to avoid saturation effects [1, 2, 15], so that the image intensity is a measure of the contrast agent concentration and the uptake in and passage through the kidney of the agent can be interpreted. The kidney enhancement is followed over time during a period of 8 minutes.

Although in the MRI images a ROI that is only covering cortical tissue can be obtained reliably in the outer shell of the kidney, one that is covering only medullary tissue can in practice not be found, due to the irregular topology of the boundary between cortex and medulla. This results in potential presence of cortical tissue in each of the voxels of the intended medullary ROI and thus a cortical contribution to the medullary signal. As was shown by de Priester et al. [16] a pure medullary signal can be obtained from the mixed signal by weighted subtraction of the cortical signal. In addition we described an algorithm [17] to automatically determine the correct weighting factor and tested its use in a series of subjects. The signals were recorded from ROIs that were automatically copied to all images after semi-automatic segmentation. For this segmentation use is made of the images before and after contrast agent injection. The operator can exclude the calyx from the automatically generated ROIs [17]. Use of this method of segmentation and this copying of the ROIs is only justified when the kidney has a constant shape and position in each image. This is the case for transplanted kidneys and we could show that in that situation the medullary signal could reliably be retrieved. [17,18].

Table 6.1: Scan parameters

Scan method: 2D spoiled Gradient Echo	Slice: 6 mm
TR: 11 ms (shortest available)	FOV : 360 x 400 mm
TE: 3.4 ms (shortest available)	Matrix: 205 x 256
Flip angle: 60° (strong T1 weighting)	Frame time: 2 seconds
Slice position: through long kidney axis and pyelum	Number of frames: 256
Breathing instructions: free breathing	

### 6.3 Slice thickness.

The information that can be retrieved from renograms depends on their signal to noise ratio (SNR), which can be increased by increasing the slice thickness.

---

However, when the slice thickness ( $h$ ) increases it can be expected that the fraction of cortical tissue present in the inner ROI (the cortical fraction,  $f_c$ ) will increase as well. Due to the algorithm used to calculate the pure medullary ROI signal this in turn will increase the noise in the signal thus possibly counteracting the gain in SNR resulting from the slice thickness increase.

The medullary ROI signal is calculated via

$$s_m(h) = \frac{s_i - f_c s_c}{1 - f_c} \quad (6.1)$$

Since  $s_m(h)$  is the pure medullary signal, it is independent of the cortical fraction and only depends on the slice thickness. The noise in this signal however is dependent of the cortical fraction and can be calculated via

$$\sigma_m(f_c) = \frac{\sqrt{\sigma_i^2 + f_c^2 \sigma_c^2}}{1 - f_c} \quad (6.2)$$

In these equations,  $\sigma_i$  and  $\sigma_c$  are the r.m.s. noise levels of the ROI signals of respectively inner and outer (cortical) ROI,  $f_c$  is the cortical fraction and  $\sigma_m$  is the r.m.s noise level in the calculated medullary ROI signal.  $s_i$ ,  $s_c$  and  $s_m$  are the respective signal levels.

As can be seen from equation (6.2) increasing  $f_c$  results in an increase of the noise in the medullary ROI signal. Therefore the determination of the optimal slice thickness becomes a trade-off between the signal to noise ratio of the raw signal in the medullary ROI and the cortical partial volume.

One approach to reduce noise is to minimize the partial volume effect by using a small slice thickness. This strategy was used in our initial scans. A thin slice obviously results in a rather noisy scan and we settled for 6 mm slice thickness. As it turned out, even this slice thickness was not sufficient to prevent serious partial volume effect. Figure 6.1 illustrates the dimension ratios of the resulting voxel. Inspection of the data of 18 transplanted kidney patients showed an average cortical fraction in the medullary ROI of 54% (min 30%, max 73%)[16-18]. Even considering the fact that this high cortical fraction is in part caused by the columns of Bertin contained in the medullary ROI, this high mean value reflects the irregular topology of the cortico-medullary boundary.

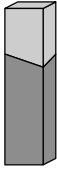


Figure 6.1: Voxel with the dimension ratios as used in our study: 1.6x1.6x 6mm. Two tissues in the voxel, resulting in partial volume effect.

An alternative approach would be to increase the slice thickness, in the hope that the cortical fraction does not increase or increases only slightly with slice thickness. In MRI the noise level remains constant and the signal level increases proportional to the slice thickness, resulting in better images and hence hopefully also a medullary renogram with a better SNR.

Besides the possible increase of the cortical fraction and its consequences for the medullary TI-signal there is another factor limiting the slice thickness. The correction algorithm for cortical contribution to the signal of the inner ROI assumes that the outer region contains only cortical tissue so that a pure cortical TI-signal can be obtained. When the slice thickness becomes too large the curvature of the kidney's circumference becomes an issue. Tall voxels in the outer ROI could leave the cortex and include other tissues. For this reason we limited our measurements to 15 mm slice thickness.

### 6.3.1 Signal to noise ratio versus slice thickness.

In theory the SNR increases linearly with the slice thickness. Since it is essential for our calculations that this is the case in our scans, we checked this by measuring the SNR as a function of slice thickness. We made dynamic scans of the lower abdomen of a volunteer with the same scan parameters as the scans we use for renogram measurements except for slice thickness (see table 6.1). The slice thickness was varied between 3 and 15 mm in steps of 3 mm and no contrast agent was used. Five ROIs were drawn in homogeneous tissue and their signal to noise ratio was calculated. Since different tissues have different signal levels, the SNR is expressed relative to its value at 6 mm. In figure 6.2 the relative signal to noise ratios ( $RSNR_{ROI,h=6}$ ) are plotted as a function of slice thickness.

Linear regression ( $r>0.995$ ) of the measurements yields

$$RSNR_{ROI,h=6}(h) = 0.116h + 0.30 \quad (6.3)$$

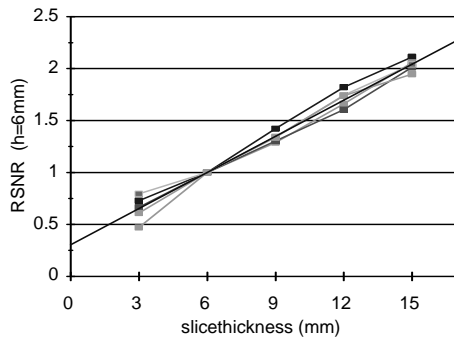


Figure 6.2: The relative signal to noise ratio ( $RSNR_{h=6}$ ) as a function of slice thickness in five ROIs.

### 6.3.2 Cortical fraction versus slice thickness.

To determine whether the cortical fraction depends on the slice thickness, we used anatomical data determined from a human kidney. A human kidney was sliced at 0.5 mm intervals and the resulting slices were stained to show the tissue type. The slices were digitized [19] and subsequently converted to a 3 dimensional matrix where each matrix element represents a volume of  $0.5 \times 0.5 \times 0.5 \text{ mm}^3$  and contains either cortex, medulla or “other”, where “other” can be veins, arteries, pyelum, etc. In this anatomical kidney model virtual MRI slices can be defined. These slices consist of voxels built up from a number of matrix elements. By determining the content of each voxel its cortical fraction can be determined as well as the cortical fraction in a ROI. Figure 6.3 and figure 6.4 show the results, including ROIs with the shape and size, as used in our MR measurements.



Figure 6.3: Example of a slice of the anatomical kidney model and a virtual MRI slice constructed from multiple element layers. In these images grey is cortex and white is medulla and black is other.

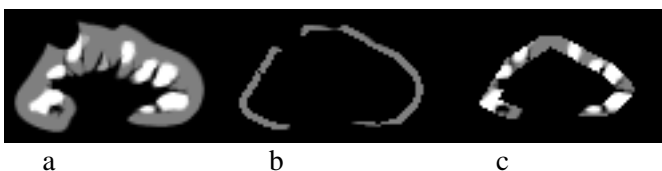


Figure 6.4: A virtual MRI slice (a) and the contents of outer (b) and inner (c) ROI.

To determine how the cortical fraction changes with increasing slice thickness, we calculated the cortical fraction in the inner ROI as a function of the slice thickness for slices between 3 and 15 mm. Since the cortical fraction also depends on the location of the slice, we generated the slices at five different locations. The mid plane of the center slice coincides with the kidney centre and its anatomical orientation is that of the coronal MRI slices as used in our clinical experiments. The mid planes of the other four slices were located at positions displaced in the AP direction by  $\pm 2.5$  and 5 mm. With increasing slice thickness this will result in more overlap of the slices. The pyelum was excluded manually according to the protocol used in the clinical studies. The cortical fraction varied with location and slice thickness. The  $f_c$  values at the 5 locations and their average are presented in table 6.2.

Table 6.2: The cortical fraction  $f_c$  observed at five slice locations and with different slice thicknesses and the average per slice over all locations. The off-sets are relative to the kidney center.

slice thickness (mm)	location off-set (mm)					avg $f_c$
	-5	-2.5	0	2.5	5	
3	0.686	0.492	0.376	0.382	0.530	0.493
6	0.672	0.513	0.413	0.398	0.566	0.512
9	0.661	0.539	0.452	0.455	0.587	0.539
12	0.657	0.564	0.500	0.520	0.612	0.571
15	0.668	0.599	0.560	0.577	0.633	0.607

Table 6.2 shows that the central slice usually has the lowest cortical fraction, explaining the tendency of  $f_c$  to increase with slice thickness.

For comparison figure 6.5 shows a histogram of values of  $f_c$  observed in dynamic MR scans of 18 renal transplants (data obtained as part of the data analysis in [16]). In this cohort the cortical fraction ranged from 0.30 to 0.73 with an average of 0.54. These scans were all done with a slice thickness of 6 mm.

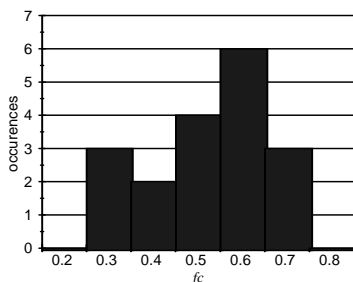


Figure 6.5: Histogram of cortical fraction distribution determined from 18 different studies.

The cortical fractions in the anatomical data set and those observed by MR have similar values. Therefore extrapolation of the trend (slow increase of  $f_c$  with thickness) observed in the anatomical data to all other kidneys is reasonable.

### 6.3.3 Signal to noise ratio versus cortical fraction.

In MRI the noise level is almost independent of slice thickness or tissue type. Therefore we use  $\sigma_i = \sigma_c = \sigma$  and in case the cortical fraction is zero  $\sigma_m = \sigma$ . The medullary signal  $s_m$  is independent of the cortical fraction. When the cortical fraction increases  $\sigma_m$  will start to differ from  $\sigma$  as a function of  $f_c$ . We can calculate the relative signal to noise ratio as a function of  $f_c$ .

$$RSNR_m(f_c) = \frac{s_m(h)/\sigma_m(f_c)}{s_m(h)/\sigma_{m,f_c=0}} = \frac{\sigma_{m,f_c=0} s_m(h)}{\sigma_m(f_c) s_m(h)} = \frac{\sigma}{\sigma_m(f_c)} \quad (6.4)$$

Combining formula (6.2) and (6.4) yields

$$RSNR_m(f_c) = \frac{\sigma}{\frac{\sqrt{\sigma_i^2 + f_c^2 \sigma_c^2}}{1 - f_c}} = \frac{(1 - f_c)\sigma}{\sqrt{1 + f_c^2}} = \frac{(1 - f_c)}{\sqrt{1 + f_c^2}} \quad (6.5)$$

In figure 6.6 the dependency of the  $RSNR_m$  on the cortical fraction as described by (6.5) is presented.

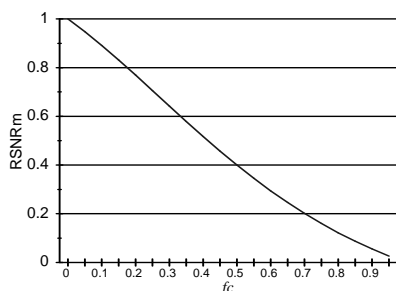


Figure 6.6: The relative signal to noise ratio ( $RSNR_m$ ) of the medulla as function of  $f_c$  with slice thickness  $h=6$ .

### 6.3.4 Relative medullary signal to noise ratio versus slice thickness.

Since the signal intensity depends on the slice thickness we can calculate the SNR as a function of slice thickness relative to the SNR at 6mm and  $f_c=0$ .



Optimal scanner settings for semi automatic renogram determination.

---

$$RSNR_{m,h=6}(f_c, h) = \frac{s_m(h) / \sigma_m(f_c)}{s_{m,h=6} / \sigma_{m,f_c=0}} = \frac{\sigma_{m,f_c=0} s_m(h)}{\sigma_m(f_c) s_{m,h=6}} = \frac{\sigma}{\sigma_m(f_c)} \frac{s_m(h)}{s_{m,h=6}} \quad (6.6)$$

Since  $s_m(h)/s_{m,h=6}$  can be approximated by (6.3), we get:

$$RSNR_{m,h=6}(f_c, h) = \frac{(1-f_c)}{\sqrt{1+f_c^2}} (0.116h + 0.30) \quad (6.7)$$

To show how the SNR depends on slice thickness, we substitute the cortical fractions from table 6.2 in equation (6.7) to obtain figure 6.7. The figure shows that for all positions, increasing the slice thickness up to 15 mm can produce a net gain in signal to noise ratio.

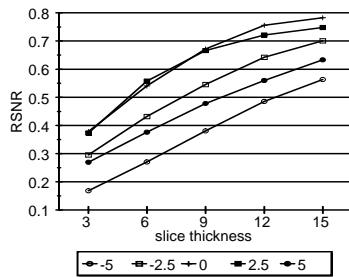


Figure 6.7: Relation between relative signal to noise ratio and slice thickness for the different slice locations in the model.

### 6.3.5 Discussion

From figure 6.7 it can be deduced that the largest slice thickness gives the best results. These results are however based on the cortical fractions obtained from the model, and thus on only one kidney. The measurements of the cortical fraction in patients, based on slices centrally in the kidney, varied as shown in figure 6.5. When we combine a higher cortical fractions ( $f_c=0.6$ ) from one of these patients with the increase of cortical fraction as observed in the central slice of the model, the RSNR would reach a maximum and decrease with further increase of slice thickness, as shown in figure 6.8. For that reason, and to prevent that the curvature of the kidney could become a problem for the cortical ROI, we advise a slice thickness of 12 to 15 mm.

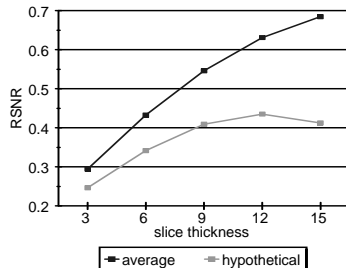


Figure 6.8: The relative signal to noise ratio based on the average  $f_c$  values of table 6.2 and a hypothetical curve based on an increase of cortical fraction as demonstrated in the middle slice of the model and a cortical fraction of 0.6 at slice thickness 6 mm.

#### *Through slice movement induced noise*

A specific problem of single slice imaging is caused by the slice selective spin saturation. If the tissue being imaged moves perpendicular to the image slice (through slice movement), non-saturated spins will enter the slice and disturb the intensity measurements. The non-saturated spin signal will add to the image intensity, especially when the movement occurs at the time where the center of k-space is scanned. The added image intensity is large in T1 weighted imaging because in that case the difference in saturation is large. The added image intensity will further be large for thin slices and high velocity of movement. In our situation, the most important movement of the kidney is caused by respiration. This certainly holds for native kidneys, but to a lesser degree it can be seen as well in the transplanted kidney. The period of respiration (4 – 6 s) and the frame to frame time of the imaging sequence (2 s) interfere so that the added signal intensity becomes a function of frame number. This means that respiratory movement of the kidney can be an important source of additional noise in the TI-signal.

Signal amplitude modulation by movement perpendicular to the slice has been treated before by Friston [20], but the problems in the abdomen are different. The movement induced intensity changes in the abdomen are more localised while at the same time the movement, and thus the intensity changes, can be larger.

## 6.4 Slice orientation.

Kidney movement due to respiration of the native kidney is approximately rectilinear. Native kidneys are located close to the musculus erector spinae and the plane of movement of the kidney is parallel to the surface of this muscle as shown in figure 6.9. This means that through plane movement can be reduced effectively

Optimal scanner settings for semi automatic renogram determination.

---

by selecting a slice orientation parallel to the movement direction (psoas surface). When imaging both kidneys at the same time, usually one slice orientation satisfies this condition in good approximation for both kidneys, so that the suggested orientation is useful for clinical functional kidney imaging as well. The experiments shown in the remainder of this section use this slice orientation.

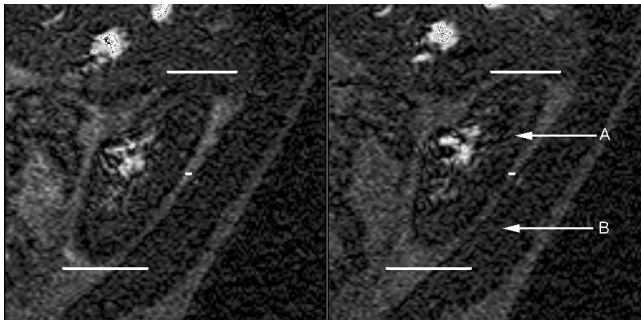


Figure 6.9: Saggital images of the kidney during different phases of breathing. The three lines have exactly the same location in both images. Via the two long lines the movement of the kidney can be observed while the small line between kidney and muscululus erector spinae shows that the distance between those two remains constant. The arrows indicate the kidney (A) and the muscululus erector spinae (B).

## 6.5 Single or multi slice

The scan parameters in table 6.1 describe single slice imaging. This method was applied as a compromise since the MRI scanner could not measure one image per two seconds in a multi slice scan. The compromise was acceptable because we do not discriminate between different areas of the kidney and the extra information gathered by using a multi slice imaging method comes at the cost of increased frame to frame time.

However, by using multi slice imaging, through slice movement induced noise should be strongly reduced. This is because the spins in multiple slices are saturated, and, except for the outer slices, when through slice movement is present, the saturated spins that are moved out of the slice are replaced with other equally saturated spins. The reduction depends on the slice distance and potentially on the slice profile.

### 6.5.1 Experiments

To check if a multi-slice approach reduces the TI-signal noise we made two dynamic scan series without contrast agent. The first series used the default

parameters of table 6.1. Figure 6.10 compares two successive single slice images of the right kidney during respiration. It can clearly be observed that the strong through plane movement that occurred between these images has caused a considerable increase in brightness in the latter image. This is particularly clear in the fat tissue below the kidney, but also intrarenal pixel intensity changes can be seen. Figure 6.11-a shows the TI-signal of the same scan for a ROI in the fat tissue. Occasional bright ROI signals occur and add to the noise behaviour of the TI-signal.

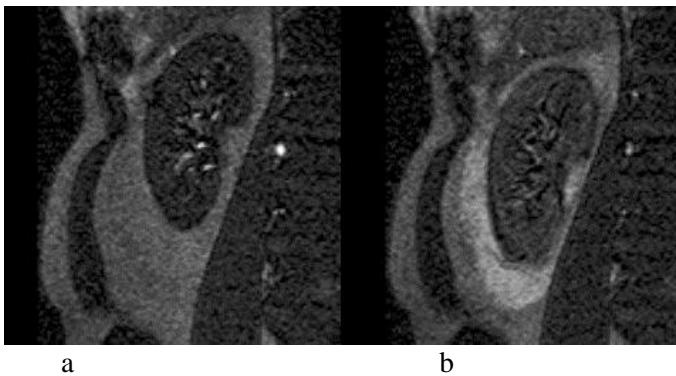


Figure 6.10: Pixel intensity changes in and around the right kidney in a single slice scan. Shown are the normal pixel intensities (a) and the pixel intensities just after end inhalation (b).

The second series used nearly the same parameters, but now the scan was a multi slice scan of three adjacent slices [21]. Scanner facilities were more favorable than at the time when the scan parameters of table 6.1 were selected and as a result, the multi slice scan repetition time remained almost the same ( $TR = 12\text{ms}$ ) while echo time ( $TE = 1.4\text{ms}$ ) was reduced. The TI-signal in this scan is shown in figure 6.11-b for the same ROI as used for figure 6.11-a.

To measure the intensity changes we placed three ROIs in the images, two inside the kidney and one in the fat below the kidney. We verified that the ROIs remained in an area of homogeneous signal in all images, recorded during the respiration displacement of the kidney. The TI-signals of the three ROIs were recorded in the single slice scan and in each of the three slices of the multi-slice scan.

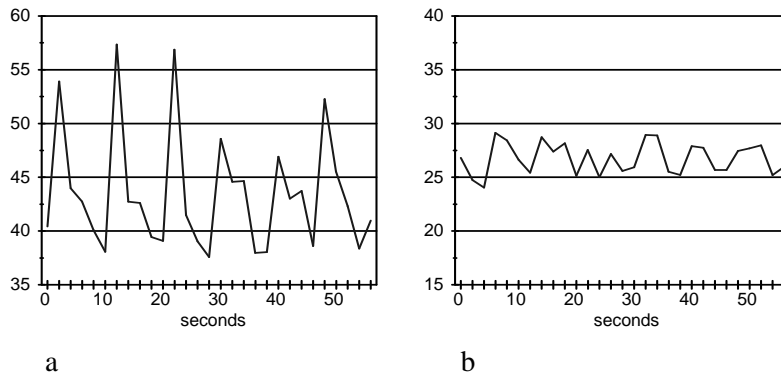


Figure 6.11: TI-signal of the ROI in the fat tissue in the single slice scan (a) and the middle slice of the multislice scan (b). The breathing period is easily recognisable in the single slice scan.

If the noise in the TI-signal is determined by the noise in each image and not also by changes in the average intensity between images, the signal-to-noise ratio of the TI-signal ( $SNR_{TI}$ ), determined from its average value and standard deviation, should be equal to the average of the signal-to-noise ratios determined from the corresponding ROI ( $SNR_{ROI}$ ) in each image separately. If changes in the average value occur the standard deviation of the TI-signal increases. We therefore calculated the signal-to-noise ratio in both ways, taking into account that the standard deviation of the TI-signal will be smaller by a factor equal to the square root of the number of pixels in the ROI because the TI-signal represents the average value of the intensity in the ROI. The latter estimate of the TI-signal signal-to-noise ratio we call expected SNR. Since the signal intensities in both scans were not equal (due to different scanner settings for TE) the signal to noise ratios could not directly be compared. Therefore we calculated the ratio between expected SNR and the actual  $SNR_{TI}$ . This is a measure for the noise induced by movement and the results are shown in table 6.3. For kidney tissue the gain is roughly a factor two.

Table 6.3: The ratio of  $SNR_{TI}$  to  $SNR_{ROI}$  in 3 ROIs.

	Single slice	MS, slice 1	MS, slice 2	MS, slice 3
Fat	0.09	0.12	0.25	0.20
Right kidney	0.47	0.54	0.76	0.71
Left kidney	0.27	0.38	0.55	0.49

### 6.5.2 Discussion

The table shows the obtained increase in SNR in the multi slice scan, especially in the central slice. The noise reduction in the multi slice scan as shown in table 6.3 is

a-symmetrical, the ratios of the outer two layers are not equal. This could be due to the different movement speeds during inhaling and exhaling.

The ratio  $SNR_{TV}/SNR_{ROI}$  in the middle slice still is not equal to 1. There are two reasons for this. The first reason is that the slice profiles with which the scanner saturates the tissue are not exact square waves so that the saturation distribution is not entirely flat over the entire slice. The second reason is analyzed by Friston for brain imaging [20]; when the RF pulses are given at slightly different moments for each slice, it is possible that tissue has moved between RF pulses so that some of it is “missed”.

## 6.6 Conclusions

From the measurements it becomes clear that in general the signal to noise ratio of both the image as well as the renograms improve with increasing slice thickness. Although, according to model calculations, the cortical fraction increases with increasing slice thickness and thus causes more noise in the medullary renogram, in general the gain in signal to noise ratio due to increasing slice thickness outweighs the losses incurred by the increased cortical fraction. Since this might not hold true for very high cortical fractions and to prevent the curvature of the kidney from interfering with a pure cortical ROI, we propose to use a slice thickness of 12 mm.

The presence of through slice movement introduces strong variations in the image intensity which appears as noise on the MR renograms. By angulating the coronal scan plane parallel to the musculus erector spinae and by using a multi slice scan these effects can be reduced considerably.

## 6.7 Acknowledgement

The preparation of the kidney and the hardware needed for digitising it to create the anatomical kidney model were kindly provided by the Department of Anatomy and Embryology, Maastricht University, the Netherlands.

## 6.8 References

- 1 R Kikinis, G von Schulthess, P Jäger, et al. Normal and Hydronephrotic Kidney: Evaluation of Renal Function with Contrast-enhanced MR Imaging. *Radiology* 1987; 165:837-842.

- 2 Takeda M, Katayama Y, Tsutui T, Komeyama T, Mizusawa T. Does Gd-DTPA enhanced MRI of the kidney represent tissue concentration of contrast media in the kidney: In vivo and in vitro study. *Mag. Res. Im.* 1994; 12:421-427.
- 3 P Heintz, Ch Ehrenheim, H Hundeshagen. Gd-DTPA in MRI and 99m Tc-DTPA in the examination of the perfusion of transplanted kidneys. *Diagnostic Imaging International* 1988; November, Supplement.
- 4 P Choyke, J Frank, M Girton, et al. Dynamic Gd-DTPA-enhanced MR Imaging of the Kidney: Experimental Results. *Radiology* 1989; 170:713-720.
- 5 M Carvlin, P Arger, H Kundel, et al. Use of Gd-DTPA and Fast Gradient-Echo and Spin-Echo MR Imaging to Demonstrate Renal Function in the Rabbit. *Radiology* 1989; 170:705-711
- 6 R Semelka, H Hricak, E Tomei, A Floth, M Stoller. Obstructive Nephropathy: Evaluation with Dynamic Gd-DTPA-enhanced MR Imaging. *Radiology* 1990; 175:797-803.
- 7 H Munechika, D Sullivan, Hedlund, et al. Evaluation of Acute Renal Failure with Magnetic Resonance Imaging Using Gradient-Echo and Gd-DTPA. *Invest Radiol* 1991; 26:22-27
- 8 O H el on, E Attlam, C Legendre, et al. Gd-DOTA-enhanced MR Imaging and Color Doppler US of Renal Allograft Necrosis. *RadioGraphics* 1992; 12:21-33.
- 9 Th Vestring, K Dietl, A Fahrenkamp, et al. Die Rindennekrose der Transplantatniere. *Fortschr. R ntgenstr* 1992; 156,6: 507-512
- 10 P Ros, J Gauger, C Stoupis, et al. Diagnosis of Renal Artery Stenosis: Feasibility of Combining MR Angiography, MR Renography, and Gadopentetate-Based Measurements of Glomerular Filtration Rate. *AJR* 1995; 165:1447-1451.
- 11 R Sharma, R Gupta, H Poptani, et al. The Magnetic Resonance Renogram in Renal Transplant Evaluation using Dynamic Contrast Enhanced MR Imaging. *Transplantation* 1995; 59: 1405-1409

- 
- 12 N Grenier, H Trillaud, C Combe, et al. Diagnosis of Renovascular Hypertension: Feasibility of Captopril-Sensitized Dynamic MR Imaging and Comparison with Captopril Scintigraphy. *AJR* 1996;166:835-843.
  - 13 T Roberts, Physiology Measurements by Contrast-Enhanced MR Imaging: Expectations and Limitations. *JMRI* 1997; 7:82-90.
  - 14 D Szolar, K Preidler, Ebner, et al. Functional Magnetic Resonance Imaging of Human Renal Allografts during the Post-Transplant Period: Preliminary Observations. *Magnetic Resonance Imaging* 1997; 15:727-735
  - 15 DenBoer JA, DePriester JA, Geerlings MJHM, et al. Quantitative model description of dynamic MRI enhancement data of the kidney. *JMRI*, submitted.
  - 16 J. A. de Priester, J. A. den Boer, E. L.W. Giele, M. H.L. Christiaans, A. Kessels, A. Hasman, J. M.A. van Engelshoven. MR Renography: An Algorithm for Calculation and Correction of Cortical Volume Averaging in Medullary Renographs. *JMRI* 2000;12:453-459.
  - 17 E Giele, J de Priester, J Blom, J den Boer, J van Engelshoven, A Hasman. Reduction of noise in medullary renograms from dynamic MR Images. *Journal of Magnetic Resonance Imaging*. *JMRI* 2000;11:149-155
  - 18 E Giele, J de Priester, J Blom, J den Boer, J van Engelshoven, A Hasman. Evaluation of two cortical fraction estimation algorithms for the calculation of dynamic magnetic resonance renograms. Accepted for publication in *Computer Methods and Programs in Biomedicine*.
  - 19 Lataster LM, Rensema JW, van Mameren H, Drukker J. Transverse sections of the elbow region in man, made into transparencies and embedded in plastic in a self-study module. *Acta Morphol Neerl.-Scand.* 22, 253, 1984
  - 20 K Friston, J Ashburner, C Frith, J Poline, J Heather, R Frackowiack. Spatial Registration and Normalization of Images. *Human Brain Mapping* 1995; 2:165-189
  - 21 Kindly provided on an experimental basis by Jan Groen of Philips Medical Systems.



Optimal scanner settings for semi automatic renogram determination.

---

## Chapter 7

---

# Discussion and Conclusions

---

### 7.1 General discussion

The research described in this thesis is one of two parts in a tandem study. It focuses on the technical problems encountered during acquisition of MR renograms while the counter part focuses on the clinical possibilities of these renograms.

Doing research in a clinical environment with patients as volunteers to test new analysis methods can lead to special problems not present in a technical or physical research lab. The progress of the experiment is dependent on the availability of patients with a particular disease. These volunteers have to be informed thoroughly and give written consent before an experiment can start which reduces the number of subjects and thus the number of experiments that can be done.

### 7.2 Conversion of images to numerical data

MRI has the ability to generate high resolution, cross-section images of the kidney, thus the contrast agent arrival can be observed in the cortex as well as in the medulla. This in contrast to radionuclide scanning. In previous research as described in literature small ROIs in cortical and medullary tissue were selected manually and the average intensity of each ROI was registered as a function of time to generate cortical and medullary enhancement curves. However, it is sometimes very difficult to visually delineate renal cortex and medulla and to place the ROIs accurately. This is especially true in small shrunken kidneys. Besides, even if cortex and medulla are discernible, the borders between the two tissues are not sharply demarcated and information about the border in the third dimension is totally lacking. The outer border of the cortex, being the outer contour of the kidney, is smooth and easily recognisable but the cortex encapsulates the medullary tissue and that border is tortuous and unpredictable. As a result the placement of a

medullary ROI is always difficult and not accurate. To prevent the voxels selected in the medullary ROI from penetrating the cortex we chose a small slice thickness of 6 mm, which at that time seemed to be a reasonable compromise between the obtainable quality of the ROI definition and the level of signal to noise ratio in the images. As it later turned out, even this small slice thickness was not enough to prevent partial volume effect.

The presence of cortical contribution is not visible in the images but can be found back in the signals. For these reasons we developed a method to correct for the cortical contribution based on the assumption that the kidney consists of two homogeneous tissue types, cortex and medulla, and that the image intensity is a linear addition of the contributions of both tissues. This was proven to be a valid assumption in the tandem study. It allows the use of weighted subtraction of the cortical signal from the medullary signal to calculate the pure medullary renogram. Once that correction is introduced the choice of slice thickness can be reconsidered, as discussed in chapter 6.

A major problem with MR renography is the low signal to noise ratio in the images, which is far lower than for example with brain imaging. Imaging in the abdomen requires the use of the MR scanner's main body coil which results in a low signal to noise ratio. The high temporal resolution demands a very short imaging time which reduces the possibilities to increase the signal to noise ratio. Also, due to the high concentration factors of the contrast agent in the kidney, a choice has to be made between allowing saturation effects or using scanner parameters which result in an even lower signal to noise ratio. We chose to avoid saturation effects since they would reduce the reliability of the renograms.

### *7.2.1 Segmentation*

To obtain the kidney contour the average of several post contrast images is subtracted from the average of several pre contrast images and this subtracted image is then thresholded. Not the entire kidney border will show early enhancement; in the area of the renal pelvis there is no cortex and thus no enhancement. Therefore the contour is closed with a default closing algorithm resulting in the convex shape on which the onion ring ROI placement is based. The obtained kidney contour was then copied to all images, assuming that their movement was negligible. In transplanted kidneys this is a reasonable assumption. In the case of native kidneys no such assumptions can be made because these kidneys move over a distance of up to centimetres during breathing. Dynamic imaging of the native kidney requires additional precautions (e.g. breath holding) or correction of movement before our method of segmentation can be applied.

---

Segmentation on single images would avoid the need for a movement correction algorithm, but is almost impossible due to the noise. Figure 7.1 shows an example of one of the more difficult cases and gives an indication of the noise in the images and the low contrast possible between kidney and surrounding tissue.

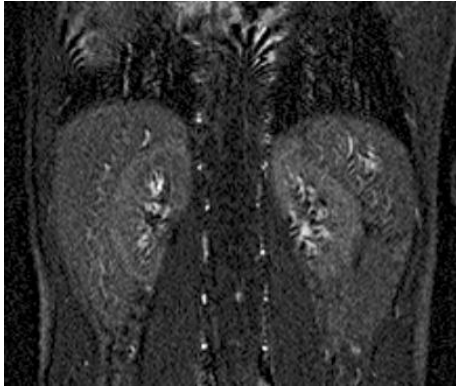


Figure 7.1: Dynamic image of two kidneys of a healthy volunteer 20 seconds after maximum contrast enhancement.

This is also the reason why segmentation based movement detection did not function (discussed further down). Since segmentation on single images did not show any promise and the above mentioned method works accurately for non-moving kidneys, we did not investigate other methods and used the method described above to segment the kidney as the basis for the ROI placement.

Noise reduction with filtering for the purpose of segmentation is made difficult by the shape and structure of the kidney, in combination with the low contrast and high noise levels. Reducing the noise, for example with a gaussian filter, enough to make edge detection possible requires a kernel which is larger than the cortex and medulla are thick. This results in blurring of the renal tissue with the renal pelvis and will reduce the contrast between kidney and periphery even further, making segmentation on these images highly unreliable.

### 7.2.2 ROI placement

The calculation of the onion rings is an extension on the kidney segmentation. The advantage of the onion ring ROI placement is that it is relatively simple. It does not require knowledge about the actual location of the cortex-medulla interface. In the images used during this research, the border between cortex and medulla was often hard to discern (and then only during the early phase of the contrast enhancement), and it is expected that in diseased kidneys the differentiation becomes even harder. The onion ring ROIs are placed independent of the exact location of cortex and

medulla and follow the outside contour of the kidney. Since the contour of the kidney is closed during segmentation the rings continue through the renal pelvis. To exclude this part of the rings we opted for a manually drawn exclusion line. This approach allows the operator to exclude other unwanted areas of the ROIs (e.g. infarcted areas) as well, but the disadvantage is that an element of subjective choice remains part of the ROI determination.

It might be worth evaluating if the thresholded subtraction image, as used for locating the kidney, can be used to automatically exclude the renal pelvis from the ROIs. Multiplication of the thresholded subtraction image with the onion rings will remove the renal pelvis from the rings but has the complication that medullary areas which do not yet show enhancement in the images used for the subtraction might become excluded as well, so a form of closing is needed which fills the medullary areas but keeps the renal pelvis open.

The main alternative to the use of onion ring ROIs are medullary ROIs selected by a radiologist based on a visual criterion and hence on the medulla signal in one or more of the images. Copying to the remaining images is still necessary. This alternative has a few advantages, which have mainly to do with the localised nature of the ROIs. Small localised ROIs enable the radiologist to indicate from which area of the kidney a renogram should be obtained and result in a lower cortical contribution in the medullary renogram. Also there is no need for a kidney segmentation as described above. The main disadvantages are (a) the low signal to noise ratio of the small ROI and (b) that despite the careful selection the likelihood of a cortical contribution in the medullary renogram remains high and the correction mechanism remains necessary.

A second alternative, which we did not investigate, is to use a combination of both discussed possibilities; using onion ring segmentation and dividing the onion rings in several parts. Although this would lower the signal to noise ratio of the resulting renograms, the results could indicate possible problem areas in the kidney. We think that, unless a serious increase in signal to noise ratio is achieved, an attempt to work with smaller ROIs will have only limited success.

### 7.2.3 ROI size

The choice of ROI size was based on a comparison of the correlation between signals originating from elementary onion rings with a thickness of 1 pixel. From a physiological point of view the hypothesis that the enhancement is independent of the location within each tissue is slightly questionable because the nephron path is highly organised, especially in the medulla. This would leave considerable timing differences in the response of a medullary ROI, depending on its radial position.

Since timing differences reduce the correlation between two equal signals notably, the observed high correlation between the elementary onion shells can be seen as a confirmation of our assumption that the enhancement behaves as if the enhancement is location invariant for each tissue.

#### *7.2.4 Exclusion of pixels from the medullary ROI*

The advantage of small ROIs in the medulla is their lower cortical contribution in comparison with our onion rings. It is however possible to reduce the cortical contribution to the medullary onion ring ROI. To achieve this we use the method described in chapter 4 where, based on the cortical renogram and the intensity changes of each individual pixel, those pixels most resembling cortex are removed from the medullary ROI. It is important to note that this method only reduces the amount of cortical tissue from the medullary ROI. The selection is based on the match between the enhancement curves of individual pixels and the cortical enhancement curve.

Pixels with a different enhancement pattern than that of the cortex will not be removed. Therefore still care has to be taken not to include pixels representing voxels which contain tissue other than cortex or medulla. The use of this method in combination with a large medullary ROI was therefore not investigated: the possible inclusion of calyx or renal pelvis may lead to unacceptable distortion of the medullary signal.

#### *7.2.5 Movement correction*

The methods described in chapter 2 to 4 were all developed using transplanted kidneys because these kidneys do not move during breathing. Since it is expected that MR renograms can also give a valuable contribution to the diagnosis of native kidneys, a method was needed that would allow the techniques developed on transplanted kidneys to be used on the moving native kidneys. Two options were available: scanning with breath holding or the use of a movement correction algorithm.

Scanning during breath holding (with intermittent breathing periods because a full scan takes at least three minutes) is potentially problematic for three reasons: a) The data series is interrupted at times when the patient is breathing and this may make interpretation of the enhancement curve uncertain. b) Whereas in the free breathing mode the spin saturation is in a steady state, this is not the case in the intermittent mode, leading to a bright first image after each breathing period (partial solutions could be the addition of a run-in period of the data acquisition after each breathing period or a continuation of the RF pulses during breathing periods; solutions not available on the actual scanner). c) It has been shown

recently by Vasbinder et al. [1] that even during breath holding the kidney moves. Especially during breath holding after inhalation (which can be maintained longer than after exhalation) the diaphragm moves, and thus the kidney moves as well. This would render the entire exercise of breath holding useless.

We therefore chose to scan during free breathing and to develop a method that could correct for the movement of the kidney in the images. We surveyed the movement and shape changes of the kidney using overlays on the images in the series. It was concluded that the rotation of the kidney is negligible and the shape changes are mainly caused by through slice movement, something which can be prevented by appropriate angulation of the scan plane. Since there is only translation of the kidneys we can shift the entire image in the opposite direction of the movement. The other structures in the images are not used and thus their location is unimportant. The method developed and the reasons to use it are discussed elaborately in chapter 5.

The main problem with the suggested movement correction remains the manual check of the results in all images. Although the time the operator has to spend is reduced considerably since he only has to acknowledge all the right movement corrections, in all the cases that something goes wrong he still has to correct manually. An advantage of the method is that this correction has no repercussions for later images. When we started our study, we chose 6 mm slice thickness (to prevent partial volume effect) and we have maintained this slice thickness during the entire study. An increase in slice thickness will result in an improved signal to noise ratio in the images and we expect an increased performance of the movement detection algorithm.

A choice we made at the beginning of the study which turned out to be rewarding was the high temporal resolution. Not only could the arterial passage be observed with sufficient detail, which was the reason for choosing it, but also the problem of movement may have been reduced considerably by the short scan time (e.g., at very short scan times there is hardly any blurring and the movement of the kidney is visible in the scan series; with relatively large scan times there is no motion, only blurring). To estimate the role of unsharpness, one should realise that of the total scan time, the signal in the central time fraction is by far the largest; this is often called "the centre of k-space". That central time fraction is the equivalent of the exposure time in normal photography and may determine to a large extent the unsharpness. At a scan time of 2 seconds, the central time fraction is likely to be less than half a second. Although at the start of our study 2 seconds per image was the minimum time we could achieve, at the end of our study it was possible to reduce the time per image, but an increase of temporal resolution was not investigated.

### 7.2.6 *Suggested changes of scanner settings*

Changes of scanner settings that were investigated are the choice of slice thickness, slice orientation and the possibility of multi-slice imaging. The small slice thickness we chose at the beginning of the study was maintained during the entire study, although the correction for cortical contribution did remove its necessity. In chapter 6 the effects on the renograms of other slice thicknesses are discussed extensively. Also used in this chapter is an anatomic computer model of the kidney which we used earlier in the study to gain some insight in the structure of the kidney, especially in the third dimension. The creation of this model was very time consuming, which is the main reason that only one kidney was modelled. From the model it was concluded that the cortical fraction is only slightly dependent on the thickness of the slice in a slice through the kidney centre.

## 7.3 **Usability of techniques for other clinical research**

The tools developed in this thesis can globally be divided into two areas. Robust data retrieval from dynamic image series of non moving kidneys (chapter 2, 3 and 4) and movement correction for such series taken from moving kidneys (chapter 5). The usability of the partial volume correction methods and algorithms for other tissues in the human body is fairly limited, since the algorithm uses highly specific properties of the kidney that may not be found in other tissues.

However, the movement correction method is based on universal principles and there are almost no limits to its use in the body for large displacements. Since its accuracy is limited to one pixel and it assumes a constant shape of the organ it is only useful in situations where there are large displacements and no notable change of shape. For this mainly abdominal imaging comes to mind.

The scan parameters as suggested in chapter 6 (thick multiple slice acquisition) have not been used in clinical series. Therefore there neither is information on the accuracy of the enhancement data, nor on the performance of the movement correction that can be reached with this acquisition method in clinical practice. Because of the reduction of noise it is expected that the results of movement correction will be more stable, reducing the number of corrections needed from an operator. Also the considerations described to prevent image intensity artefacts caused by through slice movement are valid for all single slice dynamic imaging methods.



#### **7.4 Contribution of this research to the clinical use of MR renography**

Since this study was a tandem study, as mentioned in the first paragraph, its targets were closely related to facilitating the accompanying clinical research. The method for cortical fraction estimation which was developed together with a radiologist and the movement correction algorithm are both necessary elements of the clinical investigation. Without these it would be impossible to measure the medullary renogram respectively measure renograms from native kidneys.

On the other hand the reduction of noise and the increase in accuracy in the renograms by removal of high  $f_c$  pixels or by thick multi-slice imaging are deemed useful, but no hard data is yet available how necessary they are for diagnosis. Implementation of a study using thicker slices and the method for removing high  $f_c$  pixels within a clinically acceptable time was not feasible. The first clinical results collected with our method of MR renography to date (appendix B) show that the present accuracy is sufficient for clinically interesting conclusions. However, we expect that an increase in signal to noise ratio of the images will have a positive effect on the accuracy and robustness of the movement correction algorithm. Also, the increased reliability of the ROI signals is expected to allow more precise data and this will almost certainly be relevant for any clinical practice based on clinical diagnostic use of MR renography

#### **7.5 Image processing**

The image processing methods described in this thesis make use of standard procedures in most cases. The research was in the first place meant to solve problems in MR renogram acquisition and not on developing new methods for image processing. That the methods used are often very basic is caused by the low signal to noise level in the images, which prohibits the use of more advanced techniques.

##### *7.5.1 Registration: no sub-pixel accuracy*

Something which is fairly standard by now is sub-pixel accuracy when registering two images. MR renography can, in theory, profit from sub-pixel accuracy when determining the movement of the kidney. The rounding off of movements to entire pixels and the propagation of the round off differences can be a source of errors for the motion correction. Also, the distance the kidney moves is not an exact multiple of the pixel width, resulting in a possible maximum mismatch of the ROI on the kidney of half a pixel.

In the case of error propagation the gain of using sub pixel accuracy remains questionable though. Since the motion correction algorithm still makes an error equal to or larger than 2 pixels in 13% of the cases, the main problem is not the small one pixel error that is the result of the addition of small round off differences. For the same reason the reliability of sub pixel movement will be very low.

A test on inter observer variability showed that two operators often disagreed on the exact location of the kidney.

Table 7.1: Interobserver variability in determining kidney location on 4 patient series.

Difference between operators	0	1	2	>2
Number of times	689	262	51	18

### 7.5.2 Interpolation

Assuming sub pixel accuracy to be possible, the increased accuracy of the ROI location thus achieved is only useful when it is possible to adjust the borders of the ROI to the new location. Since these are located between the pixel borders, interpolation is needed.

Due to the very low signal to noise ratio, especially in the contrast between the different tissues, interpolation to calculate the new shifted image becomes very hard. Even if it would be possible it is questionable if first calculating pixel values and then averaging these values as the input for the renogram measurement will improve accuracy.

It should also be noted that in experiments with misalignment of the ROIs on the kidney, where the ROIs were moved alternatingly up and down over a pre determined distance, a misalignment of 1 pixel did not notably influence the curves or the calculated cortical fraction. Misalignment of 2 pixels caused a notable difference in the cortical curve which also influenced the calculated cortical fraction.

### 7.5.3 Registration methods

For the movement correction we tested several fairly basic registration algorithms. There are many different types of registration methods possible which can be divided into several categories [2]. Extrinsic registration uses artificial markers which are attached to the object. In the case of kidney movement detection this would require surgery, and is thus not suitable. Intrinsic registration methods are based on properties of the image itself. These can be landmark based, where easily recognisable points in the image are used, segmentation based, where the image is

## Discussion and Conclusions

---

first segmented and the thus found structures are registered with each other, and voxel property based, which works directly on the grey values of the images. Since there are no clear landmarks in the kidney which can be used for registration this method can not be used and segmentation of the kidney on single images is not possible either. Therefore we only tested methods which are voxel property based.

Methods of which we did not describe results in this thesis are the method used by Friston and mutual information maximisation which are both voxel property based registration techniques. The method as proposed by Friston was evaluated visually, and was abandoned for the reasons mentioned in chapter 5.

Mutual information maximisation [3-5] is used for matching both inter and intra modality images and is based on the assumption that there is a coherence between pixel intensities in two images. In the case of two images in a dynamic series without contrast agent there is of course a one to one relationship. With contrast agent our assumption that the enhancement is location independent for each tissue also leads to a strong coherence and thus the registration has a strong resemblance with multi modality registration where tissues often have different intensities depending on the imaging method. However, when the signal intensities in the image are all very close together and there is a relatively high noise level, as is the case with our MR images of the kidney, the entropy is mainly determined by the noise instead of the extent of misalignment. This reduces the effectiveness of the method and results in a low success rate in aligning the kidneys.

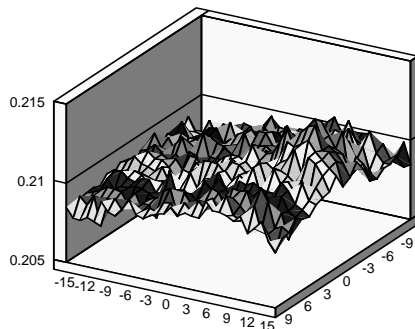


Figure 7.2: Example of mutual information maximisation registration. Compare with figure 5.2, 5.7 and 5.8.

In table 7.2 we compare the performance of the mutual information maximisation method with the results of the PDMD method. The results demonstrate that mutual information maximisation is not suitable for this kind of noisy low contrast images.

Table 7.2: Comparison between PDMD and mutual information maximisation for motion detection in two patient series.

Error size	0	1	2	3	4	>4
PDMD	410	78	17	3	2	0
Mutual information maximisation	163	173	60	30	26	26

#### 7.5.4 Processing speed

Not much attention has been paid to increasing the speed of the algorithms used, unless their slow performance made evaluation impractical (for example the image matching method for movement correction uses hill climbing). The main reasons are that (a) the research described in this thesis focused on evaluating the merits of the methods for MR renogram measurement and the optimisation of those methods focused entirely on accuracy of the results and (b) that since computers get faster every day, algorithm optimisation may become superfluous with the next computer generation.

## 7.6 Recommendations for further research

Due to time constraints several aspects could not be studied. As has already been mentioned several times, we expect that the performance of the movement correction algorithm will increase with thicker slices. This is something that should be studied as it potentially reduces the operator input for the movement correction, improving the automation of the method.

A lot of effort went into the improvement of the signal to noise ratio of the renograms. Since currently these renograms are fitted to a smooth curve described parametrically, it would be interesting to know how the accuracy of these parameters depends on the noise in the images. We have not tested the influence of a change in image time. A longer image time could result in better compromise between signal to noise and motion artefacts, but it also implies a loss of definition of the sharper features of the measured renograms. The net gain from such a change in the scan parameters could be tested objectively by comparing the means and the uncertainty of the fitted enhancement parameters.

Finally, it would be interesting to see if scans of the entire kidney, as opposed to the current single slice scan, would result in more reliable data or useful data on the kidney which is not yet available. The implementation of a 3D or multi-slice scan with enough slices to include the entire kidney would require either faster MR scanner technology or longer scan times, in which case it should of course be weighted against the associated loss of information in the enhancement data.

## 7.7 Conclusions

For the analysis of MR renograms several problems had to be solved. First, the kidney and its different functional areas had to be located in the images. Second, the image intensity changes in these areas had to be tracked. Since it turned out that mixing of these signals was unavoidable they had to be separated functionally. Third, in the case the segmentation cannot be performed on single images but has to be done on a set of images, a correction for movement needs to be developed for those cases where movement is present, as for example is the case in native kidneys. The following can be concluded.

1. Only shortly after arrival of the contrast agent the kidney shows sufficient enhancement that reliable automatic segmentation is possible.
2. Since the outer layer of the kidney consists of cortex there is no need for a separate segmentation of the cortex; (a thin) ROI following the outer contour of the kidney suffices to measure the cortical enhancement.
3. It is usually impossible to find a ROI that gives a medullary signal without cortical contamination. The medulla is poorly discernable due to a complex course of the medulla-cortex tissue border, weak contrast and partial volume.
4. Medullary enhancement is delayed with respect to cortical enhancement and this effect can be used to determine the cortical contribution to the enhancement signal in a ROI that contains cortical as well as medullary tissue. The medullary signal from the same ROI can be found by weighted subtraction.
5. In view of conclusions 3 and 4, the preferred ROI shape for the observation of medullary signal is a large ROI giving a mixed signal with a high medullary fraction. Such an area can be defined as a concentric ROI located further inside the kidney than the cortical ROI. This leads to an onion ring like configuration of the cortical and medullary ROIs.
6. The concentric nature of the onion ring type ROIs conforms to the approximately radial structure of the kidney. This has the advantage that isochronic passage of the contrast agent in the nephrons translates in sharp enhancement peaks in the ROI signal.
7. Based on correlation between the signals from single pixel onion rings, the optimal cortical ROI is two pixels wide and the optimal mixed ROI is four pixels wide.

- 
8. Calculating the medullary signal with weighted subtraction when noise is present in the signals reduces the signal to noise ratio of the resulting medullary renogram. Higher weighting factors result in lower signal to noise ratios. Matched image filtering of the image with the cortical signal can show the areas which most resemble the cortex of the kidney and can then be removed. An average noise reduction of 23% could be achieved this way.
  9. The weighting factor for the weighted subtraction is calculated based on the time delay in enhancement between cortex and medulla. Since the signals from which this factor is calculated are noisy, a method is needed that is as insensitive to noise as possible. Iteratively changing the weighting factor until the medullary renogram shows no enhancement in the initial phase, calculated with a least squared error method, proved to be a stable method.
  10. To be able to obtain renograms from native kidneys, which move with breathing, a method is needed to detect the movement of the kidney and correct for it. With normal shallow breathing the kidney only translates in the image. The main problem for motion detection during the measurement of renograms is the change in contrast between kidney and periphery (sometimes even reversed) due to the contrast agent. Using a method which uses the (FFT) phase information in the image of the kidney and its immediate surroundings it is possible to automatically detect the exact movement in 68% and with one pixel deviation in 88% of the cases.
  11. We noticed that there was a difference in the noise as estimated per slice and the noise as estimated from the renogram. It was established that the additional noise was caused by unsaturated spins moving into the imaging slice. Using a multi-slice technique reduces the noise in the signal significantly.
  12. Because we developed a method to correct for the cortical contribution to the medullary signal, we were free to use thicker slices. Thicker slices result in a better signal to noise ratio and more partial volume effect. The resulting increase in cortical contribution and thus weighting factor and noise in the medullary renogram are more than compensated for by the increased signal to noise ratio.

## 7.8 References

- [1] Vasbinder B, Kaandorp D, Ho KY, van Engelshoven J. Motion of the Distal Renal Artery During 3D Contrast-Enhanced Breathhold MRA. *Proc. Intl. Soc. Mag. Reson. med* 2001, 9:391.

## Discussion and Conclusions

---

- [2] Maintz JB. Retrospective Registration of Tomographic Brain Images. PhD thesis, Universiteit Utrecht, 1996. ISBN 90-393-1227-3
- [3] Viola P, Wells W M. Alignment by maximisation of mutual information. International journal of computer vision 1997, 24(2):137-154
- [4] Maes F, Collignon A, Vandermeulen D, Marchal G, Suetens, P. IEEE transactions on medical imaging. 1997, 16(2):187-198
- [5] Pluim J. Mutual information based registration of medical images. PhD thesis, Universiteit Utrecht, 2000. ISBN 90-393-2749-1

## Appendix A

---

# Use of a Dynamic 3D Computer Model of the Kidney for Validation of Analysis Methods and Scan Parameters in Dynamic MRI of the Kidney.

---

### Introduction

To gain insight in the methods already developed and currently under development for the extraction of medullary renograms from dynamic MR images, a need was perceived for an anatomically based model simulating the distribution per voxel of relevant tissue types in the kidney. The model, as presented in figure A.1, and some of its potential uses are discussed. One test based on the model is worked out and results are shown.

One of the main problems in the extraction of medullary renograms is the partial volume effect; both voxel partial volume as well as region of interest (ROI) partial volume effect cause a cortical contribution in the raw cortico-medullary renogram. It is in theory possible to remove this partial volume effect by means of a data processing algorithm (see below). The anatomical model can be used to validate this algorithm.

Other problems are the (semi-automatic) placement of ROIs and the amount of noise in dynamic MR images, where an increased voxel volume reduces the noise but increases the partial volume effect. The anatomical model can be used to determine the voxel size allowing an optimal balance between signal to noise and partial volume. Finally, it enables determination of rules for automatic placement of the ROIs.





The contrast agent arrives later in the medulla than in the cortex, so a signal containing both a cortical and medullary contribution will show only the cortical characteristic enhancement in the first few scans after contrast agent arrival. The cortical fraction is determined by choosing an arbitrary  $f_c$  and modifying this value until the corrected signal (the cortico-medullary signal with the cortical signal weighted with  $f_c$  subtracted) remains at its pre-arrival level for the first 5 scans (10 seconds) after contrast agent arrival. By subtracting the  $f_c$  weighted cortical curve from the cortico-medullary one, the pure medullary signal is obtained.

To estimate the influence of image noise on the determination of  $f_c$ , two slices with a different thickness were generated, resulting in two slices with different values for  $f_c$ . For both slices  $f_c$  was determined using five different noise levels. Determination of  $f_c$  was repeated 2000 times for each noise level. The noise levels were chosen at values that were representative for the noise seen in real dynamic MR kidney scans as used in our laboratory. The standard deviation of the noise is expressed as a fraction of the signal enhancement in the cortical peak.

The calculated cortical fractions have a normal (gaussian) distribution with an average value equal to the true cortical fraction. The Standard Error Estimates (SEE) are expressed as a percentage of the true value of  $f_c$ . Because of the normal distribution this also means 99% of all errors will be smaller than 3 times the SEE.

Table A.1. Standard Error Estimates for two cortical fractions and five noise levels.

Noise level Value of SD as a fraction of cortical signal peak	SEE as percentage of the cortical fraction	
	Cortical fraction=0.37	Cortical fraction=0.52
0.20	1.5 %	1.2 %
0.28	2.1 %	1.8 %
0.36	2.7 %	2.2 %
0.44	3.2 %	2.6 %
0.52	3.9 %	3.2 %

## Conclusion

With the model the accuracy of the algorithm for determining the cortical fraction can be determined. The model therefore proves to be a valuable aid for assessing and optimising new algorithms and related problems in the acquisition and processing of our renographic data.

### **Acknowledgement**

Special thanks to H. van Mameren and the Department of Anatomy and Embryology, Maastricht University, the Netherlands for their efforts.

### **References**

- [1] Mameren H van, Groenewegen W, Rensema H. "Acta Morphol Neerl.-Scand. 22, 253, 1984.

## Appendix B

Derived from the article:

---

### **Automated quantitative evaluation of diseased and non-diseased renal transplants with MR – renography.**

---

Jacobus A. de Priester , MD, Jacques A. den Boer, PhD, Maarten H.L. Christiaans, MD, PhD, Alphons G.H. Kessels, MD, Eelco L.W Giele, MSc, Arie Hasman, PhD, Jos M.A. van Engelshoven, MD, PhD

*Submitted for publication*

#### **Introduction**

Medical conditions like acute and chronic rejection, acute tubular necrosis and drug induced tubulopathy are difficult to diagnose because clinical symptoms, laboratory tests and imaging findings are often overlapping [1]. In many cases renal transplant biopsy is inevitable since a final diagnosis can only be made with histology [1,2]. Biopsy, however, has a well-known risk of complications (bleeding, AV-fistula's, etc.) that may be hazardous for the patient and the renal transplant [1,3].

MR-renography (MRR) is a new imaging technique that may improve the diagnosis of medical diseases affecting the renal transplant. This method generates functional information in terms of time dependant changes in signal intensity during passage of a MRI contrast agent through the renal transplant parenchyma [4-6]. This is expressed in signal-time curves. The major difference with scintigraphic techniques is that the high spatial resolution of MRI makes it possible to separate the cortical from the medullary structures [2, 4-13]. Because various medical diseases affect different parts of the renal transplant, such a separation may

make it possible to differentiate these diseases by specific changes in cortical and/or medullary signal curves.

Although added value in the diagnosis of renal transplant diseases has been demonstrated in various papers [2,11,13], MRR has not gained widespread acceptance as a diagnostic tool.

Probably, the reason for this is threefold. First, as we experienced at our department, post-processing is difficult. Especially the placement of regions of interest (ROI's) over cortical and medullary tissue is problematic. Due to partial volume averaging and suboptimal contrast between cortex and medulla, ROI placement is difficult and subjective, even for an experienced operator. Second, renal transplant enhancement is complex and difficult to interpret quantitatively. Apart from the early cortical enhancement peak, which is sharp and easily discernible, a complex pattern of shallow cortical and medullary peaks is observed [14]. In combination with the fair amount of noise in MR-renographs it is difficult to identify and quantify these peaks in terms of time of occurrence, height and shape. Thirdly, non linearity of response caused by signal saturation can occur easily because of high intrarenal contrast agent concentrations [10, 15]. As a result, the shape of the MR renograph can depend strongly on bolus size and imaging method.

To handle these problems we have developed methods for data acquisition and automated image analysis [16,17] as well as curve parameterisation [18, submitted parallel to this study] in which our intention has been to minimise subjective operator input. This has resulted in a dramatic decrease in post-processing time (taking less than ten minutes per study) and, more important, in an objective parametric quantification of signal curves, which has proved to be reproducible [18, submitted parallel to this study]. In our acquisition method, in which a small bolus and a strongly T1 weighted scan sequence are used, signal non linearity was estimated to be mild at most [18, submitted parallel to this study].

In the study presented here we applied our technique of objective parametric MRR to a group of patients with well functioning renal transplants and a group of patients with severely diseased renal transplants. Our objective was to assess normal parameter values and to get an impression of the disease detecting capabilities of our technique.

---

**Material and methods.***Patients*

Thirty-five renal transplant recipients were selected for this study. Group 1 consisted of 27 renal transplant recipients who were in good clinical condition and had stable renal function for a period of at least three months prior to the investigation. Group 2 was formed by eight renal transplant recipients with severely disturbed renal transplant function requiring renal dialysis.

Patients in group 1 were immunosuppressed by azathioprine (13 patients), cyclosporine (8 patients) or tacrolimus (6 patients). Cyclosporine and tacrolimus have vasoconstrictive properties, altering renal perfusion, an effect that is not known from azathioprine [19]. Because this could influence renal transplant enhancement, a subdivision of group 1 was made. In group 1A (9 men, 4 women) immunosuppression was azathioprine based, in group 1B (13 men, 8 women) cyclosporine or tacrolimus were used for immunosuppression. The mean and range of the post-transplantation intervals of group 1A was 15.3 years and 6.5 - 20.5 years respectively, that of group 1B 3.0 years and 0.4 -10.2 years.

All patients in group 2 (4 men, 4 women) were on tacrolimus-based immunosuppression. Biopsy proven diagnoses for disturbed renal transplant function were delayed graft function in 4 patients, acute rejection in 2 patients and combinations of delayed graft function and cortical necrosis in 1 patient and cortical necrosis and interstitial nephritis in 1 patient. All renal transplant recipients of group 2 were in their early post-transplantation period (mean 25.0 days, range 6 to 64 days).

None of the patients of group 1 and group 2 had a history of decreased cardiac pump function and none were on diuretics. This study was approved by the medical ethics committee of our hospital and written informed consent was obtained from all the patients.

*Laboratory data and patient preparation*

The MRI examinations were planned in the late afternoon, 8-10 hours after the last intake of their immunosuppressive drugs, to exclude influence of changing drug levels of tacrolimus or cyclosporine on the renal transplant enhancement. From a 24-hour urine sample (collected the day before the examination) the 24-hour urine volume was measured and sodium and creatinine urine concentrations were estimated. Prior to the MRI investigation a venous blood sample was taken from which serum sodium and creatinine concentrations and the trough levels of

cyclosporine and tacrolimus were estimated. From these laboratory data, creatinine clearances and fractional excretion of sodium were calculated.

As pointed by Wolf et al.[14] low hydration influences renal enhancement because it leads to an increase of the fraction of water reabsorbed from the nephrons. The concomitant rise in concentration of Gadolinium-DTPA could cause unwanted T2\* effects which decrease signal intensity. Patients with disturbed renal transplant function (group 2) were under clinical surveillance and were held at slight levels of hyperhydration. To match hydration of the non-diseased population with that of the diseased patients and to avoid underhydration, patients with normal transplant function (Group 1A and 1B) were administered 500ml sodiumchloride 0.9% intravenously one hour prior to the MRI examination.

#### *MRI procedure*

MRI was performed on a 1.5 T imager, gradient strength 10 mT/m, slew rate 15 T/m/sec (Philips ACS-NT, Philips, Best, The Netherlands). MR studies started with coronal and sagittal planscans (SE;TR/TE=182/10), followed by a multislice axial T2-weighted scan (FSE;TR/TE/TF=3000/150/20) and an oblique multislice coronal T1-weighted scan through the long axis of the renal transplant (SE;TR/TE=550/14). The long axis images were used to select the optimal scan plane for the dynamic sequence, which consisted of a run of 256 T1-enhanced spoiled gradient echo scans (TR/TE/Flip=11ms/3.4ms/60°) with a slice thickness of 6 mm, FOV 400 mm, rectangular field of view 90% and scan matrix 200x256 (resulting voxel size 6.0x1.6x1.6mm). Scans were performed every 2 seconds. After the tenth dynamic scan, Gadolinium-DTPA (Magnevist, Schering, Germany) was injected in a dose of 0.05 mmol/kg. This low dose was used to avoid T2\*-effects [17, submitted parallel to this study]. Gadolinium was injected as a rapid bolus with a flow rate of 5 ml/sec with a MR-injector pump (Medrad Spectris, Medrad, Maastricht, The Netherlands), immediately followed by a saline flush (0.9%, dose 20ml, flow rate 5ml/sec).

#### *Post-processing, curve generation and parameterisation.*

Image analysis was performed on a Sun Sparc Ultra 30 work station(Sun microsystems Netherlands, Amersfoort, The Netherlands) with EasyScil software (Philips, Best, The Netherlands).

On each of the axial T2-weighted images the renal transplant parenchyma was circumscribed with a hand drawn line. Renal volumes were then calculated by adding up the measured areas and multiplying these with the slice thickness.

Objective cortical and medullary signal-time curves were generated with the automated image analysis algorithm that was described in a previous paper [17].

Signal-time curves are often characterized by three peaks and a tail [14, 18, submitted parallel to this study]. These structures can be expected on physiological grounds [14]. Accordingly, the enhancement data were fitted with a smooth enhancement curve with these, prescribed, features (three peaks and a tail) but with an adjustable shape, as described in [18, submitted parallel to this study]. Each peak is shaped as a gamma variate function and the tail as a matched exponential decay function. Each of these composing functions has three parameters that define peak time ( $\tau$ ), amplitude ( $\mu$ ) and shape ( $\lambda$ ) [18, submitted parallel to this study]. As an example, a gamma variate function and its parameters are illustrated in Figure B.1-a. Figure B.1-b gives an example of raw and noisy enhancement data and the corresponding fitted enhancement curve with its composing functions.

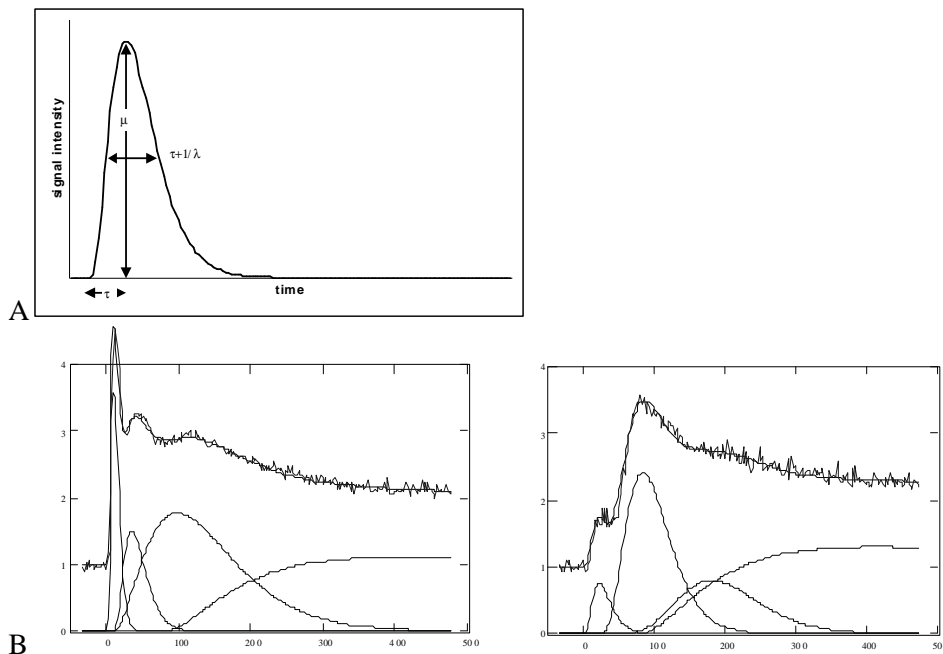


Figure B.1: (a) Gamma variate function; peak time is defined by  $\tau$ , peak amplitude (height) by  $\mu$  and curve width/shape by  $\tau + 1/\lambda$ . (b) Raw cortical and medullary signal-time curves and corresponding fitted curve with its composing functions. Cortical and medullary enhancement are characterized by three peaks and a tail that are fitted by the separate composing functions. The enhancement data and the fitted curves are offset vertically by one scale unit to visually separate them from the composing functions.



In total, therefore, four cortical and four medullary composing functions are used to fit renal enhancement curves, resulting in its description by 24 parameters (12 cortical and 12 medullary). Because several parameters were given fixed values, however, 8 cortical and 8 medullary parameters remain adjustable and after fitting these become the quantitative descriptors of renal enhancement [18, submitted parallel to this study]. These free parameters are listed in table A.2. In this table the subscripts 0 refer to the first (arterial) peak and subscripts 1 and 2 to the second and third peak, which are caused by accumulation of the contrast agent in the renal parenchyma (nephrons). Subscript 3 refers to the tail.

#### *Statistical analysis.*

For the analysis we used the observed kidney volume and the enhancement parameters per subject, together called “study parameters”.

The disease detecting capability of our method was tested in two steps. First, the study parameters from patients of group 1A and group 1B were joined and compared to those of group 2 with a t-test. Second, a forward stepwise logistic regression analysis was performed with disease as dichotomous dependent variable and the study parameters as independent variables.

To assess the homogeneity of the group of healthy volunteers, in view of possible effects of the various types of immunosuppression used in that group, the differences between the study parameters of group 1A and 1B were tested with a t-test.

## **Results.**

Laboratory findings are listed in table B.1. For healthy renal transplant recipients (group 1A and 1B) the mean creatinine clearance was higher and the mean fractionate sodium excretion was lower than for patients with diseased renal transplants (group 2). These differences were statistically significant ( $P < 0.05$ ). The high values of the fractionate sodium excretion in group 2 can be attributed to the disturbed function of the renal transplants in this group, causing high fractional loss of sodium in the urine. Despite differences between non-diseased and diseased population, the fractionate sodium excretion was well above 1% in all groups. Therefore, there was no indication that patients were dehydrated. The trough levels of cyclosporine and tacrolimus were within normal therapeutic ranges for both groups.

Table B.1: Laboratory data; means and standard deviations per group.

	Group 1A	Group 1B	Group 2
creatinine clearance (ml/min)	73,0 ± 34,8	59,0 ± 25,1	9,4 ± 9,6
fractionate sodium excretion (%)	12,1 ± 6,8	15,9 ± 5,9	57,0 ± 37,7
cyclosporine trough level (ng/mL)		0,19 ± 0,09	
tacrolimus trough level (ng/ml)		15,5 ± 4,3	18,9 ± 5,5

*Diseased (group 2) versus non-diseased (group 1A and 1B) renal transplant recipients.*

The study parameters are given in table B.2. In the diseased group, the mean medullary  $\lambda_1$  was significantly smaller than that in the non diseased group ( $P < 0.001$ ). The logistic regression analysis indicated that the combination of cortical  $\mu_0$  and medullary  $\lambda_1$  was the best predictor of renal transplant disease. Addition of other study parameters did not improve the prediction. A ROC-curve with the combination of cortical  $\lambda_1$  and medullary  $\mu_0$  as predictor of renal transplant disease is given in a ROC curve (figure B.2). The area under the curve was 0.98 (95% confidence interval: 0.96-1.0), indicating high sensitivity and specificity. For comparison, a scatter plot of cortical  $\mu_0$  and medullary  $\lambda_1$  for diseased and non-diseased patients is shown in figure B.3. In terms of MR-renographs these results are demonstrated in figure B.4 in which signal-time curves of a diseased and a non-diseased renal transplant are shown. The lower values of cortical  $\mu_0$  and medullary  $\lambda_1$  in the diseased renal transplant (figure B.4-a) are reflected as a lower amplitude of the vascular cortical peak and flattening of the first nephronal peak of the medulla, as compared to the normal renal transplant (figure B.4-b).

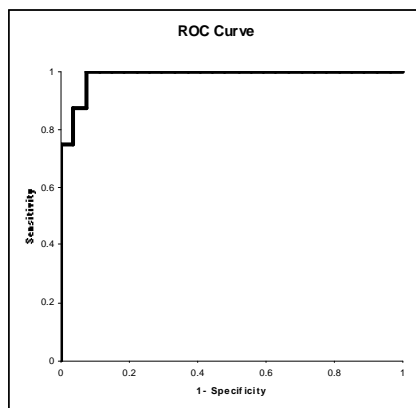


Figure B.2: ROC-curve of cortical  $\mu_0$  and medullary  $\lambda_1$  as predictors of renal transplant disease. Area under the curve is 0.98 indicating high sensitivity and specificity

Automated quantitative evaluation of diseased and non-diseased renal transplants with MR – renography.

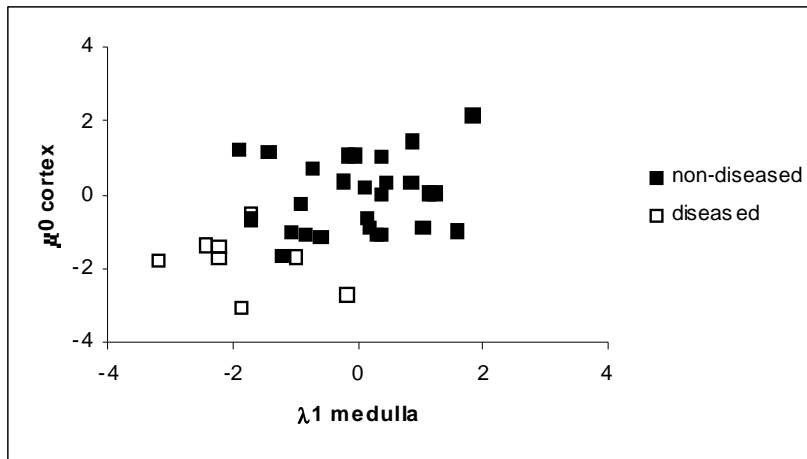


Figure B.3: Distribution of cortical  $\mu_0$  and medullary  $\lambda_1$  in diseased and non-diseased renal transplants. To enhance visualization, values are expressed as differences to the mean of the non-diseased population and are normalized to the standard deviation. A clear tendency of both parameters to be lower in the diseased group is shown.

Table B.2: Study data; means and standard deviations per group

		group 1A	group 1B	group 2
	Renal transplant volume (ml)	239,8 ± 43,1	222,6 ± 48,8	190,5 ± 53,2
	Enhancement parameters		-	-
cortex	$\mu_0$	2,3 ± 0,7	2,1 ± 0,6	1,1 ± 0,5
	$\tau_0(\text{sec})$	11,5 ± 1,5	10,4 ± 2,7	9,7 ± 2,5
	$\lambda_1(\text{sec}^{-1})$	0,099 ± 0,018	0,114 ± 0,019	0,098 ± 0,024
	$\mu_1$	0,97 ± 0,24	0,81 ± 0,30	0,47 ± 0,17
	$\tau_1(\text{sec})$	<b>23,8 ± 4,5</b>	<b>17,7 ± 4,1</b>	19,4 ± 5,1
	$\mu_2$	1,29 ± 0,28	1,08 ± 0,36	0,89 ± 0,19
	$\tau_2(\text{sec})$	<b>81,8 ± 6,2</b>	<b>71,9 ± 5,7</b>	70,1 ± 4,5
	$\mu_3$	0,87 ± 0,23	0,70 ± 0,25	0,65 ± 0,16
medulla	$\mu_0$	0,4 ± 0,2	0,6 ± 0,4	0,5 ± 0,2
	$\tau_0(\text{sec})$	24,5 ± 9,6	24,3 ± 7,3	21,6 ± 8,2
	$\lambda_1(\text{sec}^{-1})$	<b><i>0,046 ± 0,009</i></b>	<b><i>0,047 ± 0,009</i></b>	<b><i>0,029 ± 0,008</i></b>
	$\mu_1$	1,47 ± 0,59	1,26 ± 0,45	0,95 ± 0,31
	$\tau_1(\text{sec})$	63,4 ± 21,4	53,8 ± 10,8	55,3 ± 15,4
	$\mu_2$	0,43 ± 0,20	0,45 ± 0,31	0,49 ± 0,25
	$\tau_2(\text{sec})$	171,2 ± 40,8	156,8 ± 51,2	182,0 ± 71,6
	$\mu_3$	0,93 ± 0,34	0,88 ± 0,46	0,83 ± 0,35

Printed bold:statistically significant differences between group 1A and group 1B ( $P < 0.01$ ).

Printed italic and bold:statistically significant differences between group 1A+1B and group 2 ( $P < 0.001$ ).

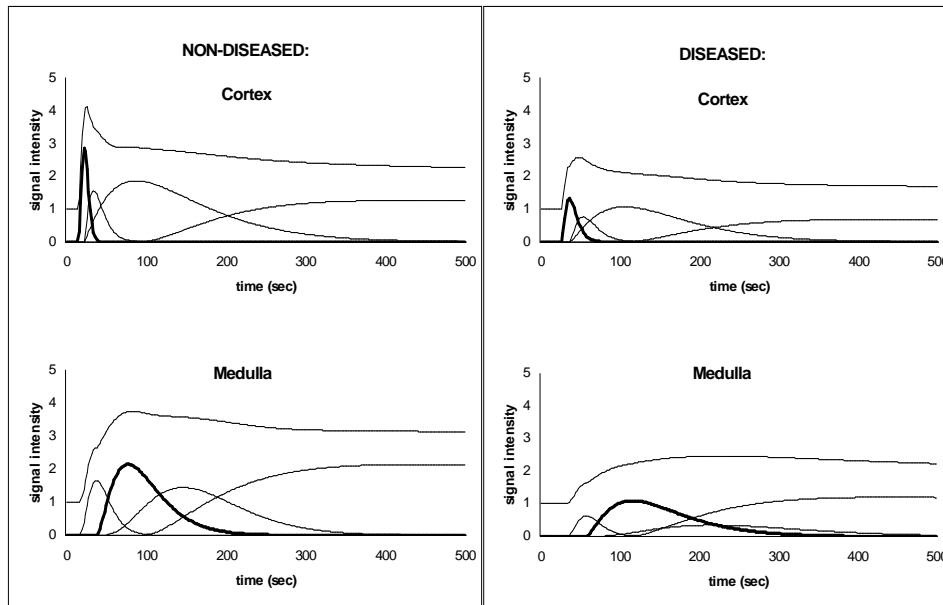


Figure B.4: Cortical and medullary enhancement curves of a diseased (a) and a non-diseased renal transplant (b); Lower values of cortical  $\mu_0$  and medullary  $\lambda_1$  in the diseased transplant reflect lower amplitude of vascular cortical peak and flattened first nephronal peak of the medulla, as compared to normal renal transplant (corresponding fit functions printed bold). Also visible differences in curve amplitudes are incidental.

#### *Non-diseased renal transplant recipients; group 1A versus group 1B.*

In renal transplant recipients with cyclosporine or tacrolimus based immunosuppression (group 1B), the peak times of the first ( $\tau_1$ ) and second ( $\tau_2$ ) parenchymal nephronal peak of cortical enhancement were significantly shorter than for patients who do not use these agents (group 1A;  $P < 0.01$ ). The other enhancement parameters, including those that predicted renal transplant disease, were not statistically different between group 1A and group 1B.

## Discussion

This report shows the first clinical results of a new quantitative analysis method for MR renographic data of renal transplants. Cortical and medullary renographs are quantified by eight parameters that describe amplitude, shape and timing of the various characteristics of the enhancement curves.

The most important result is the accurate prediction of renal transplant disease, as shown in the ROC curve (figure B.2). Diseased renal transplants are characterized by the combination of lower amplitudes of the cortical arterial perfusion peak ( $\mu_0$ ) and a flatter shape of the first medullary parenchymal nephronal peak ( $\lambda_1$ ). The cases used to define this test (by forward logistic regression) were the same as the ones for which the prediction was given. One could therefore doubt the true predictive value for other independent cases. The distribution of both variables, however, is close to normal (figure B.3) which suggests that the performance of the test is not accidental. The (statistically significant) difference in  $\lambda_1$  is an interesting finding. This has not been described previously in renal transplants and is a strong argument for MRR because no other technique can provide functional information that is strictly medullary in origin.

These results are encouraging but could have been influenced by dissimilarity of the diseased and non-diseased population in terms of immunosuppressive drug regimes. All diseased renal transplant recipients used tacrolimus which, like cyclosporine, has vasoconstrictive properties [19], whereas part of the non-diseased population used medication without this property (subgroup 1A; azathioprine). To rule out any influence of this dissimilarity, we assessed the differences in study parameters between group 1A and group 1B. This demonstrated that medullary  $\lambda_1$  and cortical  $\mu_0$  are not statistically different between these groups. Therefore, we can conclude that the disease-predictive properties of this combination of parameters is real and does not result from different immunosuppressive drug regimes.

A further interesting result of the study in the non-diseased population is that renal transplant recipients who use cyclosporine or tacrolimus (group 1B) have significantly lower cortical  $\tau_1$  and  $\tau_2$  than patients who use azathioprine (group 1A). These enhancement parameters define the peak times of the first and second cortical nephronal peak and are not the same as the parameters that differentiated between diseased and non diseased renal transplant recipients. This demonstrates that our description of enhancement is capable of resolving different aspects of kidney functionality.

The parametric curve to which our dynamic MR data are fitted is based on a physiologic model [18, submitted parallel to this study]. This implies that it should be possible to interpret our results from a physiologic perspective. The following is an attempt:

The smaller amplitude of the cortical vascular peak ( $\mu_0$ ) in diseased renal transplants means a decrease in cortical blood volume. The also visible flatter shape of the first parenchymal nephronal peak of the medulla ( $\lambda_1$ ) denotes a slower

---

washout from the medulla or a lack of isochronism of the early medullary transport in the nephrons. Considering the different types of diseases in our population it is remarkable that this trend is the same for all patients (figure B.3). It suggests that different mechanisms cause similar changes in renal dynamic behavior.

Pathophysiologic interpretation is speculative but the decreased cortical blood volume in diseased renal transplants could for instance be caused by loss of vascular structures (necrosis), vasoconstriction or interstitial disease with secondary vascular compromise. The changes in the medulla can be secondary to the events taking place in the cortex or be caused by medullary degeneration.

In renal transplant recipients who use agents with vasoconstrictive properties (group 1B; cyclosporine or tacrolimus), the peak times of the first and second cortical nephronal peak ( $\tau_1$  and  $\tau_2$ ) are significantly shorter than for patients who do not use these agents (group 1A). These parameters reflect the accumulation of Gadolinium-DTPA in the proximal and distal tubules. Similar, but not statistically significant, changes are seen in the medullary  $\tau_1$  and  $\tau_2$  (table B.2). In terms of the curve-fitting model, shorter peak times mean that flow through the nephrons is higher. This could be a reaction of the nephron apparatus to the vasoconstrictive effects of cyclosporine and tacrolimus. Rapid flow could be associated with small nephron diameter or with low concentration of the contrast agent caused by a lower reabsorption of water from the nephrons. More straightforward effects of vasoconstriction would be alterations in the arterial phases of enhancement. These are not demonstrated. Although the cortical arterial peak enhancement tends to be lower in individuals who use cyclosporine or tacrolimus (table B.2), this difference is not statistically significant.

Of course, the physiological interpretations given are speculative but they do give a suggestion of what could be inferred from the enhancement curves when sufficient experience in their interpretation is added.

Limitations of our study are that all the diseased patients had severe renal transplant dysfunction and that the types of diseases were very heterogeneous. Although we were capable to accurately demonstrate disease related changes in renal enhancement, nothing can be said about disease specificity which should be the ultimate objective of MRR. Furthermore, the sensitivity of our technique for milder forms of renal transplant disease is not proven. Additional studies with larger groups of patients and variable degrees of renal transplant dysfunction are required. The positive results from our study justify such future research.

In conclusion, our method of MR renography, that includes new methods of image analysis and parametric quantification, is highly accurate in detecting medical renal transplant disease. Because our technique is performed fully computerized it is

operator independent and postprocessing time is minimal. These are important steps forward towards the clinical use of functional MRI in renal transplant recipients and justify future research that should be directed towards disease-specific changes in MR-renographs. In this respect, functional information obtained from medullary enhancement may play a vital role.

## References

- 1 Granger and Allison. Diagnostic Radiology. Edinburgh: Churchill Livingstone; 1992;1372-1377.
- 2 Szolar DH, Preidler K, Ebner F, et al. Functional magnetic resonance imaging of human renal allografts during the post-transplant period: preliminary observations. Magn Reson Imaging 1997; 15:727-735.
- 3 Wallace S, Schwarten DE, Smith, et al. Intrarenal arteriovenous fistula; transcatheter stem occlusion. J Urol 1978; 120:282-286.
- 4 Kikinis R, Von Schultess GK, Jager P, et al. Normal and hydronephrotic kidney: Evaluation of renal function with contrast-enhanced MR imaging. Radiology 1987; 165:837-842.
- 5 Choyke PL, Frank JA, Girton ME, et al. Dynamic Gd-DTPA-enhanced MR imaging of the kidney: Experimental results. Radiology 1989; 170:713-720.
- 6 Carvlin MJ, Arger PH, Kundel HL, et al. Use of Gd-DTPA and fast gradient-echo and spin-echo MR imaging to demonstrate renal function in the rabbit. Radiology 1989; 170:705-711.
- 7 Semelka RC, Hricak H, Tomei E, Floth A, Stoller M. Obstructive Nephropathy: Evaluation with dynamic Gd-DTPA-enhanced MR imaging. Radiology 1990; 175:797-803.
- 8 Von Schultess GK, Kuoni W, Gerig G, Wuthrich R, Duewell S, Krestin G. Semiautomated ROI analysis in dynamic MR studies. Part II: Application to renal function examination. J Comput Assist Tomogr 1991; 15:733-741.
- 9 Ros PR, Gauger J, Stoupis C, et al. Diagnosis of renal artery stenosis: Feasibility of combining MR angiography, MR renography, and Gadopentetate-based measurements of glomerular filtration rate. AJR 1995; 165:1447-1451.

- 
- 10 Munechika H, Sullivan DC, Hedlund LW, et al. Evaluation of acute renal failure with magnetic resonance imaging using gradient-echo and Gd-DTPA. *Invest Radiol* 1991; 26:22-27.
  - 11 Sharma RK, Gupta RK, Poptani H, Pandey CM, Gujral RB, Bhandari M. The magnetic resonance renogram in renal transplant evaluation using dynamic contrast-enhanced MR imaging. *Transplantation* 1995; 59: 1405-1409.
  - 12 Roberts TPL. Physiologic measurements by contrast enhanced MR imaging: expectations and limitations. *JMRI* 1997; 7:82-90.
  - 13 Nakashima R, Yamashita Y, Tomiguchi S, Tsuji A, Takahashi M. Functional evaluation of transplanted kidneys by Gd-DTPA enhanced Turbo-FLASH MR imaging. *Radiat Med* 1996; 14:251-256.
  - 14 Wolf GL, Hoop B, Cannillo JA, Rogowska JA, Halpern EF. Measurement of renal transit of Gadopentetate Dimeglumine with echo-planar MR imaging. *JMRI* 1994; 4:365-372.
  - 15 Takeda M, Katayama Y, Tsutsui T, Komeyama T, Mizusawa T. Does gadolinium-diethylene triamine pentaacetic acid enhanced MRI of the kidney represent tissue concentration of contrast media in the kidney? In vivo and in vitro study. *Magn Res Imag* 1994; 12:421-427.
  - 16 DePriester JA, Giele ELW, DenBoer JA, et al. MR-renography: An algorithm for calculation and correction of cortical volume averaging in medullary renographs. *JMRI* 2000; 12:453-459.
  - 17 De Priester JA, den Boer JA, Kessels AGH, et al. MR – renography by semiautomated image analysis: performance in renal transplant recipients. *JMRI* 2001; 14:134-141.
  - 18 DenBoer JA, DePriester JA, Geerlings MJHM, et al. Quantitative model description of dynamic MRI enhancement data of the kidney. *JMRI*, submitted.
  - 19 Marsen TA, Weber F, Egink G, Suckau G, Baldamus CA. Differential transcriptional regulation of endothelin-1 by immunosuppressants FK 506 and cyclosporine A. *Fundam Clin Pharmacol* 2000; 14:401-408.



Automated quantitative evaluation of diseased and non-diseased renal transplants  
with MR – renography.

---

---

## Samenvatting

---

In dit proefschrift worden enkele technieken beschreven die gebruikt kunnen worden voor het bepalen van MR renogrammen. Renogrammen zijn curves die de concentratie van een contrastmiddel in de cortex en medulla van de nier weergeven als functie van de tijd. Om MR renogrammen te maken wordt tijdens en na de injectie van een contrast middel een serie dynamische MR scans gemaakt. Door in deze scans de helderheid te meten van de cortex en de medulla wordt het MR renogram bepaald.

Ondanks het feit dat een MR scanner doorsnede-plaatjes maakt van de nier zal het signaal dat in de medulla wordt gemeten vaak ook nog een bijdrage bevatten van de cortex, doordat er meestal ook cortex aanwezig is in de drie-dimensionele beeldelementen (voxels). Door het corticale signaal met gewogens subtractie van dit gemengde signaal af te trekken wordt het zuivere medullaire signaal verkregen. In dit proefschrift worden verschillende methodes voor het bepalen van de weefactor beschreven en de meest stabiele bepaald.

Om de reproduceerbaarheid te verbeteren en de benodigde invoer van de gebruiker te verminderen is er een methode beschreven voor de automatische segmentatie van de nier en de plaatsing van de regions of interest (ROIs) die gebruikt worden om de helderheid te meten. Deze ROIs worden geplaatst aan de hand van a priori kennis van de distributie van beide weefsels in de nier en aan de hand van analyse van de distributie van het contrastmiddel tijdens de dynamische scan.

Aangezien gewogen subtractie de signaal/ruis verhouding vermindert en deze verslechtert bij toenemende weefactor, moet de corticale bijdrage zo klein mogelijk worden gehouden. Door gebruik te maken van matched image filtering kunnen gebieden met een hoge corticale bijdrage gevonden worden en door deze vervolgens uit het ROI te verwijderen wordt de totale corticale bijdrage verminderd.

De eerste algoritmes werden ontwikkeld op beelden van getransplanteerde nieren aangezien deze niet bewegen als gevolg van de ademhaling. Om het mogelijk te maken om MR renogrammen te maken van de wel met de ademhaling bewegende natieve nieren moet deze beweging gecorrigeerd worden. In dit proefschrift worden verschillende methodes beschreven en met elkaar vergeleken.

Automated quantitative evaluation of diseased and non-diseased renal transplants with MR – renography.

---

Als laatste worden in dit proefschrift een aantal scanner parameters die gebruikt zijn tijdens dit onderzoek nog een keer onder de loep genomen. Aan de hand van de tijdens het onderzoek ontwikkelde methodes en de nieuwe mogelijkheden als gevolg van de voortschrijdende technologie wordt een set nieuwe parameters voorgesteld die zouden moeten resulteren in een verbeterde signaal/ruis verhouding in de MR renogrammen.

---

## Dankwoord

---

Onderzoek, zeker een onderzoek zoals dit dat zich met meerdere disciplines bezig houdt, is bijna onmogelijk zonder de hulp van anderen. Vanaf deze plaats wilde ik dan ook graag die mensen bedanken die hier aan hebben bijgedragen.

Als eerste is dat mijn eerste promotor Arie Hasman. We verschilden nogal eens van inzicht en dat leverde interessante en soms ook luidruchtige discussies op. Uiteindelijk wisten we altijd weer overeenstemming te bereiken om het dan een week later over iets anders oneens te zijn. Bedankt voor het geduld.

Ten tweede wilde ik graag Jacques den Boer bedanken, zowel voor het onvermoeibare (her-)lezen van mijn artikelen en suggereren van verbeteringen als vanwege zijn bijdragen aan het onderzoek. Zijn kennis is van enorme waarde geweest.

Op de TU heeft verder ook Hans Blom bijgedragen aan het nalezen en corrigeren van mijn schrijfwerk.

Van het Academisch Ziekenhuis Maastricht heb ik de nodige ondersteuning gehad. Zo werd dit onderzoek gedaan in nauwe samenwerking met Koo de Priester, die de medische kant van het onderzoek deed. Samen hebben we uren zitten puzzelen op problemen en hoe ze op te lossen. En natuurlijk is het prachtig dat jouw resultaten aantonen dat we dit niet allemaal voor niets hebben gedaan.

Professor van Engelshoven heeft als tweede promotor voor de nodige sturing op medisch gebied gezorgd en heeft zo een belangrijke bijdrage geleverd aan het onderzoek.

Marc Geerlings ben ik dankbaar voor zijn hulp bij de implementatie van de in dit proefschrift beschreven methodes. Marc kon mijn software begrijpen en hing alles aan een userinterface waardoor de methodes ook echt gebruikt konden worden. Vooral voor zijn hulp bij het temmen van Solaris ben ik hem zeer dankbaar.

Verder wilde ik de laboranten graag bedanken voor hun hulp met de MR scanner en de data archivering.

Mensen die ook zeker niet in dit rijtje mogen ontbreken zijn Henk van Mameren en alle anderen van de Anatomie en Embryologie groep van de Universiteit van

Automated quantitative evaluation of diseased and non-diseased renal transplants with MR – renography.

---

Maastricht. Dankzij hen werd het mogelijk om een nier in het echt te bestuderen en er een computermodel van te maken.

Al deze mensen wil ik niet alleen bedanken voor hun bijdragen aan het onderzoek, maar vooral ook voor de prettige samenwerking.

Verder wilde ik graag nog Philips Medical Systems bedanken voor het beschikbaar stellen van hard- en software.

En tenslotte wil ook nog al de patiënten bedanken die hebben meegedaan. Zonder hun medewerking was dit onderzoek niet mogelijk geweest.

Eelco Giele  
Januari, 2002

---

## Curriculum Vitae

---

Eelco Giele was born in Geldrop, the Netherlands, on May 12th 1971. In 1989 he finished secondary school (VWO, Strabrecht College in Geldrop) and started with his study Electrical Engineering at the Eindhoven University of Technology.

He obtained his masters degree in 1995 at the group of medical electrical engineering with his work entitled "Brain mapping with EEG signals". After a short period during which he worked for the medical electrical engineering group (amongst other things on the European IMPROVE project) he started with his PhD study.